

SEVERE PLASTIC DEFORMATION OF MAGNESIUM ALLOYS BY EQUAL CHANNEL ANGULAR PRESSING

Thesis

Submitted in partial fulfillment of the requirements for the degree of

DOCTOR OF PHILOSOPHY

by

GOPI K. R



**DEPARTMENT OF MECHANICAL ENGINEERING
NATIONAL INSTITUTE OF TECHNOLOGY KARNATAKA
SURATHKAL, MANGALORE-575025**

OCTOBER, 2017

DECLARATION

I hereby declare that the Research Thesis entitled “**SEVERE PLASTIC DEFORMATION OF MAGNESIUM ALLOYS BY EQUAL CHANNEL ANGULAR PRESSING**” which is being submitted to the **National Institute of Technology Karnataka, Surathkal** in partial fulfillment of the requirements for the award of the degree of **Doctor of Philosophy in Department of Mechanical Engineering** is a *bonafide report of the research work carried out by me*. The material contained in this Research Thesis has not been submitted to any other Universities or Institutes for the award of any degree.

Register Number: **145013ME14F04**

Name of the Research Scholar: **GOPI K. R**

Signature of the Research Scholar:

Department of Mechanical Engineering

Place: NITK-Surathkal

Date:

C E R T I F I C A T E

This is to certify that the Research Thesis entitled “**SEVERE PLASTIC DEFORMATION OF MAGNESIUM ALLOYS BY EQUAL CHANNEL ANGULAR PRESSING**” submitted by **Mr. GOPI K. R (Register Number: 145013ME14F04)** as the record of the research work carried out by him, *is accepted as the Research Thesis submission* in partial fulfillment of the requirements for the award of the degree of **Doctor of Philosophy**.

Dr. H. Shivananda Nayaka

Research Guide

Date:

Chairman-DRPC

Date:

Dedicated to

- ❖ *My beloved parents, wife and children*
- ❖ *All my Teachers and Professors who taught and encouraged me with positive thoughts*

ACKNOWLEDGEMENT

First of all, I would like to express my sincere gratitude and heartiest thanks to my supervisor **Dr. H. Shivananda Nayaka**, Assistant Professor, Department of Mechanical Engineering, National Institute of Technology Karnataka (N.I.T.K), Surathkal, for his excellent guidance and support throughout the work. This thesis could not have attained its present form, both in content and presentation without his active interest, timely support, direction and valuable guidance. The words are insufficient to express my deep feeling and heartfelt thanks to my supervisor for his unhesitated guidance throughout my doctoral work.

I take this opportunity to thank **Dr. Narendranath S**, Professor and Head, Department of Mechanical Engineering for his continuous and timely support.

I wish to express my sincere gratitude to all the faculty members of Department of Mechanical Engineering, of N.I.T.K Surathkal for their unbiased appreciation and support all through this research work.

I owe my deepest gratitude to Jaya Devadiga, Verghese, Pradeep, Sudhakar, and Sathish technicians, Machine shop, NITK, for permitting me to carry out the experimental work and use the testing facilities available here.

I would like to express my sincere thanks and gratitude to Applied Mechanics Department for their kind help, encouragement for successful completion of this Research work.

I owe my deepest gratitude to Seetharam, Sreekanth and Shashi, technicians for permitting me to carry out the experimental work and use the testing facilities available in “Strength of Materials Lab”, for successful completion of this Research work.

I would like to express my sincere thanks to **Dr. Udaya Bhat K**, Associate Professor and Head, **Dr. Shashi Bhushan Arya** and Bhaskaran, Research Scholar, Department of Metallurgical and Materials Engineering, N.I.T.K Surathkal for their continuous

support and permitting me to carry out the OM, SEM, TEM and corrosion test in their testing facilities available in their department.

I would like to express my sincere thanks to **Dr. Shashank Shekhar**, Assistant Professor and Sandeep Sahu, Research Scholar, Department of Materials Science and Engineering, IIT Kanpur for their continuous support and permitting me to carry out the experimental work and use the testing facilities available in their department.

I am indebted to all my colleagues of Department of Mechanical Engineering, N.I.T.K, for their constant help and encouragement during the entire process of this research work.

I would like to share this moment of happiness with my parents, Smt. Mohan kumari and Sri. K M Rangaraju, my daughter Lekhana and my son Namith. My Wife Smt. Sandhya deserves special thanks for her endless moral support and for her fabulous encouragement.

Above all, I am highly indebted to almighty God who blessed me with spiritual support and determination at each and every stage of this research work.

(Gopi K R)

ABSTRACT

Magnesium and its alloys possess good mechanical properties like low density, good castability, high specific strength and low cost. Requirement of magnesium alloys is more towards industrial applications, particularly in aerospace and automotive industries. The main limitation is the poor room temperature formability, with limited number of slip systems, due to their hexagonal closed packed (HCP) structure. Formability at room temperature in Mg alloys can be improved by grain refinement, as fine-grained structure improves ductility. Severe plastic deformation (SPD) is a technique where high strains are induced into the material to produce fine grained structural material. They also have few limitations, like high wear rate and low corrosion resistance, which hinders the usage of magnesium in many applications. Wear rate and corrosion resistance can be improved by subjecting the material to SPD, thereby, increase the applications of magnesium alloys.

Equal channel angular pressing (ECAP) is one of the simple and most effective methods of SPD to improve the material properties. ECAP is a process in which the workpiece is subjected to shear deformation and thus, severe plastic strain is induced into the material without any change in the cross-sectional dimension of the sample. Microstructure has major effect on mechanical properties. ECAP process leads to ultrafine-grained microstructure in the material which may show superplastic deformation at low temperature and high strain rate. In HCP structured metals, grain refinement also leads to textural changes i.e. high strengthening in some particular directions.

Magnesium alloys are available in various systems – (a) Mg-Al system where aluminum addition improves the mechanical property as well as the castability. Addition of aluminum up to 6% and more makes the alloy age-hardenable. Manganese (Mn) addition plays a vital role in grain refinement for magnesium alloys. (b) Aluminum-manganese (AM) series magnesium alloys are widely used in manufacturing of various automobile components such as seat frames, instrument panels etc., due to their better damping, better toughness, impact absorption and elongation properties compared to aluminum-zinc (AZ) series alloys.

In the present study, ECAP was performed on AM70, AM80 and AM90 alloy with varying percentage of aluminum and manganese. In spite of various applications of AM series magnesium alloy, limited work has been done to improve the physical properties of AM series magnesium cast alloys. We may further improve these properties by using ECAP, so that its application can be expanded in different areas of engineering. ECAP was carried out using hot die steel (HDS) die with channel angle (Φ) as 110° and outer arc of curvature (Ψ) as 20° using route B_C. Unprocessed and ECAP processed samples were subjected to microstructural studies and tested for mechanical properties. Strength and hardness values showed increasing trend for the initial 2 passes of ECAP processing and then started decreasing with further increase in the number of ECAP passes, even though the grain size continued to decrease in all the successive ECAP passes. However, the strength and hardness values still remained quite high when compared to the initial condition (as-cast and homogenized). This behavior was found to be correlated with texture modification in the material as a result of ECAP processing. Wear and corrosion tests were conducted to study tribological and corrosion behavior of ECAP processed samples. Results showed reduction in wear mass loss for the ECAP processed samples. Coefficient of friction (COF) was studied for different loads and improvement in COF values was observed for ECAP processed samples compared to initial condition. Potentiodynamic polarization and electrochemical impedance spectroscopy test showed improvement in corrosion resistance of ECAP processed samples. Immersion test showed similar trend with increased corrosion resistance of ECAP processed samples with low hydrogen evolution.

Key words: *Equal Channel Angular Pressing, Magnesium Alloys, Grain Refinement, Microstructure, Mechanical Properties, Fractography, Wear, Corrosion, X-ray Diffraction, Energy dispersive X-ray spectrometer*

Organization of the Thesis

Structure of the thesis includes seven chapters and is summarized as follows:

Chapter 1, Introduction to magnesium and magnesium alloys followed by brief description of SPD techniques and the reason for selection of ECAP process.

Selection of the material to carry out ECAP process and the objectives of the present work are discussed in this chapter.

Chapter 2, Literature review consists of features of various SPD Techniques, advantages and limitations. Brief discussion about ECAP process, parameters which influence the ECAP process, advantages and limitations of ECAP process is carried out. Discussion on magnesium and magnesium alloys with its drawback. Application of AM series magnesium alloys. Reported work of different researchers on ECAP processed magnesium alloys with respect to mechanical properties, wear and corrosion behavior. Motivation from literature survey and objectives of the present work are highlighted.

Chapter 3, Material composition of the received alloy and detailed explanation of experimental procedure to carry out ECAP process. Characterization of the ECAP processed samples using optical microscopy (OM), scanning electron microscopy (SEM), Transmission electron microscopy (TEM), electron backscattered diffraction (EBSD) and X-ray diffraction (XRD) analysis is explained. Procedures of microstructural analysis, tensile, wear and corrosion and the corresponding sample preparation techniques are highlighted. Equipment used to conduct microstructural characterization, analyze mechanical properties, wear and corrosion tests discussed.

Chapter 4, Chapter 5 and Chapter 6, explain the results and discussion of various experiments carried out on the three alloys AM70, AM80 and AM90. Microstructural characterization by OM, SEM, TEM, EBSD and XRD analysis has been discussed. Mechanical properties which includes hardness, tensile followed by fractography has been analyzed. Wear test with different loading conditions and sliding distances has been explained. Corrosion studies by electrochemical measurements and immersion test method has been highlighted.

Chapter 7, summarizes the conclusions followed by future work.

CONTENT

	Page No.
Declaration	
Certificate	
Acknowledgements	
Abstract	
Contents.....	i
List of Figures.....	vi
List of Tables.....	xii
Nomenclature.....	xiii
Symbols.....	xv
1. INTRODUCTION	1
1.1 Background	1
1.2 SPD techniques	2
2. LITERATURE REVIEW	5
2.1 Severe plastic deformation (SPD)	5
2.1.1 Constrained groove pressing (CGP)	6
2.1.2 Repetitive corrugation and straightening (RCS)	7
2.1.3 High pressure torsion (HPT)	7
2.1.4 Cyclic extrusion compression (CEC)	8
2.1.5 Accumulative roll-bonding (ARB)	8
2.1.6 Equal channel angular pressing (ECAP)	9
2.2 ECAP setup	10
2.3 Basic parameters in ECAP	10
2.3.1 Imposed Strain in ECAP and different die angles	11
2.3.2 Processing routes and slip systems	12

2.3.3 Effect of pressing speed	15
2.3.4 Effect of pressing temperature	15
2.3.5 Effect of back-pressure	15
2.4 Advantages and limitations of ECAP	16
2.5 Magnesium alloys and their properties	17
2.5.1 Drawback of magnesium alloys	19
2.5.2 Applications of AM series magnesium alloys	20
2.6 Strengthening mechanisms	21
2.6.1 Work hardening	21
2.6.2 Solid solution strengthening and alloying	21
2.6.3 Precipitation hardening	22
2.6.4 Grain boundary (GB) strengthening	22
2.7 Literature on microstructure and mechanical properties	23
2.8 Literature on wear behavior	28
2.9 Literature on corrosion studies	30
2.10 Motivation from literature survey	32
2.11 Objectives	32
3. EXPERIMENTAL PROCEDURE	33
3.1 Equal channel angular pressing (ECAP) setup with universal testing machine	34
3.2 Material and ECAP operation	35
3.3 Optimizing the processing temperature	37
3.4 Sample preparation for testing	38
3.4.1 Microstructural characterization	38
3.4.2 Mechanical properties evaluation	41

3.4.2.1 Tensile test	41
3.4.2.2 Vickers Microhardness (Hv)	42
3.4.3 Wear behavior	43
3.4.4 Corrosion studies	44
3.4.4.1 Electrochemical measurements	44
3.4.4.2 Immersion test	45
4. RESULTS AND DISCUSSION	48
4.1 Equal channel angular pressing of AM70 alloy	48
4.1.1 Microstructure analysis	48
4.1.2 X-ray diffraction analysis	53
4.1.3 Mechanical properties	54
4.1.3.1 Tensile behavior	54
4.1.3.2 Vickers Microhardness	56
4.1.3.3 Fractography	57
4.1.4 Wear behavior	58
4.1.4.1 Coefficient of friction (COF) during wear test	58
4.1.4.2 Wear mass loss and wear morphology	59
4.1.5 Corrosion behavior	64
4.1.5.1 Electrochemical measurements	64
(a) Potentiodynamic polarization study	64
(b) Electrochemical impedance spectroscopy (EIS)	66
4.1.5.2 Immersion test	70
4.2 Summary	71
5. RESULTS AND DISCUSSION	74
5.1 Equal channel angular pressing of AM80 alloy	74

5.1.1 Microstructure analysis	74
5.1.2 X-ray diffraction analysis	78
5.1.3 Mechanical properties	79
5.1.3.1 Tensile behavior	79
5.1.3.2 Vickers Microhardness	81
5.1.3.3 Fractography	82
5.1.4 Wear behavior	83
5.1.4.1 Coefficient of friction (COF) during wear test	83
5.1.4.2 Wear mass loss and wear morphology	83
5.1.5 Corrosion behavior	88
5.1.5.1 Electrochemical measurements	88
(a) Potentiodynamic polarization study	88
(b) Electrochemical impedance spectroscopy (EIS)	90
5.1.5.2 Immersion test	93
5.2 Summary	95
6. RESULTS AND DISCUSSION	97
6.1 Equal channel angular pressing of AM90 alloy	97
6.1.1 Microstructure analysis	97
6.1.2 X-ray diffraction analysis	102
6.1.3 Mechanical properties	103
6.1.3.1 Tensile behavior	103
6.1.3.2 Vickers Microhardness	105
6.1.3.3 Fractography	106
6.1.4 Wear behavior	107
6.1.4.1 Coefficient of friction (COF) during wear test	107

6.1.4.2 Wear mass loss and wear morphology	108
6.1.5 Corrosion behavior	112
6.1.5.1 Electrochemical measurements	112
(a) Potentiodynamic polarization study	112
(b) Electrochemical impedance spectroscopy (EIS)	114
6.1.5.2 Immersion test	117
6.2 Summary	119
6.3 Comparison of properties in ECAP processed AM70, AM80 and AM90 alloys	121
7. CONCLUSIONS	123
Scope for Future Work	125
References	127
List of Publications based on PhD research work	
Bio-data	

LIST OF FIGURES

Fig. No.	Description	Page No.
Figure 2.1	Constrained groove pressing	6
Figure 2.2	Repetitive corrugation and straightening	7
Figure 2.3	High pressure torsion	7
Figure 2.4	Cyclic extrusion compression	8
Figure 2.5	Accumulative roll-bonding	9
Figure 2.6	Schematic of ECAP setup	10
Figure 2.7	Principles of ECAP pressing	11
Figure 2.8	Various equivalent strain values for different channel angle and outer arc of curvature	12
Figure 2.9	Four fundamental processing routes	12
Figure 2.10	Slip systems for different routes and passes	13
Figure 2.11	Distortions into the cubic elements on different planes	14
Figure 2.12	Shearing patterns on different planes for different processing routes with ECAP 1 (red), 2 (mauve), 3 (green) and 4 (blue) passes respectively	14
Figure 2.13	Illustration of the ECAP die with pressing force and back-pressure force	16
Figure 2.14	Equipment with computer controlled back-pressure	16
Figure 2.15	Phase diagram for magnesium-aluminium alloy system	18
Figure 2.16	Applications of magnesium alloys	19
Figure 2.17	Alloy development	20
Figure 3.1	Flow chart of the process	33
Figure 3.2	Schematic illustration of ECAP process	34
Figure 3.3	UTM with ECAP setup	34
Figure 3.4	Machined samples to carry out ECAP	36
Figure 3.5	Split ECAP die with plunger	36
Figure 3.6	Processing route B _C	37
Figure 3.7	Sample after ECAP operation	37
Figure 3.8	(a) Initial sample and ECAP at (b) 225 °C (c) 250 °C and (d) 275	38

°C with soaking time of 15 min

Figure 3.9	(a) Optical microscope (b) Scanning electron microscope	39
Figure 3.10	Transmission electron microscope	40
Figure 3.11	(a) FE-SEM (b) Struers electro polishing machine	40
Figure 3.12	X-ray diffraction	41
Figure 3.13	Tensile test specimen dimension as per ASTM-E8	41
Figure 3.14	Shimadzu Tensile Tester	42
Figure 3.15	Omni tech microhardness tester	42
Figure 3.16	Wear test specimen preparation	43
Figure 3.17	Schematic diagram of wear test machine	44
Figure 3.18	Electrochemical workstation	45
Figure 3.19	Schematic of immersion test setup for measuring hydrogen evolution	46
Figure 3.20	Immersion test setup	47
Figure 4.1	SEM images of AM70 alloy (a) as-cast and (b) homogenized samples	49
Figure 4.2	Optical microstructures of AM70 alloy (a) as-cast (b) homogenized (c) 1P (d) 2P (e) 3P and (f) 4P samples	50
Figure 4.3	SEM images of (a) as-cast (b) homogenized and ECAP (c) 1P (d) 2P (e) 3P and (f) 4P samples	50
Figure 4.4	Grain size of as-cast, homogenized and ECAP processed samples	51
Figure 4.5	TEM images of ECAP 4P sample	51
Figure 4.6	OIM with IPF image (a) as-cast and (b) ECAP 4P samples	52
Figure 4.7	Misorientation angles of (a) as-cast and (b) ECAP 4P samples	53
Figure 4.8	XRD patterns of (a) as-cast (b) ECAP 2P and (c) ECAP 4P samples	54
Figure 4.9	Tensile properties for as-cast, homogenized and ECAP processed samples	55
Figure 4.10	Microhardness of homogenized and ECAP processed samples	57
Figure 4.11	SEM images of fractured surfaces (a) as-cast (b) homogenized (c) 1P (d) 2P (e) 3P and (f) 4P samples	58

Figure 4.12	COF curves for samples under 30 N and 40 N load with sliding distance (a) 2500 m and (b) 5000 m	58
Figure 4.13	Wear mass loss versus number of ECAP passes	59
Figure 4.14	SEM images of worn surfaces of (a) Homogenized and ECAP processed (b) 1P, (c) 2P, and (d) 4P samples under 30 N load with sliding distance 2500 m	60
Figure 4.15	SEM images of worn surfaces of (a) Homogenized and ECAP processed (b) 1P, (c) 2P, and (d) 4P samples under 40 N load with sliding distance 2500 m	61
Figure 4.16	SEM images of worn surfaces of (a) Homogenized and ECAP processed (b) 1P, (c) 2P, and (d) 4P samples under 30 N load with sliding distance 5000 m	62
Figure 4.17	SEM images of worn surfaces of (a) Homogenized and ECAP processed (b) 1P, (c) 2P, and (d) 4P samples under 40 N load with sliding distance 5000 m	62
Figure 4.18	EDS analysis for (a) Homogenized and (b) ECAP processed 2P sample under 30 N load	63
Figure 4.19	EDS analysis for (a) Homogenized and (b) ECAP processed 2P sample under 40 N load	63
Figure 4.20	Electrochemical potentiodynamic polarization plots of unprocessed and ECAP processed samples	65
Figure 4.21	Nyquist plots of unprocessed and ECAP processed samples	67
Figure 4.22	Equivalent circuit (Randles circuit) for analyzing of the EIS characteristics	68
Figure 4.23	R_t verses number of ECAP passes	68
Figure 4.24	XRD of ECAP processed 3 pass corrosion sample	69
Figure 4.25	SEM images of corrosion samples for different ECAP passes	69
Figure 4.26	SEM images of immersed samples (a) as-cast (b) homogenized and ECAP processed (c) 1P, (d) 2P, (e) 3P, and (f) 4P samples	70
Figure 4.27	SEM images with EDS and elemental mapping of ECAP 3P sample	71
Figure 5.1	Microstructures of (a) as-cast (b) Homogenized (c) 1P (d) 2P (e) 3P and (f) 4P ECAP samples	75

Figure 5.2	SEM micrographs of ECAP (a) as-cast (b) Homogenized (c) 1P (d) 2P (e) 3P and (f) 4P samples	76
Figure 5.3	Grain size of as-cast, homogenized and ECAP processed samples	76
Figure 5.4	TEM images of ECAP 4 pass sample	77
Figure 5.5	OIM with IPF image of (a) as-cast and (b) ECAP 4P samples	77
Figure 5.6	Misorientation angle grain distribution of (a) as-cast and (b) ECAP 4 pass sample	78
Figure 5.7	XRD profile of (a) as-cast (b) ECAP 2 pass and (c) ECAP 4 pass samples	79
Figure 5.8	Tensile properties for as-cast, homogenized and ECAP processed samples	80
Figure 5.9	Microhardness values of homogenized and ECAP processed samples	81
Figure 5.10	SEM micrographs of fractured surfaces (a) as-cast (b) homogenized and ECAP (c) 1P (d) 2P (e) 3P and (f) 4P samples	82
Figure 5.11	COF curves for samples under 30 N and 40 N load with sliding distance (a) 2500 m and (b) 5000 m	83
Figure 5.12	Wear mass loss versus number of ECAP passes	84
Figure 5.13	SEM images of worn surfaces of (a) Homogenized and ECAP processed (b) 1P, (c) 2P, and (d) 4P samples under 30 N load with sliding distance 2500 m	85
Figure 5.14	SEM images of worn surfaces of (a) Homogenized and ECAP processed (b) 1P, (c) 2P, and (d) 4P samples under 40 N load with sliding distance 2500 m	85
Figure 5.15	SEM images of worn surfaces of (a) Homogenized and ECAP processed (b) 1P, (c) 2P, and (d) 4P samples under 30 N load with sliding distance 5000 m	86
Figure 5.16	SEM images of worn surfaces of (a) Homogenized and ECAP processed (b) 1P, (c) 2P, and (d) 4P samples under 40 N load with sliding distance 5000 m	86
Figure 5.17	EDS analysis for (a) Homogenized and (b) ECAP processed 2P sample under 30 N load	87
Figure 5.18	EDS analysis for (a) Homogenized and (b) ECAP processed 2P	87

sample under 40 N load

Figure 5.19	Electrochemical potentiodynamic polarization plots of unprocessed and ECAP processed samples	89
Figure 5.20	Nyquist plots of unprocessed and ECAP processed samples	90
Figure 5.21	R_t verses number of ECAP passes	91
Figure 5.22	XRD of ECAP processed 3 pass corrosion sample	92
Figure 5.23	SEM images of corrosion samples for different ECAP passes	93
Figure 5.24	SEM images of immersed samples (a) as-cast (b) homogenized and ECAP processed (c) 1P, (d) 2P, (e) 3P, and (f) 4P samples	94
Figure 5.25	SEM images with EDS and elemental mapping of ECAP 3P sample	94
Figure 6.1	Optical micrographs of (a) as-cast (b) homogenized and ECAP (c) 1P, (d) 2P, (e) 3P and (f) 4P samples	98
Figure 6.2	SEM images of (a) As-cast (b) Homogenized and ECAP (c) 1P (d) 2P (e) 3P and (f) 4P samples	99
Figure 6.3	Grain size of as-cast, homogenized and ECAP processed samples	100
Figure 6.4	TEM micrographs of ECAP 4 pass sample	100
Figure 6.5	OIM micrographs with IPF image (a) as-cast and (b) ECAP 4 pass samples	101
Figure 6.6	Misorientation angle grain distribution of (a) as-cast and (b) ECAP 4 pass sample	101
Figure 6.7	XRD profile of (a) as-cast, (b) ECAP 2 pass and (c) ECAP 4 pass samples	103
Figure 6.8	Tensile properties of initial condition and ECAP processed samples	104
Figure 6.9	Vickers microhardness values of homogenized and ECAP processed samples	106
Figure 6.10	SEM micrographs of fractured surfaces (a) as-cast (b) homogenized and ECAP (c) 1P (d) 2P (e) 3P and (f) 4P samples	107
Figure 6.11	COF curves for samples under 30 N and 40 N load with sliding distance (a) 2500 m and (b) 5000 m	107

Figure 6.12	Wear mass loss versus number of ECAP passes	108
Figure 6.13	SEM images of worn surfaces of (a) Homogenized and ECAP processed (b) 1P, (c) 2P, and (d) 4P samples under 30 N load with sliding distance 2500 m	109
Figure 6.14	SEM images of worn surfaces of (a) Homogenized and ECAP processed (b) 1P, (c) 2P, and (d) 4P samples under 40 N load with sliding distance 2500 m	109
Figure 6.15	SEM images of worn surfaces of (a) Homogenized and ECAP processed (b) 1P, (c) 2P, and (d) 4P samples under 30 N load with sliding distance 5000 m	110
Figure 6.16	SEM images of worn surfaces of (a) Homogenized and ECAP processed (b) 1P, (c) 2P, and (d) 4P samples under 40 N load with sliding distance 5000 m	110
Figure 6.17	EDS analysis for (a) Homogenized and (b) ECAP processed 2P sample under 30 N load	111
Figure 6.18	EDS analysis for (a) Homogenized and (b) ECAP processed 2P sample under 40 N load	112
Figure 6.19	Electrochemical potentiodynamic polarization plots of unprocessed and ECAP processed samples	113
Figure 6.20	Nyquist plots of unprocessed and ECAP processed samples	115
Figure 6.21	R_t verses number of ECAP passes	115
Figure 6.22	XRD of ECAP processed 3 pass corrosion sample	116
Figure 6.23	SEM images of corrosion samples for different ECAP passes	117
Figure 6.24	SEM images of immersed samples (a) as-cast (b) homogenized and ECAP processed (c) 1P, (d) 2P, (e) 3P, and (f) 4P samples	118
Figure 6.25	SEM images with EDS and elemental mapping of ECAP 3P sample	118

LIST OF TABLES

Table No.	Description	Page No.
Table 3.1	Nominal compositions of AM series magnesium alloys	35
Table 4.1	Mechanical properties of AM70 alloy processed by ECAP up to 4 passes	55
Table 4.2	Electrochemical kinetic parameters like corrosion potential, corrosion current density, Tafel slopes (β_a & β_c) and corrosion rate (mm/y)	65
Table 4.3	Fitted R_t values for unprocessed and ECAP processed sample	68
Table 4.4	Corrosion rate of immersed samples verses number of ECAP passes	70
Table 5.1	Mechanical properties of AM80 alloy processed by ECAP up to 4 passes	81
Table 5.2	Electrochemical kinetic parameters like corrosion potential, corrosion current density, Tafel slopes (β_a & β_c) and corrosion rate (mm/y)	89
Table 5.3	Fitted R_t values for unprocessed and ECAP processed sample	92
Table 5.4	Corrosion rate of immersed samples verses number of ECAP passes	93
Table 6.1	Mechanical properties of AM90 alloy processed by ECAP up to 4 passes	105
Table 6.2	Electrochemical kinetic parameters like corrosion potential, corrosion current density, Tafel slopes (β_a & β_c) and corrosion rate (mm/y)	114
Table 6.3	Fitted R_t values for unprocessed and ECAP processed sample	116
Table 6.4	Corrosion rate of immersed samples verses number of ECAP passes	117

NOMENCLATURE

ECAP	: Equal Channel Angular Pressing
SPD	: Severe Plastic Deformation
UFG	: Ultrafine grain
HCP	: Hexagonal Closed Pack
CGP	: Constrained Groove Pressing
ARB	: Accumulative Roll Bonding
HPT	: High Pressure Torsion
RCS	: Repetitive Corrugation and Straightening
HPTE	: High Pressure Torsion Extrusion
CEC	: Cyclic Extrusion Compression
ATB	: Accumulative Torsion Back
STS	: Severe Torsion Straining
CCDF	: Cyclic Closed-Die Forging
SSMR	: Super Short Multi-pass Rolling
AM	: Aluminium-Manganese
HDS	: Hot Die Steel
EDS	: Energy Dispersive X-ray Spectroscopy
UTM	: Universal Testing Machine
OM	: Optical Microscopy
SEM	: Scanning Electron Microscopy
FE-SEM	: Field Emission Scanning Electron Microscope
TEM	: Transmission Electron Microscopy
XRD	: X-ray Diffraction
EBSD	: Electron Back-Scatter Diffraction
OIM	: Orientation Imaging Microscopy
IPF	: Inverse Pole Figure

LAGB	: Low Angle Grain Boundaries
HAGB	: High Angle Grain Boundaries
SAED	: Selected Area Electron Diffraction
ASTM	: American Society for Testing and Materials
DRX	: Dynamic Recrystallization
UTS	: Ultimate Tensile Strength
YS	: Yield Strength
SCE	: Saturated Calomel Electrode
EIS	: Electrochemical Impedance Spectroscopy

SYMBOLS

Φ	: Die channel angle
Ψ	: Outer arc of curvature
ϵ_N	: Equivalent strain
σ	: Yield stress
σ_o	: Friction stress
k	: Locking parameter
d	: Grain size
\emptyset	: Diameter
Hv	: Vickers microhardness
ρ	: Metal density
ΔW	: Weight loss rate
V_H	: Hydrogen evolution rate
P_H	: Corrosion rate
E_{corr}	: Corrosion potential
I_{corr}	: Corrosion current density
β_a	: Anodic constant
β_c	: Cathodic constant

CHAPTER 1

INTRODUCTION

1.1 Background

Now-a-days, selection of material for engineering applications is a great challenge which has to satisfy all engineering requirements in terms of low density, low cost and high specific strength. Requirement towards lighter and stronger materials for aerospace and automotive industry led to the development of advanced materials. Lighter the material, lesser is the strength and is a major drawback in the field of aerospace and automotive industries. Industries are aiming for the materials with reduced weight and energy saving in the field of construction, aerospace and electrical industries.

Magnesium and its alloys are considered as structural metallic materials in the 21st century due to their properties like low density, good castability, high specific strength, good recyclability and reasonable cost. They have great potentials for industrial applications in the field of transportation or automotive and aerospace (Kojima, 2000; Valiev et al. 2006). Superior specific stiffness and strength of Mg alloys are of prime concern in automotive industries to reduce vehicle weight and hence fuel consumption (Mordike and Ebert, 2001). Magnesium is the lightest structural metal and it is one third lighter by weight than aluminum and hence gives higher specific strength and stiffness than any of the other common structural metals. Magnesium alloys has a hexagonal close-packed (HCP) crystal structure, which affects the fundamental properties of these alloys. Plastic deformation of the hexagonal lattice is more complicated than in cubic lattice structured metals like aluminum, copper and Iron. Therefore, magnesium alloys are typically used as cast alloys. However, as a consequence of their HCP structure, magnesium alloys have principally been fabricated, not by plastic forming, but by casting. Improvement in the workability and strength of magnesium alloys is required for expanding their applications in automotive engineering. Despite these advantages, they have few limitations in industrial applications because the formability of magnesium alloys at

room temperature is rather poor due to their hexagonal closed packed (HCP) structure with limited slip systems which causes poor ductility. To overcome the above limitations over the past few decades, researchers have developed severe plastic deformation (SPD) techniques. SPD is one of the methods of obtaining very fine crystalline structure in different bulk metals and alloys, which possess different crystallographic structure. SPD is a technique where large strains are induced into the material in order to achieve remarkable grain refinement to the sub-micrometer or nanometer range. The structural changes caused by SPD are reflected in improved mechanical properties of metals, which includes increased hardness and yield stress. Yet, the drawback of ultrafine grained structure materials is their limited ductility.

1.2 SPD techniques

Two approaches are used to produce bulk nanostructured / ultra-fine grained (grain size is less than 1 μm) metallic materials. The first is top-down approach, where the existing coarse-grained materials are processed to produce ultrafine grained or nanostructured material. The second is bottom-up approach in which nanostructured materials are assembled from individual atoms, molecules or nanoscale building blocks such as nanoparticles. Top-down method includes Equal Channel Angular Pressing/Extrusion (ECAP/E) (Valiev et al. 2006), Accumulative Roll Bonding (ARB) (del Valle et al. 2005), Accumulative Back Extrusion (ABE) (Fatemi-Varzaneh and Zarei-Hanzaki, 2009), High Pressure Torsion (HPT) (Sakai et al. 2005), Cyclic Extrusion Compression (CEC) (Chen et al. 2008), Friction stir processing (FSP) (Darras et al. 2007), Twist extrusion (Beygelzimer et al. 2009), Reciprocating extrusion (Lee et al. 2007), Repetitive Corrugation and Straightening (RCS) (Rajinikanth et al. (2008)), Severe torsion straining (STS) (Nakamura et al. 2004), Cylinder covered compression (CCC) (Xin et al. 2007), Submerged friction stir processing (SFSP) (Hofmann and Vecchio, 2005), Constrained groove pressing (CGP) (Shin et al. 2002) and Repetitive upsetting (RU) (Guo et al. 2012).

ECAP is considered to be an attractive SPD technique, being capable of producing ultrafine-grained bulk materials and having potentials for scale-up and mass production (Kim and Kim, 2004). Grain refinement by severe plastic deformation (SPD), particularly by equal channel angular pressing (ECAP) has become an

efficient and effective way for improving mechanical behavior of materials. Accordingly, significant efforts are made to develop Mg alloys with ultra-fine grains of size varying between 100 nm to 1000 nm. Since the pioneering work of Hall and Petch, materials engineers and scientists have been attracted by materials with small grain sizes. Finer grain size increases strength of the material and provides the potential for super plastic deformation at moderate temperatures and high strain rates (Verlinden, 2005). Strength of the metals and alloys increase with decrease in grain size of the material at low temperatures and weakens at high temperature (Azushima et al. 2008) and it was explained by the Hall-Petch equation (1.1) (Hall, 1951; Petch, 1953; George E. Dieter, 1988),

$$\sigma = \sigma_o + \frac{k}{\sqrt{d}} \dots\dots\dots(1.1)$$

Where,

σ = Yield stress (MPa)

σ_o = “Friction stress” representing the overall resistance of the crystal lattice to dislocation movement (MPa)

k = “Locking parameter”, which measures the relative hardening contribution of the grain boundaries

d = Grain size (μm)

Ultra-fine grained materials are those materials which possess homogeneous and equiaxed grain structure with average grain size less than 1 μm and most of the grains are in high angle of misorientation. LAGB are those which consist of misorientation less than 15 degrees and HAGB with misorientation greater than 15 degrees. Even though magnesium possesses better properties there are some limitations like wear and corrosion which hinders the usage of magnesium in many applications (Hoche et al. 2005; Wang et al. 2003). Wear resistance can be improved to increase the application of magnesium alloys for movable parts, which helps in reduction of fuel consumption and emissions (Majumdar et al. 2003; Zhang et al. 2008). Wear resistance can be improved by strengthening the material by grain refinement (El Aal et al. 2010). In general, wear leads to loss of material and increase in clearance in moving parts (Wang et al. 2011). Improvement in wear and corrosion properties is necessary because in real time application, the components of magnesium alloy may

be subjected to impact and load application where there will be loss of material. Also, they may be exposed to some extremely reactive corrosive environments, which leads to high level of corrosion because magnesium is more prone to corrosion. Therefore, it is important to study the wear and corrosion behavior of this material and its applications can be expanded in different areas.

The fastest growing application for magnesium is the high pressure die casting for automotive components. AM series magnesium alloys which is widely used for die-casting and automobile parts such as seat frame, instrument panels, stirring frame door inner etc, because of their better damping capacity and elongation properties. They have better toughness, impact absorption properties, better noise and vibration dampening characteristics than aluminium and excellent castability (Watanabe et al. 2010). AM alloys are extensively used magnesium alloys due to their excellent combination of strength and ductility. Aluminium and manganese are the major alloying elements, where Al improves strength and hardness of the material and addition of Mn improves the corrosion resistance by removing iron and other heavy metal elements (Avedessian and Baker, 1999).

In spite of various applications of AM series magnesium alloy, limited work has been done to improve the physical and mechanical properties of AM series magnesium cast alloys and studies on wear and corrosion behavior of magnesium alloys is limited. Since AM series magnesium alloys possesses better damping, elongation, and impact absorption properties, we may further improve these properties by using ECAP so that its application can be expanded in different areas of engineering.

Present Work

AM (Aluminium-Manganese) series magnesium alloys were processed by ECAP and various studies on microstructural changes and mechanical properties has been made. Further, mechanical properties are correlated with the microstructure and the results are discussed under various section of the thesis. Dry sliding pin-on-disc wear test was performed to study the wear behavior of ECAP processed samples compared to initial condition (as-cast and homogenized). Electrochemical measurements and immersion test were conducted to investigate the corrosion behavior of ECAP processed samples in comparison to unprocessed condition.

CHAPTER 2

LITERATURE REVIEW

Literature review gives brief discussion on different severe plastic deformation (SPD) techniques used for fabricating ultra-fine grained material and introduction to magnesium and magnesium alloy. SPD techniques are discussed with the available literature and the motivation followed by objectives of the present work has been derived. It also includes the literature of the SPD processed materials with respect to microstructure, mechanical, wear and corrosion properties. SPD produces fine crystalline structure in different bulk materials. Strains are induced to attain grain refinement in the material. Microstructural changes caused by SPD increases the material properties like increased hardness and yield stress but poor ductility. Coarse-grained materials are converted to ultra-fine grain by imposing high strain into the material to introduce dislocations and are re-assembled to form a group of grain boundaries. Few conventional metal working processes like rolling or extrusion are restricted to produce ultra-fine grain (UFG) structures due to some reasons like firstly, due to the limitation of imposing strains into the material because this processes causes reduction in the cross-sectional area of the specimen. Secondly, the imposed strains are not sufficient to produce UFG materials due to low workability at lower temperature conditions (Valiev et al. 2000).

2.1 Severe plastic deformation (SPD)

Severe plastic deformation is a process where material is highly strained without any change in dimension of the specimen resulting in ultra-fine grained materials (Lowe and Valiev 2004). Few SPD techniques include constrained groove pressing (CGP) (Shin et al. 2002; Yadav et al. 2016), equal channel angular pressing (ECAP) (Furukawa et al. 2001; Valiev et al. 2006; Surendarnath et al. 2014), repetitive corrugation and straightening (RCS) (Zhu et al. 2001; Sunil, 2015), high pressure torsion (HPT) (Zhilyaev and Langdon 2008; Choi et al. 2015; Huot 2016), torsion extrusion (Jahedi and Paydar 2010; Khosravifard et al. 2012), high pressure torsion

extrusion (HPTE) (Ivanisenko et al. 2016), cyclic extrusion compression (CEC) (Lin et al. 2009; Huang et al. 2015; Tian et al. 2015), compression and backward extrusion (Jung et al. 2014), accumulative torsion back (ATB) (Faraji and Jafarzadeh 2012), severe torsion straining (STS) (Nakamura et al. 2004), cyclic closed-die forging (CCDF) (Liao et al. 2015; Guo et al. 2017), accumulative roll-bonding (ARB) (Saito et al. 1999; Raei et al. 2011; Yu et al. 2014) and super short multi-pass rolling (SSMR) (Eto et al. 2006; Etou et al. 2008) etc. and among these few SPD techniques are discussed in this chapter.

2.1.1 Constrained groove pressing (CGP)

CGP process is carried out as shown in figure 2.1. Die consists of asymmetrically grooved plates which are constrained by cylinder wall. When pressing is carried out between the upper plate and the lower plate, the inclined portion of the specimen undergoes shear deformation with plane strain condition. But, there is no deformation in the flat region. During next press, flat plates were used and the initial deformed areas were exposed for reverse deformation whereas the initial region which was undeformed during first pass stays undeformed or unchanged. With further pressing, sample is rotated by 180° and the undeformed region will be deformed because of the asymmetry of the grooved die. By this homogeneous strain will be achieved and by repeating the procedure very high plastic strain can be induced in the sample with no change in specimen dimensions.

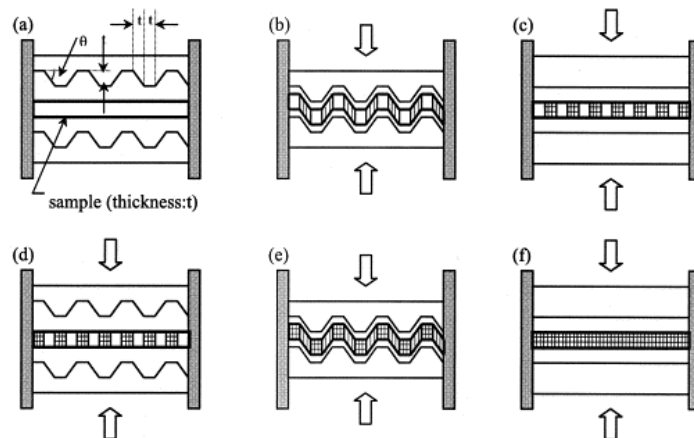


Figure 2.1 Constrained groove pressing (Shin et al. 2002)

2.1.2 Repetitive corrugation and straightening (RCS)

RCS is a process where sample is continuously subjected to bending and straightening without major change in dimension of the sample and high strains are induced which results in grain refinement. It consists of corrugated rolls for bending the sample during first stage and flat rolls for straightening the sample during second stage as shown in figure 2.2.

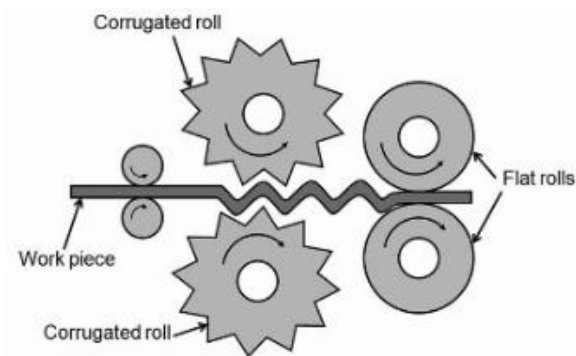


Figure 2.2 Repetitive corrugation and straightening (Sunil et al. 2015)

2.1.3 High pressure torsion (HPT)

HPT process was initially investigated by Bridgman and the schematic is as shown in figure 2.3. Samples are prepared in disk form and are located between the anvils and compressive pressure is applied on the disk at room temperature. Along with pressure, torsional strain is also applied through the lower anvil. Frictional forces on the surface causes the deformation to take place with quasi-hydrostatic pressure.

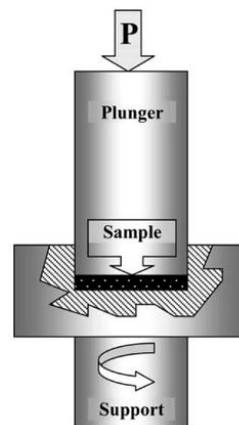


Figure 2.3 High pressure torsion (Zhilyaev and Langdon 2008)

2.1.4 Cyclic extrusion compression (CEC)

CEC process is shown in figure 2.4. Sample is allowed to pass through the cylindrical chamber of diameter D using ram A into other cylindrical chamber passing through diameter d as shown in figure 2.4. Similarly ram or plunger B is used to press the sample back to initial cylindrical chamber. The process continues and large strains are induced into the material and grain refinement occurs and during final extrusion process, ram B is removed to release the processed sample from the chamber.

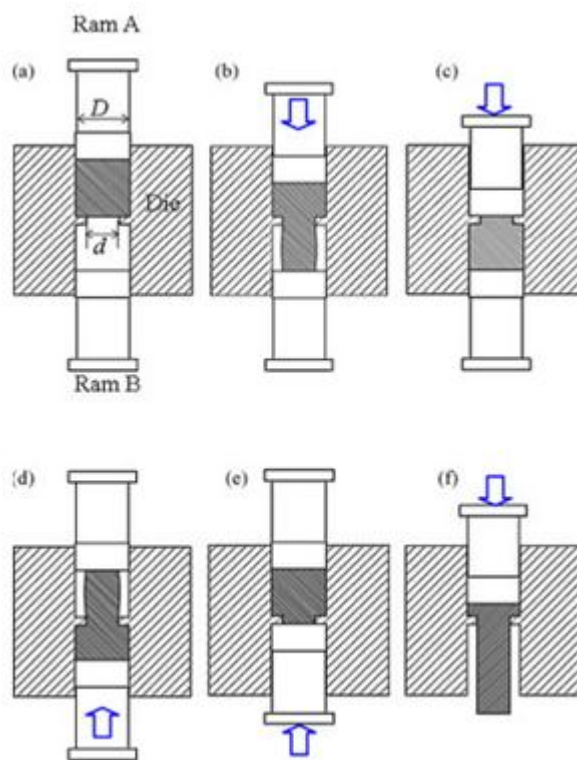


Figure 2.4 Cyclic extrusion compression (Lin et al. 2009)

2.1.5 Accumulative roll-bonding (ARB)

ARB technique uses rollers to deform the material and is shown in figure 2.5. Accumulative roll bonding is an extension of the conventional rolling process to succeed ultra-fine grains and to improve mechanical properties. ARB was initially developed by Saito et al. (1999) and includes surface treatment of two sheets of materials followed by stacking and roll bonding. Then the rolled sheets are again separated by cutting them and stacked and the process continues and the same thickness is maintained as the initial one,

but high strain will be induced in the processed sheet which contains grain-refined microstructure that improves the properties of the material.

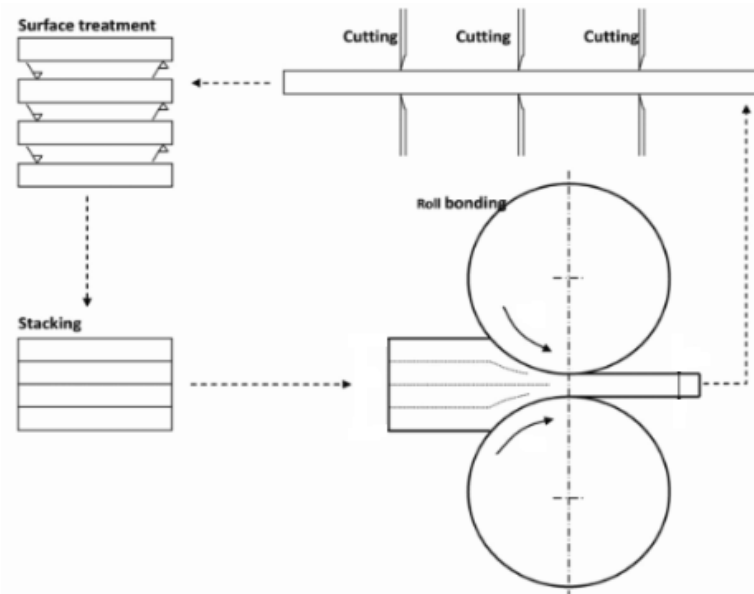


Figure 2.5 Accumulative roll-bonding (Yu et al. 2014)

2.1.6 Equal channel angular pressing (ECAP)

ECAP was proposed by Segal in the year 1977 and it is a process where high plastic strains are introduced in a material with no change in cross-section dimension of the specimen. During ECAP, simple shear process takes place when sample passes through the channel. ECAP is one of the simplest SPD process as it requires lower force and tool pressure. ECAP is found as an appropriate tool to examine the relation between the imposed strain and the microstructural development. Moreover, the grain size is to be reduced to improve the material properties such as tensile strength, ductility, and formability, as the structural material is used in many industrial applications. ECAP process is carried out by pressing a sample through a metal die consisting of two channels at die angle (Φ) and outer arc of curvature (Ψ). ECAP processed samples that emerge out from the die will possess the same cross-sectional dimensions similar to unprocessed sample condition. Repetitive pressings need to be conducted to impose high strains into the material. The total strain in the sample is calculated by using equation 2.1 (Azushima et al. 2008) for one pass and the total strain for 'n' number of passes is given by $n \times \epsilon$.

$$\varepsilon = \frac{1}{\sqrt{3}} \left\{ 2 \cot \left(\frac{\phi}{2} + \frac{\psi}{2} \right) + \psi \operatorname{cosec} \left(\frac{\phi}{2} + \frac{\psi}{2} \right) \right\} \dots\dots\dots (2.1)$$

Where, ε implies strain, Φ represents die angle, Ψ denotes outer arc of curvature.

2.2 ECAP setup

ECAP die is a split die which consists of polished metal plates of equal dimension which are joined using bolts. Channels are fabricated and designed for the required channel angle (Φ) and outer arc of curvature (Ψ). These dies can be used for laboratory work and proper care to be taken while tightening the die bolts during each pass of the specimen. Molybdenum disulfide (MoS_2) can be used to avoid the frictional losses between die and specimen (Valiev et al. 2006). Schematic of ECAP die is shown in figure 2.6.

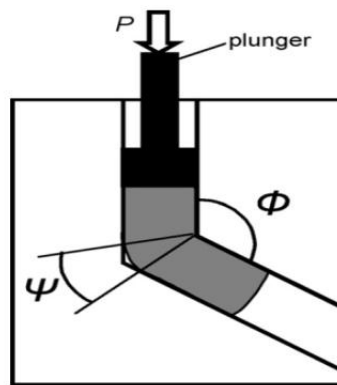


Figure 2.6 Schematic of ECAP setup (Azushima et al. 2008)

2.3 Basic parameters in ECAP

ECAP is characterized by numerous parameters and these parameters play an important role in influencing the properties of ultra-fine grained material.

- Imposed strain in ECAP and different die angles
- Processing routes and slip systems
- Effect of pressing speed
- Effect of pressing temperature
- Effect of back-pressure

2.3.1 Imposed Strain in ECAP and different die angles

Large strains are imposed in the material by ECAP process (Valiev et al. 2006). Strain can be measured by analytical method with different die patterns as represented in figure 2.7, where Φ represents the channel angle and Ψ is outer arc of curvature and intersection takes place between the two. Figure 2.7 shows three situations where $\Psi = 0^\circ$, $\Psi = (\pi - \Phi)^\circ$ and $0^\circ < \Psi < (\pi - \Phi)^\circ$. Frictional losses can be neglected by considering the sample as a lubricated specimen. A square element named as abcd, passes via channel and the theoretical shear plane and gets distorted as labelled a'b'c'd'. It may be shown from the shear strain and γ is represented as,

$$\gamma = 2 \cot\left(\frac{\Phi}{2}\right) \dots\dots\dots (2.2)$$

For Fig.2.3 (b), it gives

$$\gamma = \Psi \dots\dots\dots (2.3)$$

and similarly for Fig.2.3 (c),

$$\gamma = 2 \cot\left(\frac{\Phi}{2} + \frac{\Psi}{2}\right) + \psi \operatorname{cosec}\left(\frac{\Phi}{2} + \frac{\Psi}{2}\right) \dots\dots\dots (2.4)$$

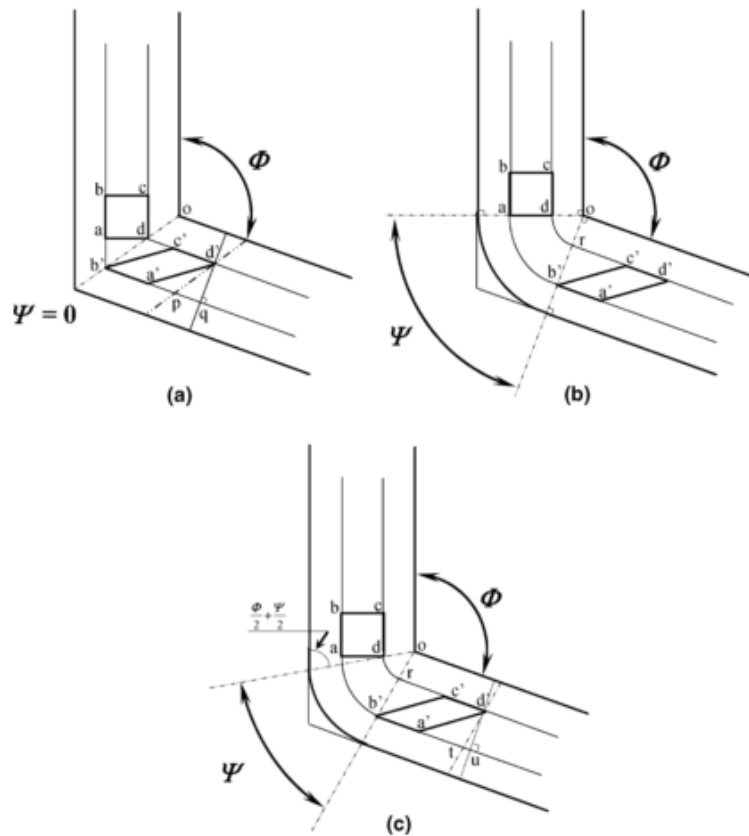


Figure 2.7 Principles of ECAP pressing (Iwahashi et al. 1996)

Finally the equivalent strain for N number of passes,

$$\epsilon_N = \frac{N}{\sqrt{3}} \left[2 \cot \left(\frac{\Phi}{2} + \frac{\Psi}{2} \right) + \psi \operatorname{cosec} \left(\frac{\Phi}{2} + \frac{\Psi}{2} \right) \right] \dots \dots \dots (2.5)$$

For different channel angle (Φ) and outer arc of curvature (Ψ), the variation in equivalent strain is represented in figure 2.8.

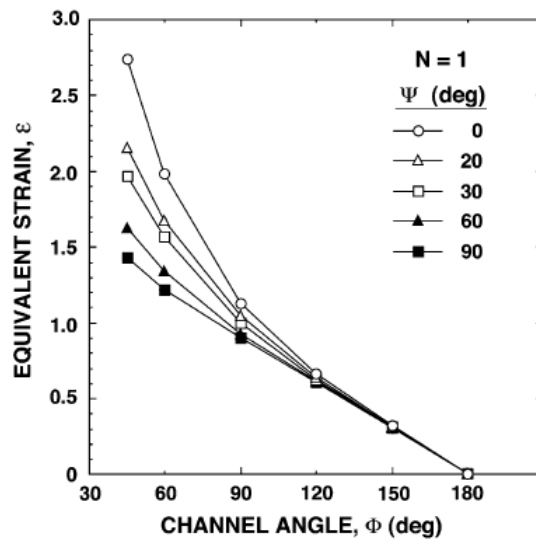


Figure 2.8 Various equivalent strain values for different channel angle and outer arc of curvature (Furuno et al. 2004)

2.3.2 Processing routes and slip systems

There are four processing routes which are shown in figure 2.9. In route A, the sample is pressed using plunger without rotating the sample. In route B_A, the sample will be rotated by 90° in alternate directions during the successive passes.

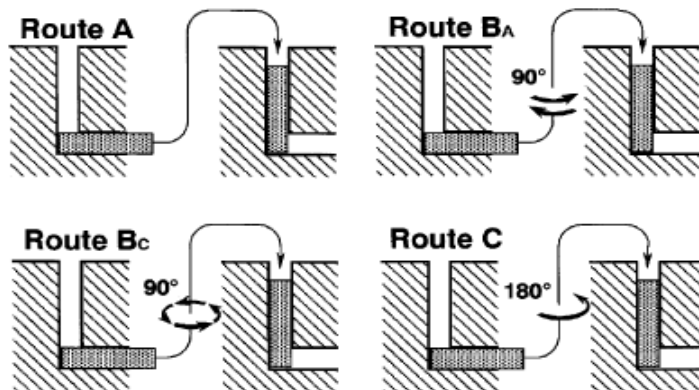


Figure 2.9 Four fundamental processing routes (Djavanroodi and Ebrahimi, 2010)

In routes B_C, the sample is made to rotate by 90° in the same direction either clockwise or anti-clockwise during each pass and during route C, the sample is allowed to rotate by 180° during consecutive passes. The slip systems which are connected with different routes x, y and z planes are the orthogonal planes are shown in figure 2.10. Numbers 1 to 4 represents ECAP passes. By using route C, continues shearing takes place on the same plane during consecutive pass but the shearing direction is reversed during each pass and the strain will be restored after each even number of passes. It is observed that route B_C is a redundant strain imposing process similar to route C, because slip taking place in 1st pass will be cancelled by slip taking place during the 3rd pass and slip during 2nd pass is cancelled by slip during 4th pass. It can be observed from figure that route A and route B_A are not redundant and possesses two distinct shear planes that intersects at 90° angle in route A and four different shear planes at 120° in route B_A (Valiev et al. 2006). The distortions and shearing patterns introduced into a cubic element on the x, y and z are show in figure 2.11 and 2.12.

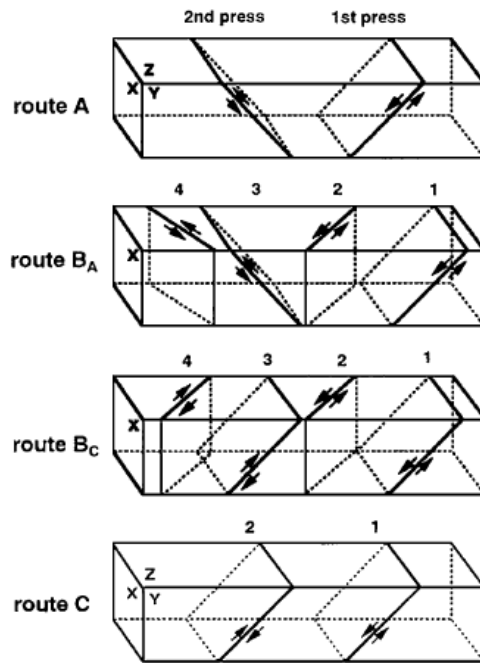


Figure 2.10 Slip systems for different routes and passes (Lee and Langdon, 1999)

Route	Plane	Number of pressings								
		0	1	2	3	4	5	6	7	8
A	X	□	□	▭	▭	▭	▭	▭	▭	▭
	Y	□	▭	▭	▭	▭	▭	▭	▭	▭
	Z	□	□	□	□	□	□	□	□	□
B _A	X	□	▭	▭	▭	▭	▭	▭	▭	▭
	Y	□	▭	▭	▭	▭	▭	▭	▭	▭
	Z	□	▭	▭	▭	▭	▭	▭	▭	▭
B _C	X	□	▭	▭	▭	▭	▭	▭	▭	▭
	Y	□	▭	▭	▭	▭	▭	▭	▭	▭
	Z	□	▭	▭	▭	▭	▭	▭	▭	▭
C	X	□	▭	▭	▭	▭	▭	▭	▭	▭
	Y	□	▭	▭	▭	▭	▭	▭	▭	▭
	Z	□	▭	▭	▭	▭	▭	▭	▭	▭

Figure 2.11 Distortions into the cubic elements on different planes (Furukawa et al. 1998)

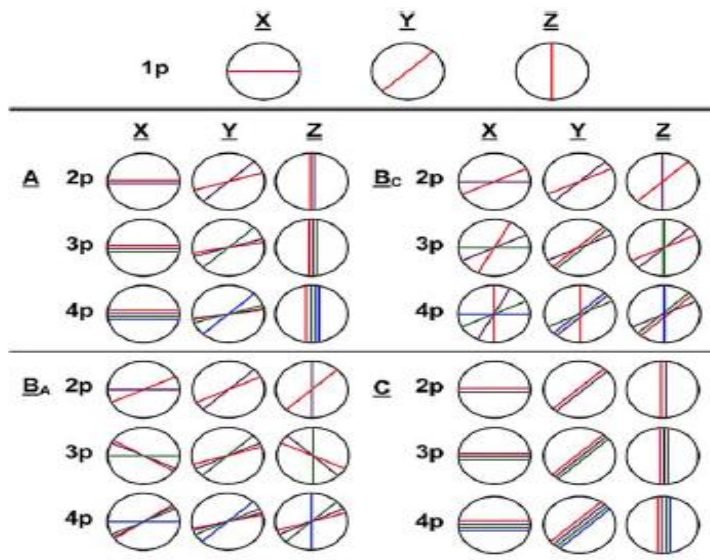


Figure 2.12 Shearing patterns on different planes for different processing routes with ECAP 1 (red), 2 (mauve), 3 (green) and 4 (blue) passes respectively (Furukawa et al. 2002)

2.3.3 Effect of pressing speed

ECAP process is carried out by hydraulic press that possesses relatively high ram speeds with a range of 1 to 20 mm/s. Some results have shown that the ram speed does not have much impact on the homogeneous size of the ultrafine grains produced by ECAP. Since recovery takes place easily when pressing is carried out at lower speeds and these slower speeds helps to produce homogeneous and uniform microstructures (Valiev et al. 2006).

2.3.4 Effect of pressing temperature

During ECAP, temperature plays a major factor and selection of temperature depends on the type of material. We have to monitor carefully to maintain the die temperature of ± 5 K during ECAP. By monitoring the die heating process, it was recognized that it took about 1 hour to get the required die temperature and 10 minutes for stabilization (Valiev et al. 2006). Grain size increases with increase in pressing temperature and grain refinement took place with variation in temperatures, but transition of high angle grain boundaries to low angle grain boundaries 473 K in pure Al and at temperature 573 K for Al-3% Mg alloy and Al-3% Mg-0.2% Sc exhibited high angle grain boundaries at all temperatures during pressing (Yamashita et al. 2000). ECAP at lower temperature gives higher ultimate tensile strength (UTS) and ECAP at 150 °C, AM60 alloy reported the highest UTS of 310 MPa and higher ductility was retained of about 15% (Kulyasova et al. 2009).

2.3.5 Effect of back-pressure

Researchers reported few ECAP designs provided with back-pressure facility which is system controlled as represented in figure 2.13 and 2.14. By imposing back-pressure, increase of workability was observed in processed samples. Few researchers reported that Cu was processed by ECAP without back-pressure and found that surface cracks appear on the processed specimen of 12 to 13 passes. With the application of back-pressure, ECAP processed samples showed no surface cracks after 16 or more number of passes (Valiev et al. 2006).

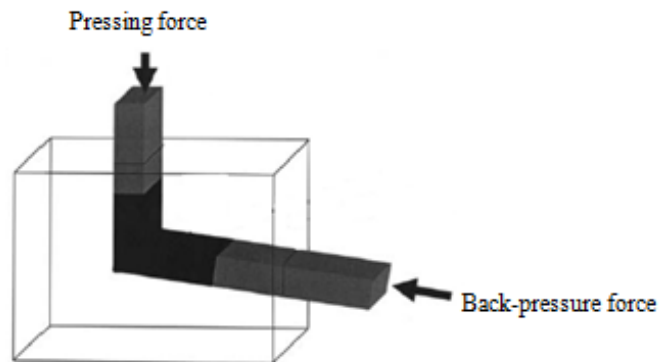


Figure 2.13 Illustration of the ECAP die with pressing force and back-pressure force (Valiev et al. 2006)

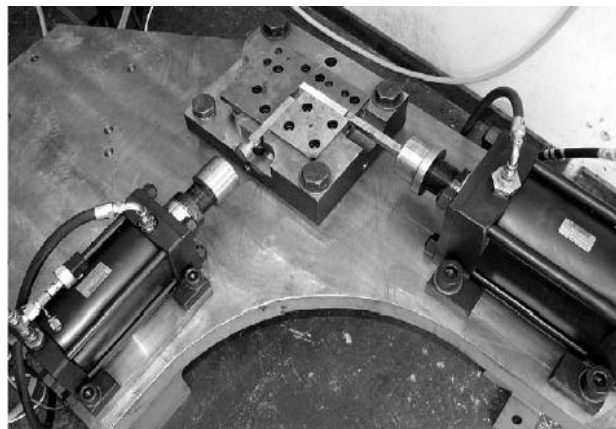


Figure 2.14 Equipment with computer controlled back-pressure (Stolyarov et al. 2003)

One more advantage is homogeneity of material flow during the ECAP process. During ECAP process, dead zone will be created due to improper filling of the outer angle of the ECAP die in case of strain-hardenable materials and also uniformity in microstructure is not achieved during grain refinement particularly at the bottom area of the specimen. With the application of back-pressure, the formation of dead zones are avoided and more grain refinement can be achieved in less number of passes (Valiev et al. 2006).

2.4 Advantages and limitations of ECAP

Advantages of ECAP process in comparison to other SPD processes (R.Z Valiev et al. 2006; Figueiredo and Langdon, 2009; Zrnik et al. 2008):

- Easy method to induce high strain into the work material by shear deformation
- Grain size reduces with increase in number of ECAP passes and increment in yield strength was achieved
- Used to produce large billets
- High pressure not required during ECAP process and it is advantageous in avoiding damage to machine and tools
- Preferred technique to develop the material properties with both hot and cold working
- Flexibility of the material was improved effectively in the ECAP process.

Few limitations of ECAP process are (Raab et al. 2004):

- Length of the specimen is limited i.e., the aspect ratio (length to diameter) should be smaller to avoid bending of the specimen while pressing.
- The ram or plunger has a restricted travel distance and this makes the ECAP process a discontinuous process which leads to lower production efficiency.
- Ends of the specimen exhibits non-uniform microstructure and also macro cracks leads to wastage of material.

2.5 Magnesium alloys and their properties

Magnesium is the lightest structural metal with a specific density of about 1.74 g/cm^3 and one third lighter in weight compared to aluminium and hence gives higher specific strength and stiffness than any of the other common structural metals. Magnesium alloys usually consists of aluminium, zirconium, rare-earths, manganese, zinc, silicon and copper. Mg alloys has a hexagonal close-packed (HCP) crystal structure, which affects the material properties and the plastic deformation of the HCP lattice is more complex than cubic metals like aluminium, steel and copper. So magnesium alloys are normally used as cast alloys and research on wrought alloys has been increased widely later by 2003. Cast alloys components used in modern cars and engine blocks made of magnesium has been used in high-performance

automobiles and also to build camera bodies and lense components. Alloying elements like aluminium, zinc, thorium and zirconium support in precipitation hardening. Manganese has less effect on tensile strength properties but slightly increases the yield strength of the material. Manganese improves the corrosion resistance properties of Mg-Al based alloys by eliminating iron and other heavy-metal elements and it is recommended to use manganese of about 0.4 % as per ASTM B93-94a (Luo and Sachdev, 2007).

Magnesium and its alloys are matched for the automotive applications due to their light weight which leads to good fuel economy which are very much essential in automotive industries. New material will be selected based on technical requirements of components manufacturing and also it should be economical. (Aghion et al. 2003).

Figure 2.15 represents the magnesium-aluminium phase diagram.

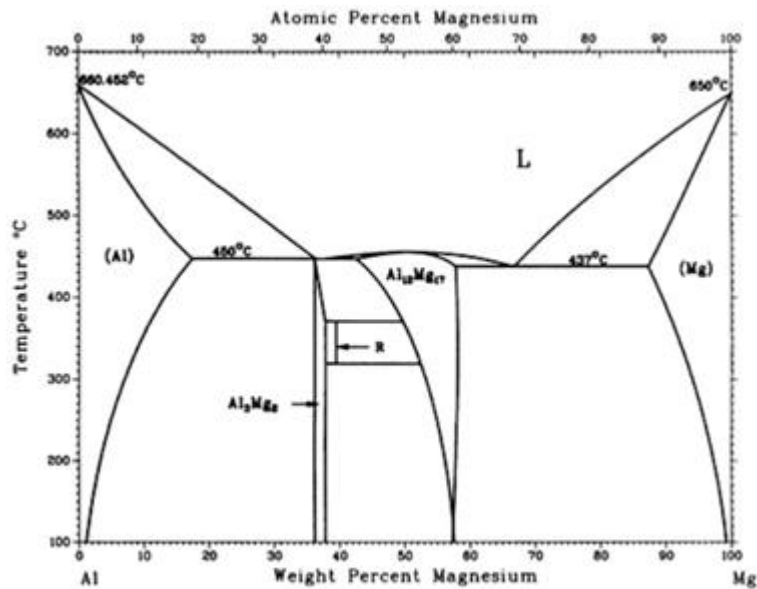


Figure 2.15 Phase diagram for magnesium-aluminium alloy system (ASM Handbook Vol. 3, 1992)

Some of the properties and applications of magnesium and its alloys are:

- Possess good impact resistant and damping capacity and it is more operational in high-speed automobiles
- Because of light weight and superior machinability properties, they are used in the manufacture of auto parts, aerospace equipment, fixtures, and other material handling equipment

- Used in automotive applications like gearboxes, alloy wheels, brake pedal brackets, valve covers, camera cases and clutch housings and few are shown in figure 2.16.
- Production of magnesium alloys by high-pressure die casting and gravity casting and it is the leading method of casting which provides high efficiency at lower cost

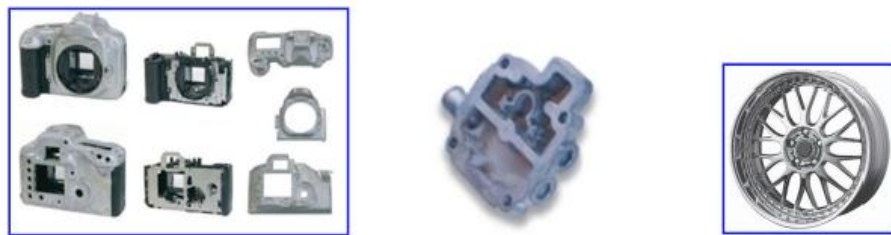


Figure 2.16 Applications of magnesium alloys

2.5.1 Drawback of magnesium alloys

Magnesium lies in some poor properties such as limited ductility, formability, stiffness and corrosion resistance. Some of the disadvantages of magnesium and its alloys are:

- low elastic modulus
- low toughness
- limited cold workability
- reduced strength and creep resistance at higher temperatures
- more prone to chemical reaction
- high degree of shrinkage on solidification
- reduced corrosion resistance

Due to HCP crystal structure, the ductility has been reduced and the solubility of alloying elements is limited, which restricts in improving the mechanical properties and chemical behavior of magnesium alloy. A reduced application of magnesium and its alloys in the older days resulted in limited research work. Few improved casting alloys are existing and fewer wrought alloys. Alloy development based on the

requirement of mechanical properties is as shown in figure 2.17 (Mordike and Ebert, 2001).

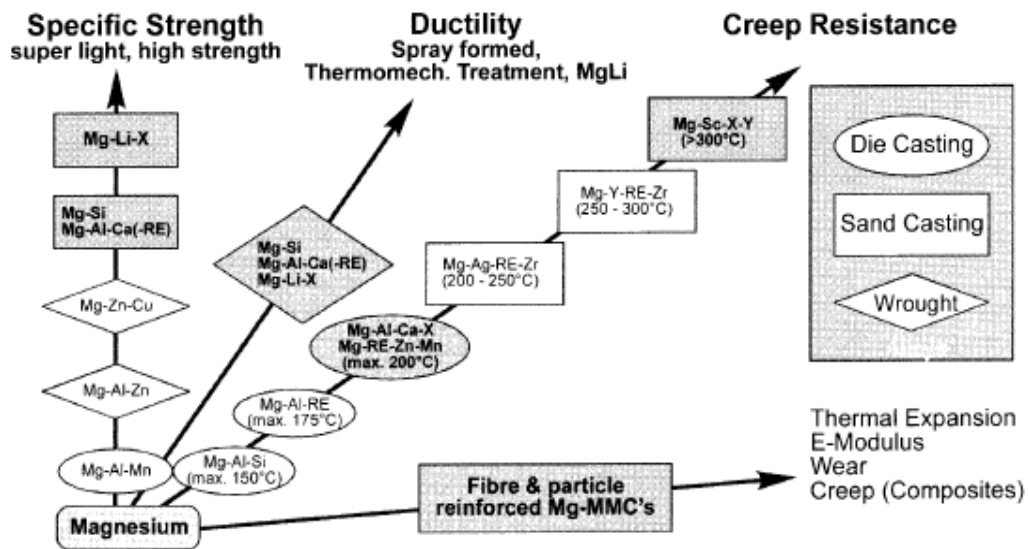


Figure 2.17 Alloy development (Mordike and Ebert, 2001)

2.5.2 Applications of AM series magnesium alloys

Available systems of magnesium alloys are Mg-Al-Zn-Mn (AZ), Mg-Al-Mn (AM), Mg-Al-Si (AS) and Mg-Al-rare earth (AE) series. Aluminium is the common alloying element for magnesium and addition of small amount of manganese improves corrosion resistance (Luo et al. 1995). AM series magnesium alloys possess good ductility, improved noise and vibration dampening characteristics compared to aluminium and excellent castability. Commercial magnesium alloys like AM60B and AM50A are widely used due to their good combination of physical and mechanical properties and excellent die castability, good corrosion resistance and economical. Most common die-casting magnesium alloys used AM series due to their improved elevated-temperature performance in specific areas like drive-train components such as intake manifolds, gearbox housing, transfer cases, oil pans and crankcases and also improved creep strength. Reduced creep strength in manufacturing of various housings may results in a clamping load reduction of bolted joints that causes poor bearing-housing contact which leads to oil leaks and increased vibration and noise (Aghion et al. 2003). AM series alloys have good damping properties in case of

impact and energy absorption requirements, high ductility magnesium alloys AM50 and AM60B are used. Die casting alloys AM60 used for production of automotive wheels and also other components that require good elongation and toughness with sound strength properties (Luo et al. 1995).

2.6 Strengthening mechanisms

Strengthening mechanisms are the ability to modify the mechanical properties of materials and can be used for different applications. Plastic deformation occurs due to the movement of dislocations and multiplies which results in macroscopic deformation. Mechanical properties (tensile and yield) are enhanced by introducing a mechanism which prohibit the movement of dislocations. Dislocation movements can be controlled by firstly, the interaction of stress fields with neighboring dislocations and solute particles. Secondly, the grain boundaries and secondary phase particles which acts as barrier. Few strengthening mechanisms (Dieter, 1988; Friedrich and Mordike, 2006) are:

2.6.1 Work hardening

Dislocations (Lavrentev, 1980) play a major role in work hardening and they interact with one another to generate stress fields with the material. These stress fields hinder the dislocation motion by attraction or repulsive interactions. If there is a crossing of two dislocations, it leads to occurrence of dislocation tangles, causing jog formation which oppose the movement of dislocation. These jogs and tangles act as pinning or jamming points which impede the dislocation movement. Dislocation density is related to yield strength and with increase in dislocation density the yield strength increases and causes shear stress to increase which are necessary to move the dislocations. The dislocation density cannot be increased infinitely as the material may lose its crystalline structure.

2.6.2 Solid solution strengthening and alloying

In this mechanism (Fleischer and Peckner, 1964), solute atoms of one element are added to another which resulted in either interstitial point defect within the crystal. These solute atoms are responsible for lattice distortions which obstruct the dislocation movement with increased yield stress. Stress fields are present around the

solute atoms which interact with these dislocations. These solute atoms impart tensile or compressive stresses to the lattice and depending on the solute size, they interfere with adjacent dislocations and causes solute atoms to behave as potential barriers. Yield strength increases with increased concentration of solute atoms and the amount of solute that can be added is limited. Solid solution strengthening mechanism generally depends on the solute atoms concentration, shear modulus, size, valency and the symmetry of solute stress field.

2.6.3 Precipitation hardening

Precipitation hardening was proposed by Gerold and Nabarro (1979). Most of the binary systems showed formation of secondary phases by increased alloy concentration limit and also with suitable mechanical treatment or heat treatment. Secondary phases behave as pinning points like solutes although they are not single atoms and dislocations may interact with the precipitate atoms in the following ways.

- Dislocations would cut through the precipitate atoms if the atoms are small and forms new surfaces
- If precipitate atoms are large, looping of the dislocations may occur resulting in the enlargement of dislocations. Therefore a critical radius of 30 nm may be selected by which the enlarged dislocations cut through the obstacle. Hence the dislocations freely loop or bow to overcome the hindrance.

2.6.4 Grain boundary (GB) strengthening

Grain size plays a major role on the properties of polycrystalline materials due to their varying crystallographic orientations. During plastic deformation, slip movement occurs and grain boundaries behave as a barrier to dislocation motion for reasons like (Callister and Rethwisch, 2011):

- Dislocation changes the direction of motion due to different grain orientations and
- Discontinuity of slip planes between one grain to another grain.

The required stress for dislocation movement from one grain to other, depends on the grain size in order to deform plastically. Dislocations per grain reduces with average

grain size and fewer dislocations per grain resulted in reduced dislocation pressure which are accumulated at grain boundaries, which makes dislocations difficult to move into adjacent grains and this relationship is explained by Hall-Petch equation (Dieter, 1988). Yield strength of the material increases with reduction in grain size and beyond a critical limit the grain size cannot be reduced. As the grain size decreases, lattice mismatch occurs because of the generation of free volume. Below 10 nm grain size, slide of grain boundaries occurs known as grain-boundary sliding. It is very difficult to fit the dislocations within the grain if the grain size gets too small and also the stress required to move them is less.

2.7 Literature on microstructure and mechanical properties

New processes have been introduced by many researchers to develop materials with better properties based on the requirement for industrial applications. Particularly ECAP processes carried out using different materials like aluminium, copper, magnesium and their alloys by varying the process parameters which makes results effective.

Iwahashi et al. (1997) witnessed that ECAP process on aluminum provides subsequent development of the microstructure by pressing the sample with or without rotation through 180°. Rotation of the samples during each pass is beneficial as it causes rapid elimination of the elongated grains and helps in the evolution of low angle grain boundaries (LAGB) into high angle grain boundaries (HAGB).

Komura et al. (2001) reported that grain size of aluminum alloy may be reduced from 200 μm to 0.2 μm using the process of ECAP and the obtained microstructure comprises of homogeneous arrangement of grains with HAGB. Maximum ductility can be obtained by processing through route B_C in which the samples are allowed to rotate by 90° in same direction during each pass within the ECAP die.

Matsubara et al. (2003) carried out ECAP at 473 K up to 2 passes and the grain refinement took place from an average of 50 μm to 12 μm after extrusion. An average grain size of 0.7 μm was achieved after extrusion and ECAP at 473 K. No much improvement in ductility was achieved after extrusion. Mg-9% Al alloy was also

processed by ECAP at a temperature of 573 K and it was found that it is not possible to achieve a sub micrometer grain size because of simultaneous grain growth at the above temperature.

Figueiredo and Langdon (2006) observed that grain size of extruded ZK60 magnesium alloy after ECAP was reduced to $\sim 0.8\mu\text{m}$. Superplastic ductilities were attained for a maximum temperature of 473 K with strain rate of $2.0 \times 10^{-4} \text{ s}^{-1}$. Homogeneity was checked by performing microhardness tests at different points in three perpendicular directions.

Miyahara et al. (2006) conducted ECAP on AZ61 alloy at 473 and 523 K and the average grain size was reduced to 0.6 and 1.3 μm , respectively for four passes. Maximum elongation was attained at 473K with a strain rate of $3.3 \times 10^{-4} \text{ s}^{-1}$. Elongation obtained for extruded condition was only 70% compared to ECAP processed sample.

Furui et al. (2007) reported that grain refinement was carried out in two stages, one is extrusion followed by ECAP on magnesium alloy. Average grain size obtained after extrusion was 3 to 10 μm and 1 to 7 μm after ECAP compared to average grain of 60 to 70 μm for as-cast condition. ECAP was conducted at lower temperature of 373 K with die channel angle of 135° .

Suwas et al. (2007) reported that pure magnesium can be deformed by ECAE at 250 $^\circ\text{C}$ by using routes A, B_C and C and every route forms characteristic texture. The textures showed the strain path and get sharpened with increase in ECAE passes. A heterogeneous grain size of 6-8 μm was attained by route B_C and C and few large grains of 20 μm were also observed but the samples processed through route A showed large portion of coarse grains.

Jiang et al. (2008) experimented Al-Mg-Mn alloy by using ECAP process at 350 $^\circ\text{C}$ up to 6 passes and fine-grained structure with grain size of 2 μm was obtained. Annealing was carried out at 400 $^\circ\text{C}$ for a period of 1 hr and no major grain growth occurred but large amount of LAGB was transformed into HAGB. Annealing continued at 450 $^\circ\text{C}$ for 1 hr and drastic grain growth occurred and fine-grained

microstructure was replaced by a coarse-grained microstructure with HAGB. With increase in annealing temperature, strength decreased which is due to the relaxation of internal stresses and also the grain growth.

Figueiredo and Langdon (2009) reported that grain refinement mechanism was different in f.c.c metals when compared to magnesium alloys which were processed by ECAP, because it mainly depends on the microstructure of the unprocessed alloy. Experiments showed that after ECAP 1 pass, homogeneous grain structure was obtained by using an alloy with an initial fine microstructure before processing and if the material possess initial coarse-grained structure then it forms heterogeneous grain structure after ECAP 1 pass.

Kulyasova et al. (2009) showed that ECAP of AM60 alloy produced microstructure with grain size down to $1\mu\text{m}$ at the lowest temperature ($150\text{ }^{\circ}\text{C}$) and also reported the highest UTS (310 MPa) and also retained the same ductility as that of the initial coarse-grained condition.

Ma et al. (2009) conducted multi-pass ECAP on ZE41A alloy and the grain size obtained after 32 passes is $1.5\ \mu\text{m}$ and it was due to dynamic recrystallization (DRX) during ECAP. This has led to homogeneous distribution of equiaxed grains. In 8 passes sample, microstructure showed a mixture of ultra-fined and also elongated coarse grains.

Masoudpanah and Mahmudi (2009) mentioned that ECAP processed AZ31 alloy showed improvements in strength and hardness properties with increase in number of ECAP passes with addition of RE and calcium. ECAP processed samples showed reduced yield stress because of the texture modification and increased tensile and ductility properties due to dispersive strengthening effects as compared to extruded samples.

Biswas et al. (2010) observed that a large plastic strain or deformation was induced by ECAP using route A in pure magnesium. Process was carried out by reducing the temperature step by step and the average grain size obtained was $\sim 250\ \text{nm}$. With slow reduction in the temperature, grain size decrease with increase in grain boundary area

which activated non-basal slip and increased the low-temperature workability. Hardness of the material increases with a reduction in the grain size following Hall-Petch relationship.

Ding et al. (2010) conducted ECAP up to 6 passes on ZE41 alloy and reduced grain size to an average of 2 μm . Yield strength obtained after ECAP 6 passes was 230 MPa and elongation of 20% compared to yield strength of initial condition samples of 160 MPa and 8% before ECAP process.

Masoudpanah and Mahmudi (2010) reported that strength obtained after ECAP of AZ31 is less compared to extruded AZ31 alloy at a temperature of 523 K because of texture softening during ECAP process but tensile and ductility was not affected. Presence of RE and Ca in AZ31 alloy after ECAP showed increased strength due to dispersive strengthening effects of the secondary particles and increased ductility due to fine grained microstructure.

Mohamed Ibrahim et al. (2011) observed that increase in ECAP passes and the imposed strain causes formation of UFG microstructure with HAGB misorientation angles for Al-Cu homogenized and non-homogenized alloys. Homogenized microstructures with reduced grain sizes with higher HAGB were obtained in case of homogenized alloys compared to non-homogenized alloys. This indicates that the homogenization process may help in quicker evolution to achieve the ultra-fine grain microstructure.

Yan et al. (2011) processed ZA62 alloy by ECAP and the grain size reduced from 100 μm to 2 μm . After 10 passes, secondary particles mixed with matrix and formed stripes like structures and the size of the stripes was around 0.5 μm . Mechanical properties were considerably improved and increased yield strength and elongation was achieved after 4 and 8 passes of ECAP.

Chen et al. (2012) carried out ECAP up to 4 passes at room temperature and observed significant grain refinement of Al-xMg alloys. Increase in misorientation was induced by particles along grain boundaries was observed using electron back scattered diffraction (EBSD) analysis. With higher ECAP passes, strength increased for Al-6

wt% Mg and the elongation reduces from 31.7% to 5.5%. Annealing after ECAP showed good results in case of both strength and ductility.

Akbaripanah et al. (2013-a) conducted ECAP process on AM60 magnesium alloy and produced an average grain size of 19.2 to 2.3 μm of through 6 passes. Yield strength and ultimate tensile strength has reduced after ECAP 2 pass due to texture softening. Maximum strength was obtained up to ECAP 2 pass and with further passes the strength decreased.

Akbaripanah et al. (2013-b) reported that extruded and ECAP processed cast AM60 at 220 °C had significant improvement in yield strength and ultimate tensile strength up to ECAP 2 passes and decreased with further passes. The production rate rises if ECAP was conducted with lower number of passes. One of the reasons for their increased UTS may be the bimodal grain structure of the ECAP 2 pass sample.

Dumitru et al. (2014) processed ZK60 magnesium alloy through ECAP at 250 °C by route B_C. After the first 2 passes, microstructure refines, but coarse grains were still visible and small recrystallized grain were observed at the grain boundaries. Further grain refinement with increase in number of ECAP passes resulted in equiaxed microstructure due to the occurrence of recrystallization processes (dynamic, metadynamic and static recrystallization). Grain size after 4 passes was reduced from 3.8 μm to 2.4 μm for the fine grains and 37.3 μm to 10.9 μm for the coarse ones.

Jahadi et al. (2014) conducted microstructure studies using SEM and showed significant refinement of grains by means of ECAP for AM30 alloy. Average grain size was reduced from 20.4 μm to 3.9 μm and ductility increased by 53% after 4 passes and variation in grain sizes decreased with higher ECAP passes. Ultimate strength showed an increase in the 2nd and 3rd passes. This is due to the higher rate of texture softening with respect to the strengthening effects during grain refinement.

Mostaed et al. (2014) processed ZK60 alloy by ECAP up to 3 passes and homogeneous grain structure was achieved with an average size of 600 nm. After 4 passes, further refinement was not possible. Corrosion studies by electrochemical method showed that the ECAP process does not have any significant effect on

corrosion resistance due to grain refinement. But corrosion rate monitoring by weight loss method showed improvement in corrosion resistance of ECAP processed samples compared to extruded samples.

Sunil et al. (2014) produced AZ31 alloy that was processed at 300 °C by ECAP and a bimodal fine grain structure was achieved. Improved hardness and wettability was observed with increase in ECAP passes. It was clearly witnessed that the working temperature and processing route play a significant role in microstructure evolution.

Fintova and Kunz (2015) processed AZ91 alloy up to 6 ECAP passes by using route B_C at 300 °C temperature and found that the microstructure to be bimodal. Microstructure showed areas with smaller grains along with large distribution of small particles of Mg₁₇Al₁₂. It also showed areas with larger grains and reduced amount of Mg₁₇Al₁₂ particles. ECAP treatment increased the yield stress from 87 to 160 MPa and tensile strength from 167 to 321 MPa followed by ductility from 3.1 to 15.4%.

Mostaed et al. (2015) carried out ECAP up to 4 passes at 200 °C temperature for ZM21 alloy and homogenous ultra-fine grain structure was achieved with grain size of 700 nm. Microstructural characterizations showed that the grain refinement and texture weakening during ECAP 1 pass increased the tensile strength of the sample. With further pass i.e., for 2 pass, yield stress was reduced from 212 to 110 MPa due to the development of new basal texture and elongation increased from 20% to 40%.

Suh et al. (2015) processed AZ31 sheets by ECAP and carried out microstructural characterization. The grain size of 8 μm was achieved at 225 °C compared to grain size 15 μm for rolled sheet. The reason is the occurrence of DRX during ECAP process and the texture analysis conducted by X-ray diffraction indicated that the ECAP processed sheets possessed weakened texture and also developed new texture.

2.8 Literature on wear behavior

Cheng et al. (2007) discussed experiment on the wear resistance of TiNi alloy processed by ECAP at varying loads and sliding distances. Homogeneous and fine

grained microstructure resulted in higher wear resistance. Wear mechanism was found to be micro-ploughing and delamination.

El Aal et al. (2010) studied wear of ECAP processed Al-Cu alloy by using pin-on-disc wear setup. Wear rate decreased with increase in ECAP passes because of increased microhardness by grain refinement. Increase of Cu percentage increased the wear resistance due to secondary phase particles (CuAl_2) and the wear mechanism was found to be adhesive and delamination wear. Due to increase in sliding distance the wear mass loss increased and the wear mechanism changed from adhesive to abrasive wear.

Wang et al. (2011) conducted wear test on ECAP processed aluminium alloy (Al-1050). It was found that coefficient of friction obtained for ECAP processed and unprocessed alloys were similar and also ECAP processed samples exhibited decreased wear resistance and increased wear mass loss with increase in ECAP passes. Wear resistance decreased due to grain refinement and loss of a strain hardening ability and wear mechanism was found to be severe wear mechanism.

Xu et al. (2013) carried out dry sliding wear test on ECAP processed AZ31 magnesium alloy. ECAP samples led to the reduction in fluctuations of the coefficient of friction (COF) due to improvement in mechanical properties. Wear mass loss was found to be lesser, when compared to wear mass loss of unprocessed alloy. Wear mechanism was known to be abrasive and oxidation wear.

Taltavull et al. (2014) observed the wear behavior of AM50B magnesium alloy. Abrasion and oxidation wear mechanisms were found for lower loads (10-40 N) and delamination, adhesion and oxidation wear mechanism were found for intermediate loads (40-80 N). Plastic deformation wear mechanism was found at higher loads (80-150 N).

Chegini et al. (2015) conducted wear test on Al-7075 alloy by pin-on-disc under different loads. Obtained results showed that the wear resistance was improved significantly by grain refinement during ECAP process. Weight loss rate increased

due to increase in applied load and wear mechanisms were identified as adhesive and delamination wear.

Hu et al. (2015) conducted wear studies on extrusion shear (ES) processed AZ31B magnesium alloy by dry sliding test. Result indicated that the wear resistance of ES processed alloy was increased due to refined microstructure. Friction coefficients and volumetric wear rate of ES processed alloy were less compared to direct extruded alloy. Wear mechanism was found to be abrasion and oxidation.

Sharifzadeh et al. (2015) investigated wear behavior and corrosion properties of pure magnesium formed by friction stir extrusion. The microstructure of the extruded sample reduced the coefficient of friction and improved the wear resistance. Fine grain improved the corrosion resistance of the produced samples.

2.9 Literature on corrosion studies

Pardo et al. (2008) studied the corrosion performance of AZ31, AZ80 and AZ91D alloys by electrochemical measurements. Fine distribution of $Mg_{17}Al_{12}$ particles and aluminium enrichment on the surface of corroded samples limited the advancement of corrosion.

Hadzima et al. (2009) observed that ECAP processed AZ31 magnesium alloy showed higher charge transfer resistance compared to cast material by conducting electrochemical impedance spectroscopy. Fine-grain microstructure influenced the corrosion resistance.

Jiang et al. (2009) conducted corrosion studies on ECAP processed ZE41A alloy using aqueous NaCl solution and the results showed nobler corrosion potential and reduced corrosion current density which led to improved corrosion resistance due to refined microstructure and homogeneously dispersed secondary phase particles.

Ralston and Birbilis (2010) conducted a review on magnesium and other alloys regarding the influence of grain size on corrosion. Grain refinement increases the corrosion resistance of magnesium alloys. The primary reason for improvements in

corrosion resistance for grain-refined materials is attributed to an improvement in passive film formation and adhesion due to increased grain boundary density.

Orlov et al. (2011) reported that ZK60 unprocessed and ECAP processed samples were subjected to corrosion studies by electrochemical measurements and immersion test using 0.1 M NaCl and the results showed improved corrosion resistance of ECAP processed samples due to redistribution of solutes (Zn and Zr) within the microstructure and grain refinement.

Argade et al. (2012) conducted corrosion studies on Mg-Y-RE alloy. UFG microstructure exhibited highest polarization resistance with positive pitting and repassivation potentials in comparison to unprocessed condition. Immersion test showed improved corrosion resistance for UFG samples.

Minarik et al. (2013) investigated corrosion behavior of magnesium alloys (AE21 and AE42) by electrochemical impedance spectroscopy (EIS) in 0.1 M NaCl solution. Enhancement of corrosion resistance was influenced by Al-rich $Al_{11}RE_3$ dispersed particles and UFG structure and uniform distribution of the secondary elements compared to the unprocessed material.

Mostaed et al. (2014) studied corrosion performance on ECAP processed ZK60 alloy by electrochemical measurements and immersion test by using phosphate buffer electrolyte. Results showed enhanced corrosion resistance in ultra-fine grained (UFG) alloy compared to extruded material. Increase in corrosion resistance is due to second phase refinement and redistribution.

2.10 Motivation from literature survey

The following points were observed from the literature survey.

- Literature shows inconsistency in the outcome obtained from ECAP process on mechanical, wear and corrosion properties of magnesium alloy. Therefore further investigation is necessary on the above properties.
- Loss of material or any damages due to impact and load application and also it may be exposed to environments where it is extremely reactive which leads to high level of corrosion, therefore the study wear and corrosion behavior of magnesium alloy to be carried out.
- AM series magnesium alloys have good ductility, better noise and vibration dampening characteristics and castability property. They are used in impact and energy absorption requirements in crash conditions. Presence of aluminium increases the strength and variation in the percentage of manganese increases the corrosion resistance properties.
- Limited work has been reported on AM series magnesium alloy using ECAP process.

2.11 Objectives

Based on the developments in the area of magnesium alloys with SPD process using ECAP technique, following objectives have been derived.

- To study the microstructural changes of magnesium alloys processed by ECAP process.
- To investigate the mechanical properties of as-cast and ECAP processed AM70, AM80 and AM90 magnesium alloys.
- To study the wear behavior of as-cast and ECAP processed AM70, AM80 and AM90 magnesium alloys.
- To examine the corrosion behavior of as-cast and ECAP processed AM70, AM80 and AM90 magnesium alloys.

CHAPTER 3

EXPERIMENTAL PROCEDURE

Following flow chart shows the different processing steps carried out for material processing followed by various testing conducted on unprocessed and ECAP processed material using different characterization and testing equipment's. Overall research methodology is illustrated in flow chart (Fig. 3.1).

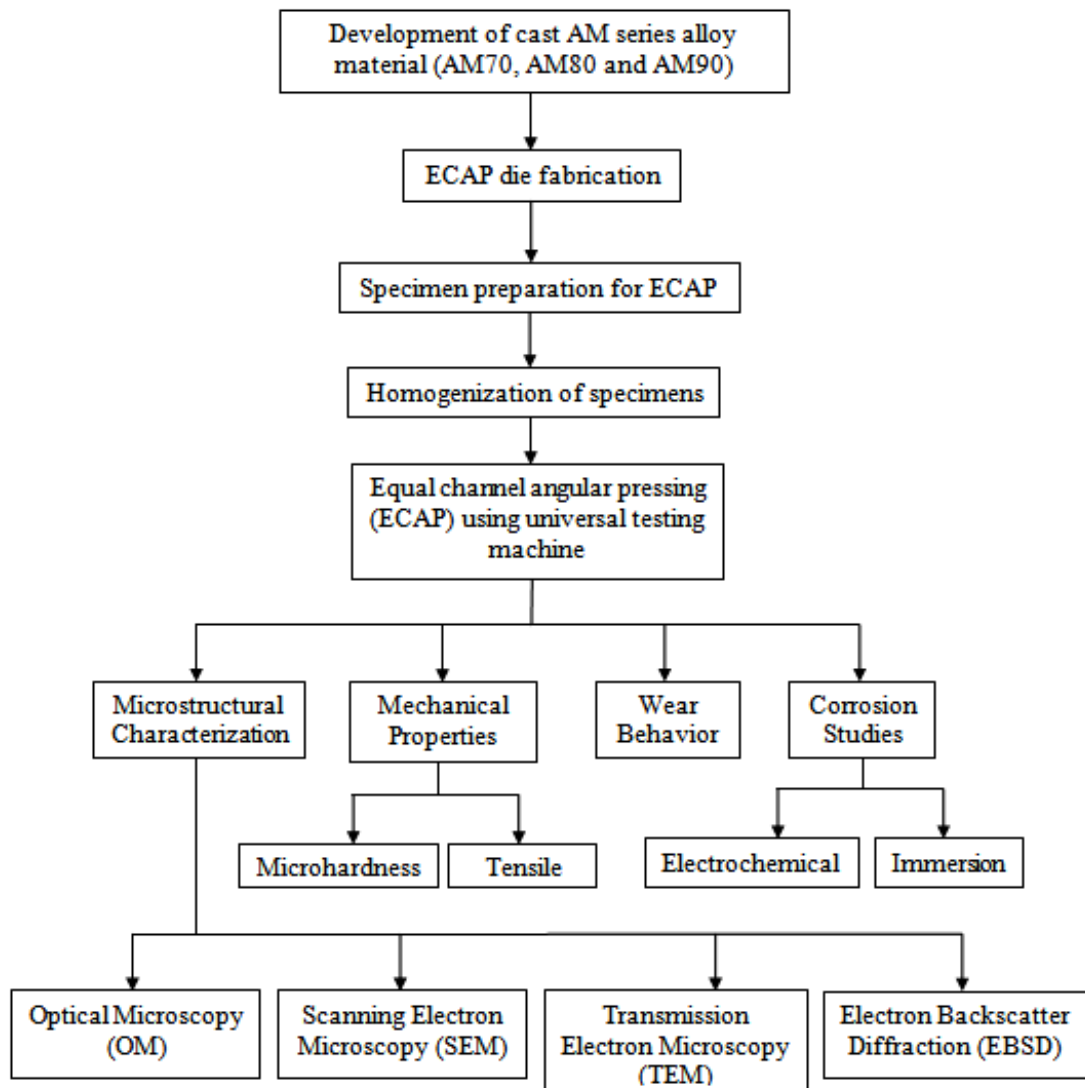


Figure 3.1 Flow chart of the process

3.1 Equal channel angular pressing (ECAP) setup with universal testing machine

ECAP is performed using a die consisting of two blocks fabricated from hot die steel (HDS) and held together using 6 large bolts (M14). It is relatively a simple task to establish the facility for conventional ECAP, by machining a two-piece split dies consisting of a highly polished smooth plate bolted to a second polished plate containing a square-sided channel. Illustration of ECAP process is as shown in figure 3.2.

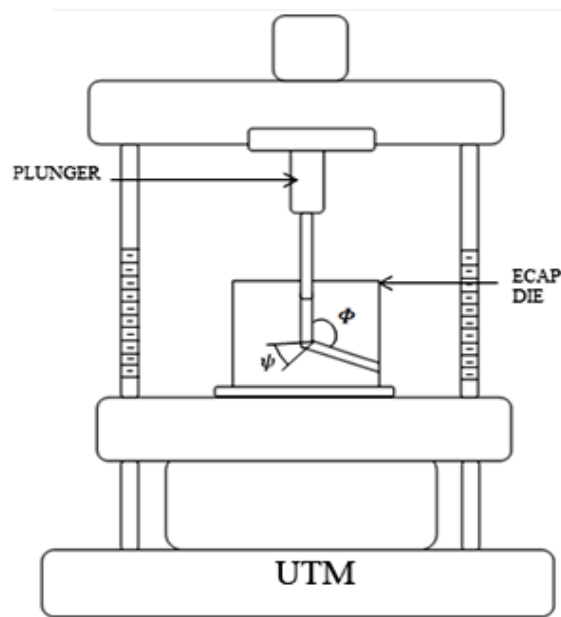


Figure 3.2 Schematic illustration of ECAP process



Figure 3.3 UTM with ECAP setup

The die was machined to a channel angle (Φ) of 110° and an outer arc of curvature (Ψ) of 20° to pass the material by using universal testing machine (UTM) and was arranged on the base plate of the UTM which is aligned to the center of the spindle as shown in figure. 3.2 and figure 3.3.

3.2 Material and ECAP operation

Nominal compositions of the cast magnesium alloys are illustrated in the Table 3.1. Cast Mg alloys (AM series) were procured from Venuka Engineering Private Ltd, Telangana, India. Material was available in the form of rectangle ingots of $240\text{ mm} \times 100\text{ mm} \times 24\text{ mm}$. Procured materials were cut into $20\text{ mm} \times 20\text{ mm}$ square sectioned rods of length 100 mm. Further the materials were turned to 15.8 mm in diameter and length to 95 mm rod and is illustrated in figure 3.4. The prepared samples were homogenized at 400°C for 24 hours in a furnace to make sure the constituents are uniformly distributed within the matrix.

Table 3.1 Nominal compositions of AM series magnesium alloys

Alloy	% Al	% Mn	% Zn	% Si	% Cu	% Ni	% Fe	Mg
AM70	7.1	0.35	0.04	0.08	0.03	0.01	0.003	Balance
AM80	8.22	0.39	0.09	0.07	0.03	0.01	0.004	Balance
AM90	9.06	0.42	0.08	0.03	0.02	0.01	0.003	Balance

ECAP die (Fig.3.5) is placed on the base plate of UTM and plunger is aligned exactly to the center of die where the specimen is placed for pressing. The die was machined to a channel angle (Φ) of 110° and an outer arc of curvature (Ψ) of 20° . Die was homogeneously heated by 4 electrical resistance heaters, placed along the vertical channel. At the intersection of the channels, temperature was monitored throughout the process using thermocouples inserted in the die located near the intersection point (Mostaed, E et al. 2014). ECAP process was carried out at different temperatures to optimize the exact temperature at which the ECAP process can be conducted. Firstly, the die is heated to the required temperature and temperature is controlled by the temperature controller which is provided with the heating facility. Sample is placed in the die and need to make sure that the temperature of the specimen also reached the required temperature. A suitable lubricant such as Molybdenum disulphide (MoS_2) or

graphite is generally used to minimize the frictional effects between samples and die walls. Molybdenum disulphide (MoS_2) is applied on the surface of sample and die walls to minimize the friction during the ECAP process. After attaining the required temperature, the sample is pressed by applying a load at the rate of 1 mm/sec using plunger attached to the UTM for deformation of the specimen. The channels are intersected to impose the total strain on the material to get ultra-fine grain (UFG) structure. The process is repeated by using route B_C , where the samples were rotated by 90° between two successive passes as shown in figure 3.6. The processed samples after ECAP operation is shown in figure 3.7. Pressing was done using plunger fixed to the spindle of the UTM giving an equivalent strain of ~ 0.8 (Iwahashi et al. 1996) per ECAP pass.



Figure 3.4 Machined samples to carry out ECAP



Figure 3.5 Split ECAP die with plunger

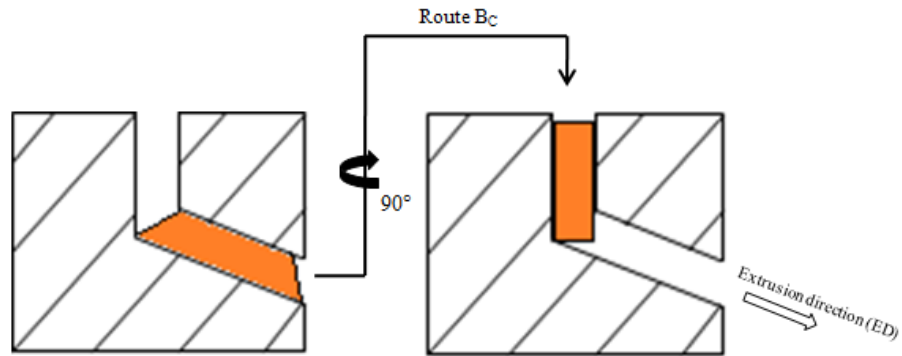


Figure 3.6 Processing route B_c

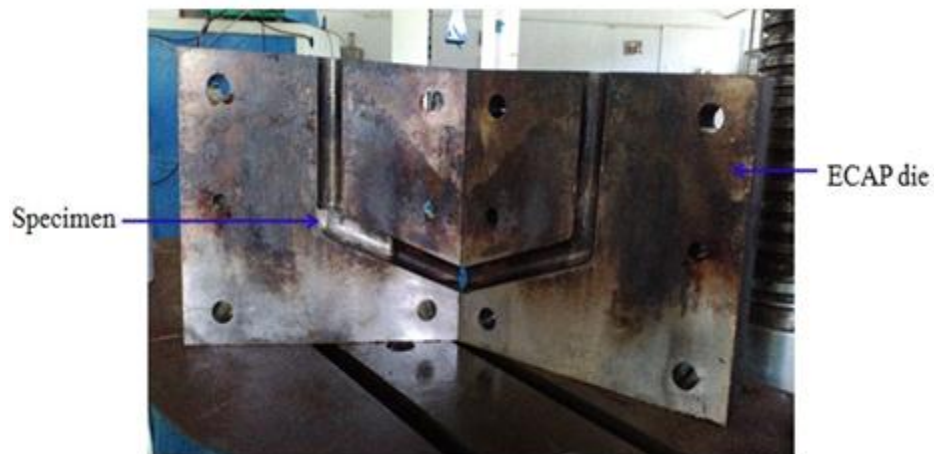


Figure 3.7 Sample after ECAP operation

ECAP process was continued up to four passes. Total strain (ϵ) accumulated after 'n' number of ECAP passes can be calculated using the equation 2.5.

3.3 Optimizing the processing temperature

ECAP process was carried out at different temperatures. Samples of 15.8 mm diameter and 95 mm in length (Fig.3.8a) were processed at temperatures varying from 225 °C to 275 °C and the samples are shown in figure 3.8 (b-d). Sample processed at 225 °C temperature showed large surface cracks as shown in figure 3.8 (b). At 250 °C, surface cracks were reduced as represented in figure 3.8 (c) and at 275 °C temperature, samples were produced with no surface cracks with a soaking time of 15 min and pressing speed of 1 mm/s as shown in figure 3.8 (d). Therefore, 275 °C

temperature was considered for processing the samples through ECAP process, because it is difficult to deform magnesium at lower temperature, due to hexagonal closed packed (HCP) structure with limited slip systems.

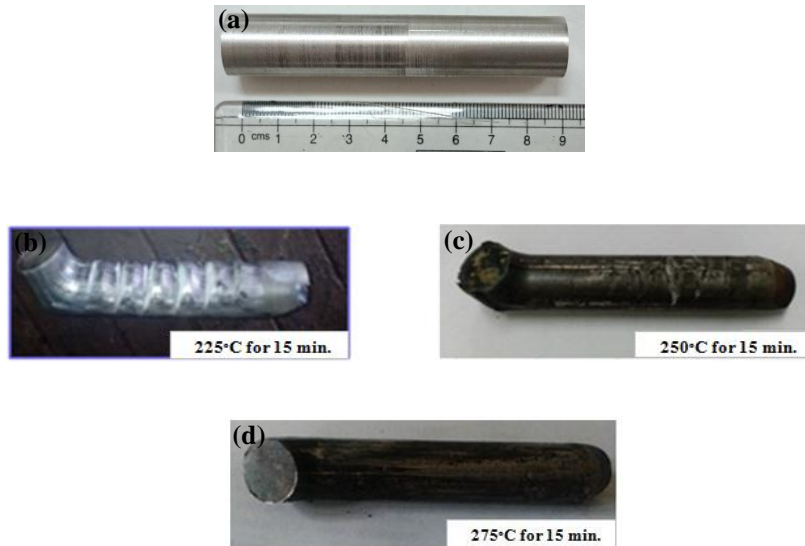


Figure 3.8 (a) Initial sample and ECAP processed samples at (b) 225 °C (c) 250 °C and (d) 275 °C with soaking time of 15 min

3.4 Sample preparation for testing

After the ECAP process, samples are prepared for microstructural characterization, analysis of mechanical properties, wear behavior and corrosion studies.

3.4.1 Microstructural characterization

Microstructure evaluation of as-cast, homogenized and ECAP processed samples of AM cast magnesium alloys (AM70, AM80 and AM90) were investigated. Slices were cut from each sample from a distance of ~10 mm from the tail of the bar. This region was selected to avoid any inhomogeneities that may occur due to distortions near the front and back regions of the samples. Cross-sections perpendicular to the pressing direction of ECAP processed samples are prepared by mechanical polishing with silicon carbide abrasive papers (grades of 400, 800, 1000, 1200, 1500, 2000 or 2/0) followed by cloth polishing using diamond paste and kerosene for obtaining mirror finish surface and finally washed using acetone. Etchant was prepared by using 4.2 g picric acid, 70 ml ethanol, 10 ml acetic acid and 10 ml distilled water (Akbaripanah et

al. 2013-a). Etching was carried by dipping the polished samples for approximately 5 s, so that sample turns light brown in color and washed with distilled water and dried thoroughly.

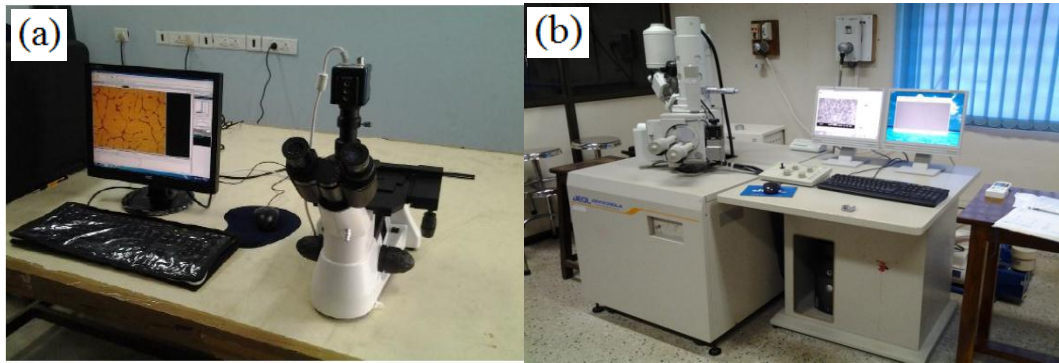


Figure 3.9 (a) Optical microscope (b) Scanning electron microscope

Microstructures were observed using optical microscope (OM) by image analyzer (BIOVIS Software) which is shown in figure 3.9(a) and average grain sizes were measured by linear intercepts method (ASTM E-112). Same samples were observed under scanning electron microscope (SEM-JEOL JSM 6380LA) (Figure 3.9(b)) attached with energy-dispersive x-ray spectroscopy (EDS) to study the surface morphology and localized chemical composition. Microstructures were also examined using Transmission Electron Microscope (TEM-JEOL-JEM 2100) as shown in figure 3.10. Sample preparation for TEM analysis involved the following steps:

1. Slicing of samples to around $\sim 100 \mu\text{m}$.
2. Thinning of sliced samples by polishing using fine emery to $\sim 40 \mu\text{m}$ thick.

Then, discs of diameter 3 mm were punched out of the polished sample. Dimpling was done to reduce the thickness to about 5 to 10 μm and finally, ion milling (Gatan-PIPS 691) was carried out on dimpled sample for producing a small perforation on the sample. TEM was carried out to observe the ultrafine grains, dislocations due to grain refinement and selected area electron diffraction (SAED) patterns were extracted from the samples to observe the diffraction spots. Dislocations are the crystallographic defects within the crystal structure which influences the properties of the material.



Figure 3.10 Transmission electron microscope

Microstructures are also analyzed by electron backscatter diffraction (EBSD) using Field Emission Scanning Electron Microscope (JEOL JSM-7100F) as shown in figure 3.11(a), for grain structure, grain size and grain boundaries misorientation angles. For EBSD analysis, samples were electropolished using Struers AC2 electrolyte at $-30\text{ }^{\circ}\text{C}$ for a period of 80 s at 16 V with Struers electropolishing machine as shown in figure 3.11(b). Immediately, the sample was loaded to Field Emission Scanning Electron Microscope (FE-SEM) to get the indexing from the microstructure. EBSD was carried out using 20 kV voltage and step size of $0.25\text{ }\mu\text{m}$. Obtained results were analyzed using HKL Channel 5 software.



(b)



Figure 3.11 (a) FE-SEM (b) Struers electro polishing machine

X-ray diffraction (XRD) was carried out to know phases existing in the as-cast and ECAP processed samples. XRD (JEOL DX GE-2P) was performed using a diffractometer with Ni filter operated at 20 mA and 30 kV with Cu- α radiation. XRD machine is shown in figure 3.12. Scan rate was fixed to 2°/min with diffraction angle (2θ) range between 20° to 90°.



Figure 3.12 X-ray diffraction

3.4.2 Mechanical properties evaluation

3.4.2.1 Tensile test

Tensile samples were prepared according to ASTM-E8 standard with 16 mm gauge length. A schematic tensile specimen has been illustrated in figure 3.13. Three samples were tested for each condition. Uniaxial tensile testing was done at ambient temperature (~25 °C) using UTM (Shimadzu AG-X plus™) equipped with 100 kN load cell and operated with a steady cross-head speed of 0.25 mm/min during all the tensile tests as shown in figure 3.14.

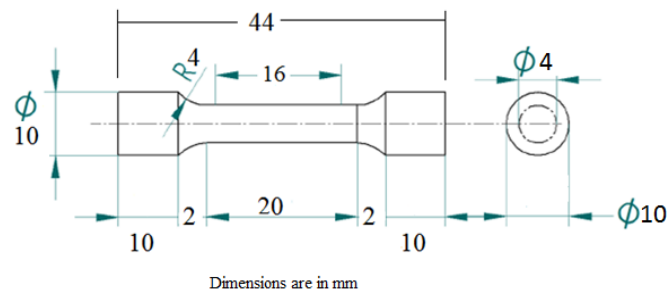


Figure 3.13 Tensile test specimen dimension as per ASTM-E8



Figure 3.14 Shimadzu Tensile Tester

3.4.2.2 Vickers Microhardness (Hv)

Vickers microhardness test was carried out to measure the hardness of material using Omni tech (MVH-S-AUTO) microhardness tester, fitted with Vickers indenter. The tester is shown in figure 3.15. Vickers microhardness test was conducted by applying small loads for a short time period and there will be no distortion on the microstructure due to application of smaller loads.



Figure 3.15 Omni tech microhardness tester

Typical loads are very light ranging from few grams to one or several kilograms. Also, since the indentation is very small, the hardness can be checked within the grain itself. But in case of macrohardness, more load will be applied and there will be

chances of damaging the material surface. Microhardness test was carried out at 10-12 locations on the surface of microstructure at equal intervals by applying a load of 25 g and dwell time of 15 s. Indentations were taken at equal intervals on middle area of the sectioned region for each of the sample to avoid any irregularities that may take place due to deformation near head and tail regions of processed samples.

3.4.3. Wear behavior

Wear test specimens were prepared by taking the central region of the unprocessed and ECAP processed samples. The specimens were turned to a dimension of 6 mm in diameter and 28 mm in length as per ASTM G99-05 and the schematic is as shown in figure 3.16. Wear tests were performed at room temperature under dry sliding condition using pin-on-disc tribometer (DUCOM-TR-20LE-PHM 400-CHM 600) wear test machine and the schematic is shown in figure 3.17. Tests were carried out on hard and polished disc (EN31 steel) with HRC 65 hardness. Prior to wear test the samples were subjected to grinding with SiC papers (1500 and 2000 grit) and followed by cleaning using ultrasonicator for 5-10 min and finally dried.

Wear resistance was measured by a weight loss technique. Samples were subjected to 30 N and 40 N load with sliding distance of 2500 m and 5000 m at a sliding speed of 3 m/s with track diameter of 110 mm.

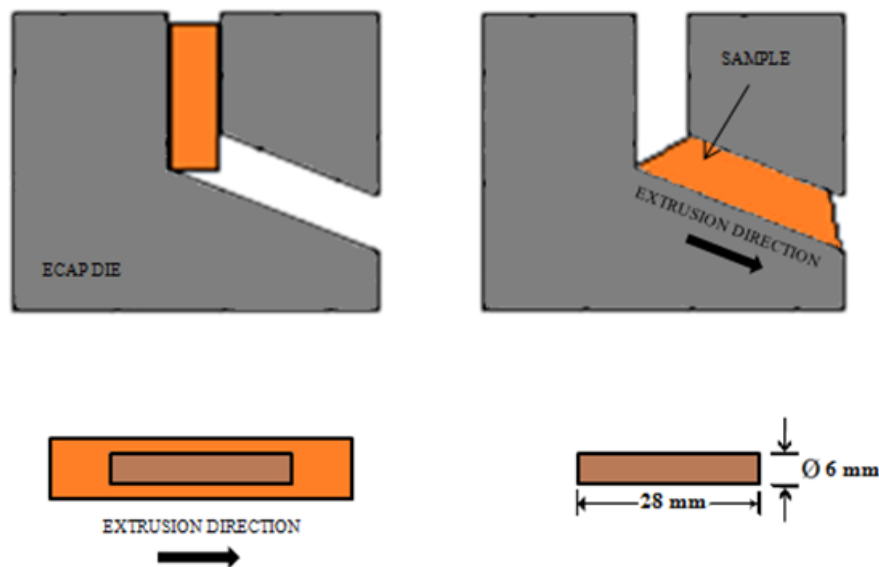


Figure 3.16 Wear test specimen preparation

Initial and final weight of the samples were measured. Prior to each test, disc surface was cleaned with 1000 grit SiC paper and cleaned with acetone to remove the debris on the surface. Worn surfaces of homogenized and ECAP processed samples were analyzed using SEM, attached with EDS, to study the wear mechanism.

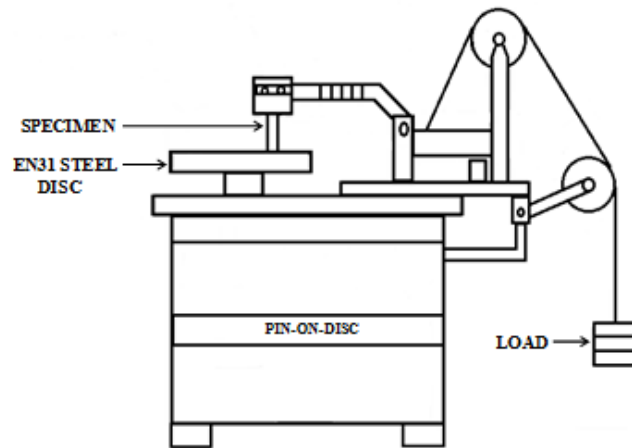


Figure 3.17 Schematic diagram of wear test machine

3.4.4. Corrosion studies

3.4.4.1. Electrochemical measurements

All the specimens used for electrochemical corrosion studies were polished to obtain mirror finished surfaces and properly cleaned using acetone. Electrochemical measurements were carried out using an electrochemical workstation (EC lab-Biologic SP-150) with a standard three-electrode system containing a saturated calomel electrode (SCE) as reference electrode, a platinum wire as counter electrode, and the sample with 1 cm² surface area exposed to solution was used as working electrode. The aqueous solution of 0.1M NaCl was prepared using A.R. grade NaCl in distilled water used as electrolyte and the pH of solution was maintained at 7.5. Dilute electrolyte was selected as test electrolyte because it is a standard electrolyte for initial screening as it imitates environments that might commonly be encountered during service of Mg components and it is dilute enough to allow subtle electrochemical differences that can be detected (Orlov et al. 2011). During each experiment, samples were polished using SiC paper (400-2000 grit). Electrochemical tests like potentiodynamic polarization test and electrochemical impedance spectroscopy (EIS) test were carried out in 0.1M wt.% NaCl solution at room

temperature. Potentiodynamic polarization experiments were carried out at a scan rate of 0.5 mV/s. The cathodic and anodic portions of the generated Tafel plots were accordingly extrapolated to calculate the corrosion potential (E_{corr}) and corrosion current density (I_{corr}). EIS test was carried out with a frequency ranges from 100 kHz to 10 mHz and the amplitude of sinusoidal potential signal is 5 mV. Surface morphology of the tested samples were examined by SEM. The corrosion product was removed using 200 g/L of chromic acid and 10 g/L of AgNO_3 solutions. EC lab-Biologic SP-150 workstation is as shown in figure 3.18.



Figure 3.18 Electrochemical workstation

3.4.4.2. Immersion test

Immersion test was performed according to ASTM G31-72. For immersion study the samples were cut perpendicular to the extrusion direction. Samples were polished using 400-2000 grit SiC emery paper and cloth polishing using 0.25 μm diamond paste and cleaned in acetone using ultrasonicator. The sample was kept in a beaker containing the 0.1M NaCl electrolyte solution and a funnel mounted with burette is placed over the specimen, which confirms the collection of hydrogen evolved from the sample surface. Initially, funnel mounted with burette is full of the test solution. Hydrogen evolved from the sample gets collected by the funnel and it enters into the burette and steadily displaces the level of test solution in the burette and is measured by the burette scale. By this, the volume of the hydrogen evolved was measured by reading the position of solution level in the burette and the schematic is shown in figure 3.19. Tests were carried out by immersing the samples in 0.1M NaCl solution

of pH 7.5 at room temperature for 120 h. Hydrogen evolution from the samples were recorded. After the test, the samples were cleaned in chromic acid and dried.

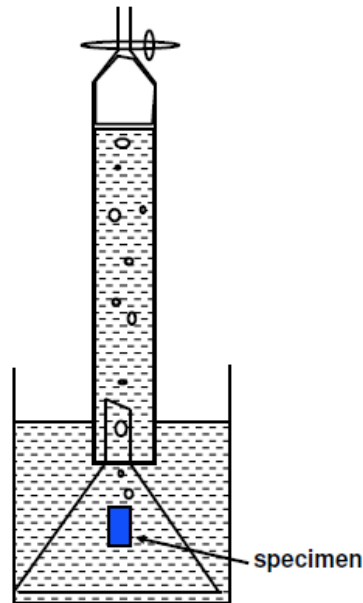
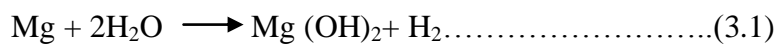


Figure 3.19 Schematic of immersion test setup for measuring hydrogen evolution (Song et al. 2001)

Hydrogen evolution method is more reliable which can be used to study the time dependent corrosion behavior of the alloys and immersion test setup is as shown in figure 3.20. Based on the overall corrosion reaction (given in Eq. 3.1), 1 mol of hydrogen gas evolved corresponds to 1 mol of magnesium corroded. Therefore, the measurement of the hydrogen evolved is equivalent to the measurement of the weight loss of the metal as (Makar and Kruger, 1993):



Weight loss method is the fundamental and simplest way of measuring the corrosion rate. This can be converted to an average corrosion rate (mm/y) using following equations as (Shi et al. 2010 and ASM Corrosion Handbook. 1987).

$$P_H = 3.65 \Delta W / \rho \dots \dots \dots (3.2)$$

Where, ρ = Metal density (g/cm^3)

$$\Delta W = \text{Weight loss rate} (\text{mg}/\text{cm}^2/\text{d})$$

One mol (24.31 g) of Mg metal corroded for each mol (22.4 L) of hydrogen gas produced. Therefore, the hydrogen evolution rate, V_H ($\text{ml}/\text{cm}^2/\text{d}$), is related to the metallic weight loss rate is given by (Song and Atrens, 2003),

$$\Delta W = 1.085V_H \dots \dots \dots (3.3)$$

Where, V_H = Hydrogen evolution rate (ml/cm²/d)



Figure 3.20 Immersion test setup

CHAPTER 4

RESULTS AND DISCUSSION

4.1 Equal channel angular pressing of AM70 alloy

AM70 alloy was processed by ECAP at 275 °C up to 4 passes using route B_C. Microstructures of the ECAP processed samples were characterized using optical microscope and SEM. Samples processed at ECAP 4 pass were observed under TEM. Microstructures of as-cast and 4 pass ECAP processed samples are also analyzed by EBSD for grain structure and grain boundaries misorientation angles. XRD was conducted to identify the different phases in the samples. Tensile and microhardness test was carried out for samples up to 4 pass and the results are discussed in the following sections. Samples were subjected to wear test to know the wear behavior and corrosion studies were conducted to measure the corrosion resistance of the material.

4.1.1 Microstructure analysis

Figure 4.1 (a) shows the SEM images of the as-cast magnesium alloy AM70. It consists of α -Mg as the matrix and a large volume of β -Mg₁₇Al₁₂ as secondary phase (Czerwinski, 2011). β phase is randomly distributed over the entire matrix and the grain boundaries are not clear. Average grain size was found to be 45 μ m. As-cast material was subjected to homogenization at 400 °C for 24 hours. During homogenization, secondary β phase dissolve in the matrix and the traces of the secondary phase are seen along the grain boundaries.

Grain boundaries are clearly visible, thus each grain can be distinguished. Average grain size of the homogenized material (Figure 4.1(b)) was found to be 100 μ m. Increase in grain size for the homogenized sample is due to static recrystallization process occurring during homogenization process.

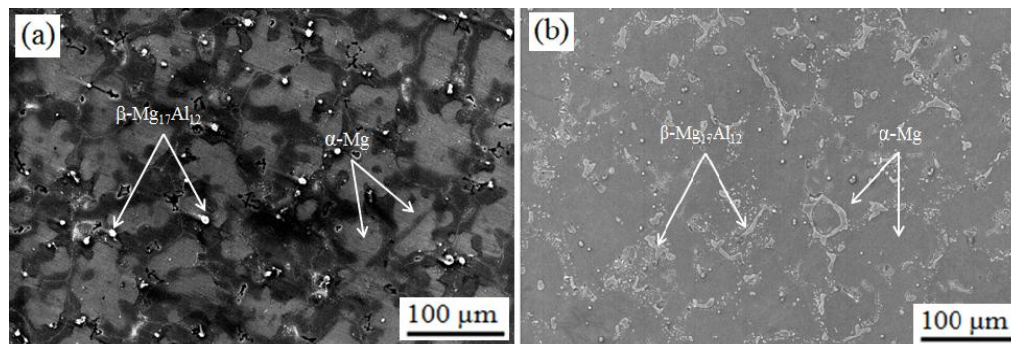


Figure 4.1 SEM images of AM70 alloy (a) as-cast and (b) homogenized samples

Homogenized samples are subjected to ECAP up to 4 passes at 275 °C. During the first pass, initial coarse grains were broken into too many finer grains, in such a way that smaller grains were encircled by larger grains which leads to heterogeneous or bimodal structure of material and is shown in figure 4.2(c). More refinement occurs at initial passes which may be dependent on high rate of dislocation. Grains are bimodal after 1st ECAP pass with some large grains of 55 to 65 μm surrounded with arrays of smaller grains of 30 to 35 μm and the average grain size found to be 60 μm . Further grain refinement occurs during the second, third and fourth passes. It is clear from figure 4.2 (d-f), i.e., for 2, 3 and 4 pass, homogeneous and refined microstructure was obtained. Grain size after 4 passes was found to be an average of 1 μm . Reasonable homogeneity and equiaxed microstructure at higher passes may be due to dynamic recrystallization (DRX) during ECAP process or static recrystallization prior to the ECAP process during heating until desired temperature is attained (Akbaripناه et al. 2013-b).

Figure 4.3 (a-f) shows SEM images of unprocessed (as-cast and homogenized) and ECAP processed samples from 1 to 4 pass. In figure 4.3 (b), secondary phase particles can be found in great proportion at grain boundaries but not inside the grain. Figure 4.3 (e) and (f) show the microstructure of the 3 and 4 pass samples. Average grain sizes as observed from the microstructures are 8 μm and 1 μm respectively for 3 pass and 4 pass samples. This homogeneous grain refinement is because of dynamic recrystallization during ECAP process (Akbaripناه et al. 2013-a, b). Grain sizes of as-cast, homogenized and ECAP processed samples are shown in figure 4.4 measured by linear intercept method.

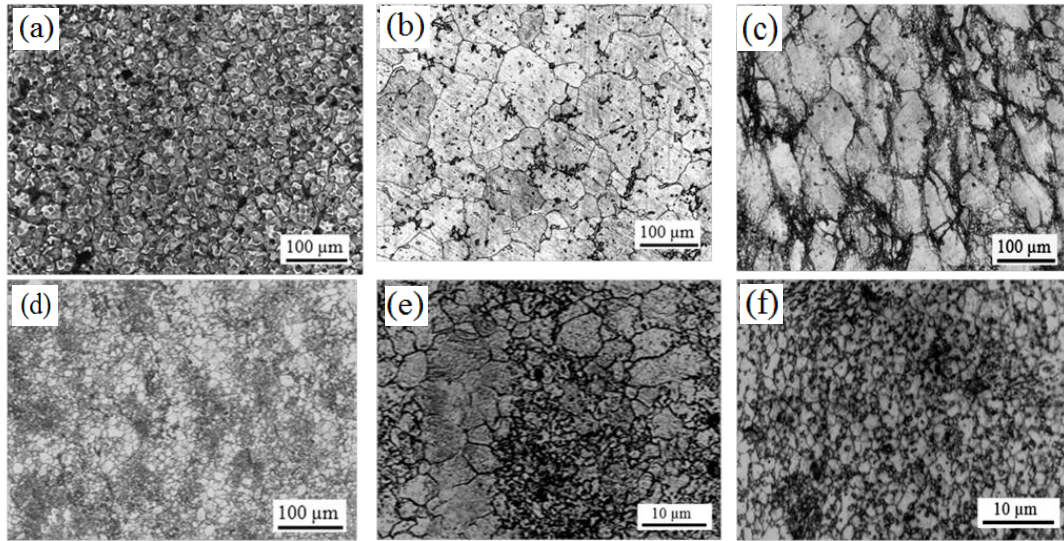


Figure 4.2 Optical microstructures of AM70 alloy (a) as-cast (b) homogenized (c) 1P (d) 2P (e) 3P and (f) 4P samples

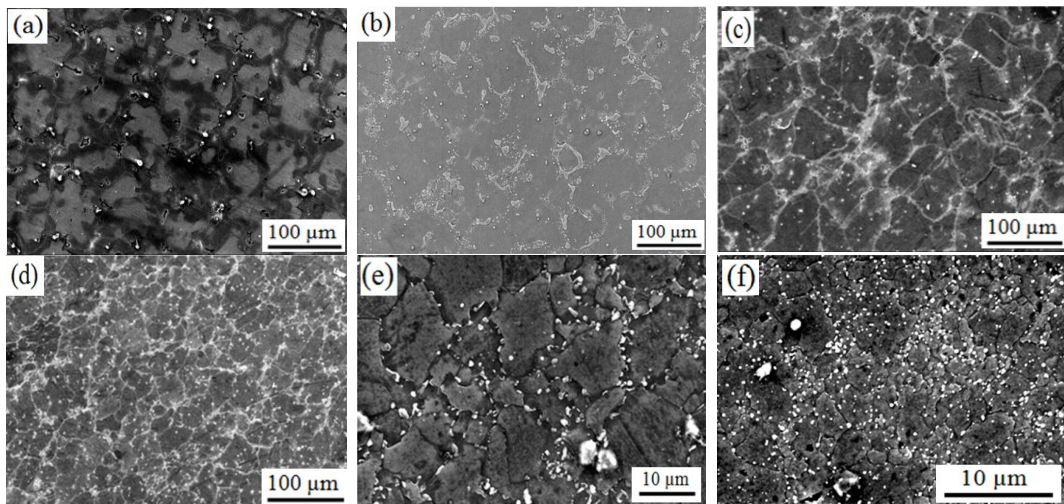


Figure 4.3 SEM images of (a) as-cast (b) homogenized and ECAP (c) 1P (d) 2P (e) 3P and (f) 4P samples

Figure 4.5 (a) and (b) shows TEM image and SAED patterns of ECAP 4 pass sample. Microstructure consists of refined grains with high volume of dislocation density. ECAP process causes subdivision of grains due to dislocation generation and with higher passes, dislocation pile-up takes place at grain boundaries causing high dislocation density. Space between these dislocations reduces with ECAP passes, which leads to the formation of fine grains (Chino et al. 2008). Diffraction spots in SAED patterns are in the form of circles, indicating large fraction of fine grains with HAGBs.

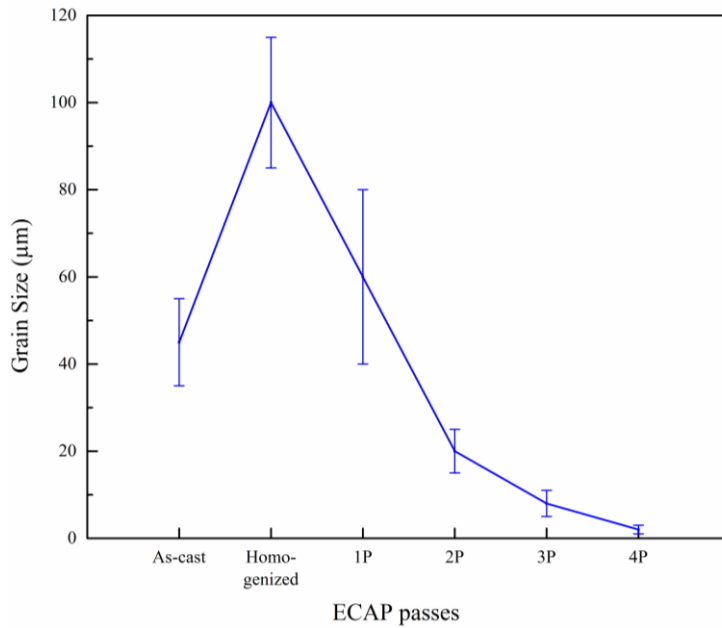


Figure 4.4 Grain size of as-cast, homogenized and ECAP processed samples

Few diffraction spots are separated and not continuous, which may be due to the presence of coarse grains with LAGBs. Some diffraction spots look stretched or elongated which point out the presence of high internal stress due to diffusion of some grain boundaries and are in high energy states (Stolyarov et al. 2001). Orientation Imaging Microscopy (OIM) with the Inverse Pole Figure (IPF) map is shown in figure 4.6. Colors present in IPF map represent the crystal orientations in different directions as shown in figure. As-cast alloy shows a heterogeneous structure and finer grains can be seen in processed 4 pass sample.

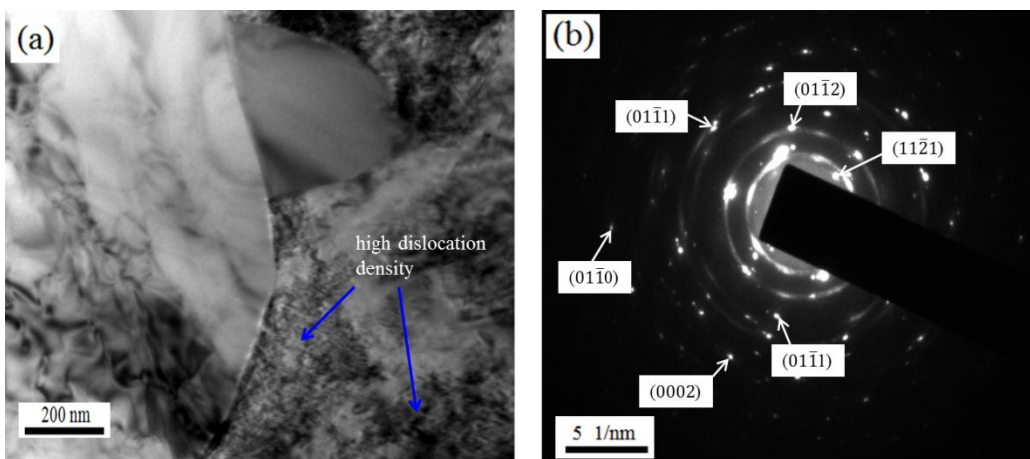


Figure 4.5 TEM images of ECAP 4P sample

Distribution of grain boundaries is observed with clear increase in misorientation angles as shown in figure 4.7. Strong peaks are observed in both as-cast and ECAP 4 pass sample in low angle area ($<5^\circ$) and dispersed groups of peaks were observed at higher angles. Development of misorientation can be observed at an angle of $\sim 10^\circ$ to $\sim 60^\circ$. Frequency of misorientation is reduced below 5° for ECAP 4 pass sample. From figure 4.3 (e) and (f), it was observed that refinement rate is reduced at higher passes compared to initial passes and also by increasing the strain (increasing ECAP passes) a transition from LAGBs to HAGBs occurs, conducting to a more stable microstructure because it is well-known that the dynamic recrystallization occurs on grain boundaries (Dumitru et al.2014). With increase in number of ECAP passes, frequency of HAGBs increases. Even though frequency of LAGBs has decreased with increase in HAGBs during higher passes, there is no much change in grain size. Fraction of recrystallized grains increases with increase in strain due to the higher rate of nucleation during recrystallization, which results in a relatively uniform microstructure with ultrafine grains as shown in figure 4.2(f) and 4.3(f). Obtained results shows that majority of grain refinement takes place during initial stages of ECAP and higher deformation produces more HAGBs (Biswas et al. 2010 and Jin et al. 2006).

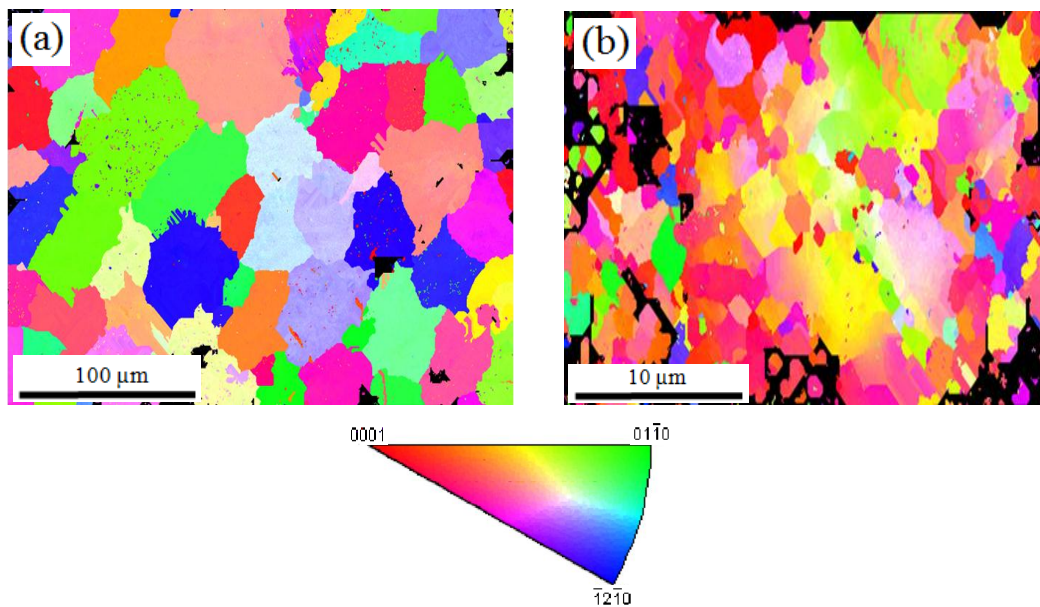


Figure 4.6 OIM with IPF image (a) as-cast and (b) ECAP 4P samples

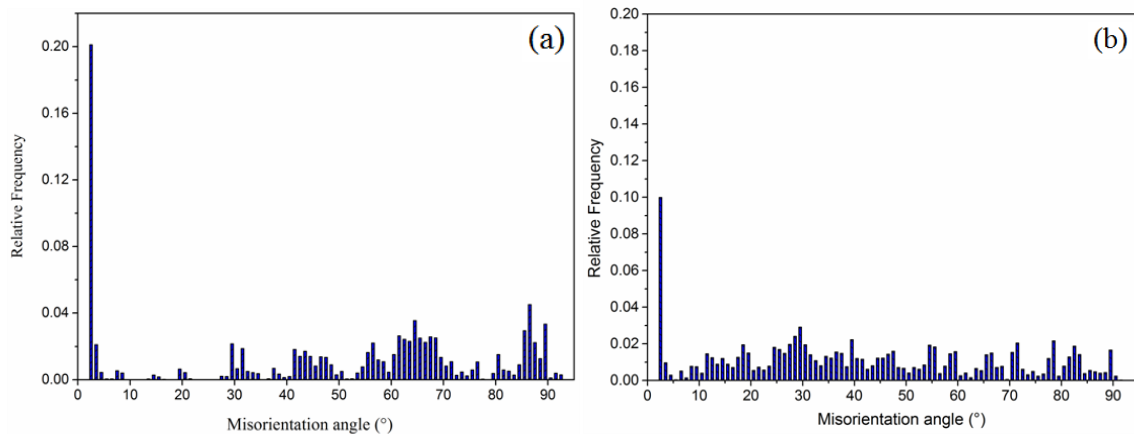


Figure 4.7 Misorientation angles of (a) as-cast and (b) ECAP 4P samples

4.1.2. X-ray diffraction analysis

Figure 4.8 shows the X-ray diffraction (XRD) patterns of as-cast, ECAP processed 2 and 4 pass samples. XRD revealed the existence of $Mg_{17}Al_{12}$, Mg_2Al_3 and $MnAl_6$ phases in the magnesium matrix. The existence of these phases or particles improves the mechanical properties and they are considered as the source for strengthening in magnesium alloy (Gong et al. 2009; Li et al. 2009). The precipitate $Mg_{17}Al_{12}$ and $MnAl_6$ shows increment in intensity at $\sim 57^\circ$ for ECAP 2 pass sample, but the other peaks showed reduction in the intensity with the number of ECAP passes. This variation can be related to precipitation orientation which occurs during grain growth (Dumitru et al. 2014). It was noticed that the planes $(10\bar{1}0)$, (0002) and $(10\bar{1}2)$ for as-cast material shows a strong trend of intensity while, no such tendency occurs during ECAP 4 pass. Intensity of plane $(10\bar{1}1)$ was increased after ECAP 2 and 4 pass but more decrease was observed for $(10\bar{1}0)$ plane. These changes may be due to the grain refinement during ECAP. From figure 4.8, strong intensity was observed for as-cast sample and this intensity gradually decreases during the ECAP process and it can be observed from ECAP 2 and 4 pass samples. Shear deformation which took place during the ECAP process eliminated the existing texture and due to that, intensity decreases with increase in number of ECAP pass. As the ECAP passes increases the initial textures is completely removed and in the meantime, shear deformation by ECAP gives rise to new texture (Feng and Ai, 2009).

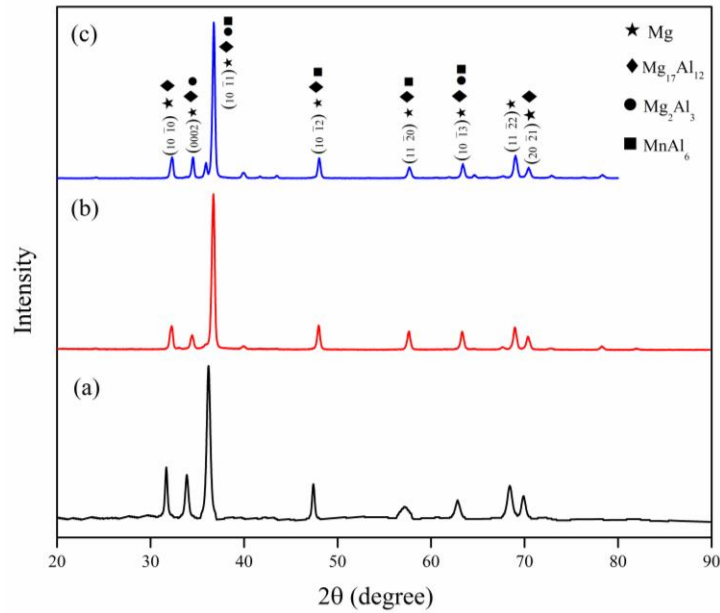


Figure 4.8 XRD patterns of (a) as-cast (b) ECAP 2P and (c) ECAP 4P samples

4.1.3 Mechanical properties

4.1.3.1 Tensile behavior

Tensile test are carried out for as-cast, homogenized and ECAP processed samples. Stress-strain diagram for as-cast, homogenized and ECAP processed samples are shown in figure 4.9 and the summary of the tensile properties are shown in table 4.1. From the plot, it is observed that ultimate tensile strength (UTS) is increased up to 2 pass but decreased with further passes. UTS of 2 pass ECAP processed sample was 282 MPa, which is 112% and 34% larger as compared to the UTS of as-cast of 133 MPa and homogenized sample of 210 MPa. After 2 pass, elongation was 20.7% compared with 3.1% for the as-cast sample. UTS obtained for 3 pass 4 pass samples are 255 MPa and 242 MPa, respectively. Yield strength (YS) obtained for 2 pass ECAP sample was 170 MPa, which is 188% and 79% larger as compared to as-cast of 59 MPa and homogenized sample of 95 MPa. YS obtained for 3 pass 4 pass samples are 135 MPa and 120 MPa.

Increase in UTS is due to grain boundary strengthening mechanism. This is according to Hall-Petch equation, which states that, reduced grain size leads to increase in UTS (Valiev et al. 2006). It may also be due to the increment in precipitation of intermetallic phases in the matrix of the material as shown in figure 4.8. UTS was

maximum for 2 pass as shown in graph i.e., refinement rate was maximum and deviation observed in UTS may be due to, firstly, decrease in grain refinement rate (Figure 4.2(e) and (f)). Second, due to DRX that happened during ECAP process which leads to elimination of dislocations and also because of static recrystallization prior to ECAP process.

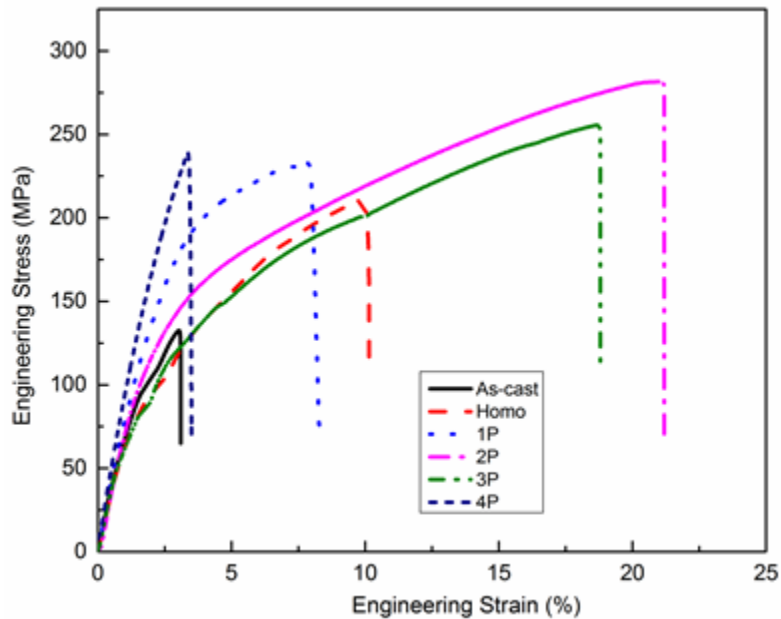


Figure 4.9 Tensile properties for as-cast, homogenized and ECAP processed samples

Table 4.1 Mechanical properties of AM70 alloy processed by ECAP up to 4 passes.

ECAP passes	UTS (MPa)	YS (MPa)	% Elongation
As-cast	133±6.5	59±8.2	3.1±0.12
Homogenized	210±5.1	95±6.8	10.25±0.15
1 Pass	233±6.2	114±5.5	7.61±0.13
2 Pass	282±4.5	170±6.2	20.7±0.10
3 Pass	255±6.6	135±4.0	18.71±0.15
4 Pass	242±5.5	120±7.3	3.95±0.17

Thirdly, even though the grain size of ECAP processed material decreased there was a reduction in UTS. This may be because of the weakening of texture fiber or texture modification, due to increase in texture intensity and the Schmid factor (Mostaed et al. 2014) that occurs in HCP structure of magnesium. From figure 4.8, fluctuations in

the intensity of planes are observed for peaks $(10\bar{1}0)$, $(10\bar{1}1)$, $(10\bar{1}2)$, $(11\bar{2}0)$, $(10\bar{1}3)$, $(11\bar{2}2)$, $(20\bar{2}1)$ and including the basal plane (0002) . This behavior shows that there is a change in texture during ECAP process with the activation of prismatic and pyramidal slip, which may be influenced by the generation of new grain boundaries. Due to limited slip systems of Mg alloys, strength is greatly influenced by texture modification and slip usually takes place on basal planes. Strength increases with decrease in the grain size up to certain limit, if texture remains constant (Akbaripناه et al. 2013-a). The effect of texture softening is stronger compared to strengthening effect during grain refinement of ECAP 3 and 4 pass. The characteristic feature of ECAP processed samples is their enhanced ductility as compared to the as-cast condition. This may be because of strain hardening occurred in the material. Finally we can observe from figure 4.9. that, even though there was decrease in UTS after 2 passes, UTS and YS of 3 and 4 pass held quite high values compared to as-cast and homogenized alloys.

4.1.3.2 Vickers Microhardness

Vickers microhardness test (H_v) was performed on the ECAP processed sample in a direction perpendicular to the sample flow direction in ECAP die. Figure 4.10 illustrates the relationship between microhardness and number of ECAP passes. With increase in ECAP passes, microhardness value increased from 60 H_v for as-cast sample to 91 H_v for ECAP 2 pass sample. This is because of grain refinement and strain hardening, which causes the grain growth at grain boundaries. But with higher ECAP passes, slight reduction in microhardness values is observed. This may be due to formation or nucleation of new grains which obstructs the effect of strain hardening. Uniformity of microhardness for 1 pass and 2 pass are less compared to 3 pass sample. Enhancement in uniformity of microhardness with increasing ECAP passes may be because of homogeneous microstructure (Shaarbaf and Toroghinejad, 2008). Variation in microhardness is related to UTS and is found to be interdependent with each other.

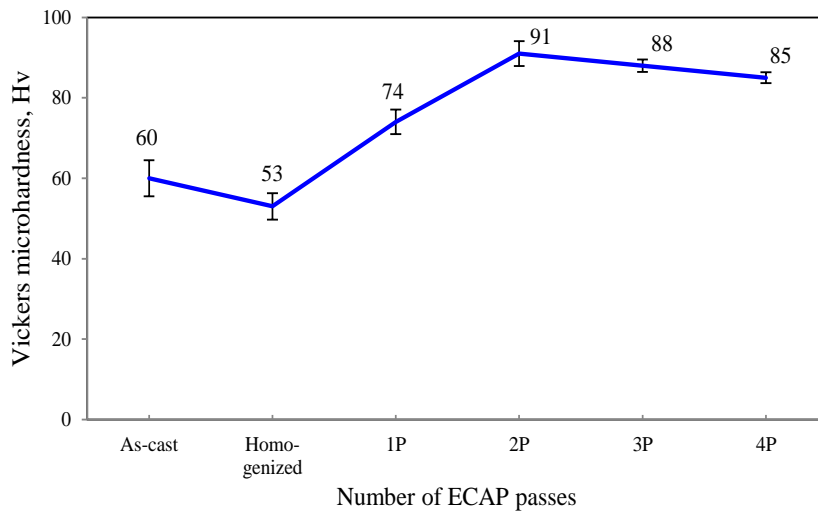


Figure 4.10 Microhardness of homogenized and ECAP processed samples

From figures 4.2 and 4.3, with increase in ECAP passes grain size decreases. But from figure 4.10, microhardness decreases after 3 passes and from figure 4.9, UTS also reduces after 3 passes. This shows that ECAP processed samples do not have the same texture throughout as observed in XRD in figure 4.8. Hardness and grain size can be related based on Hall-Petch relationship (Hakamada et al. 2007).

4.1.3.3 Fractography

SEM images of fractured surfaces (after tensile test) of as-cast, homogenized and ECAP processed at 1, 2, 3 and 4 pass tensile specimens are shown in figure 4.11. Tearing ridges are visible on fractured surface of as-cast, homogenized and one pass ECAP processed samples (Figure 4.11 (a-c)). This is due to plastic deformation of the material. For the 2 pass sample, cleavage planes are observed as shown in figure 4.11 (d). The frequency of cleavage planes decreased as grain size reduced with higher number of ECAP passes and fewer cleavage planes were observed on fracture surfaces for ECAP 4 pass sample. Initially, it looked like a mixed mode of ductile and brittle fracture. After 2 passes, fracture surface with high fraction of fine and equiaxed dimples are observed, which are nearly homogeneous in size and represents the features of ductile fracture.

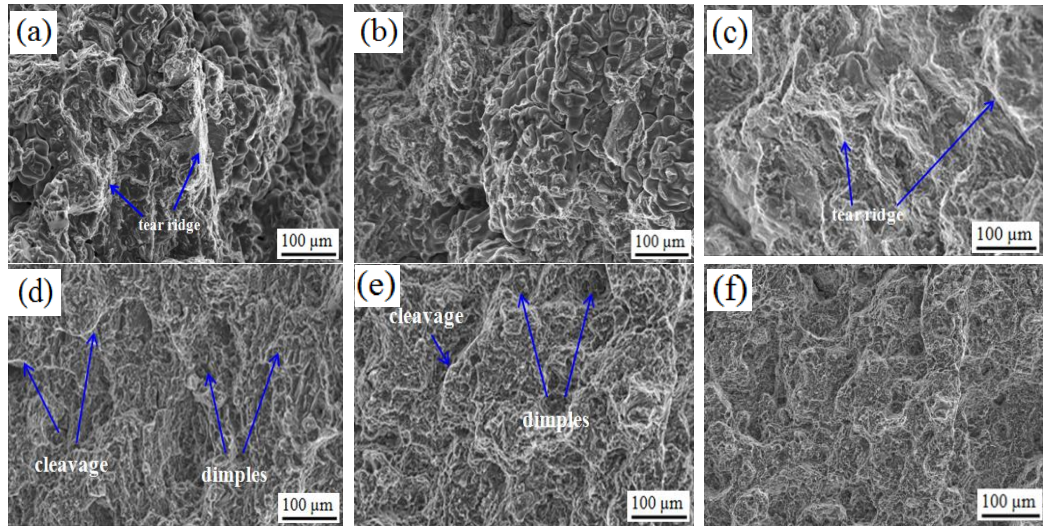


Figure 4.11 SEM images of fractured surfaces (a) as-cast (b) homogenized (c) 1P (d) 2P (e) 3P and (f) 4P samples

4.1.4 Wear behavior

4.1.4.1 Coefficient of friction (COF) during wear test

Wear test carried out for 30 N and 40 N under sliding distance 2500 m and 5000 m. The COF curves are plotted for different loads and sliding distances for unprocessed and ECAP processed samples as shown in figure 4.12 (a) and (b). Figure 4.12 (a) shows the variation in friction for sliding distance 2500 m and in figure 4.12 (b) for 5000 m. Fluctuation is more for sliding distance 2500 m and 5000 m with 30 N load as shown in figure 4.12 (a) and (b).

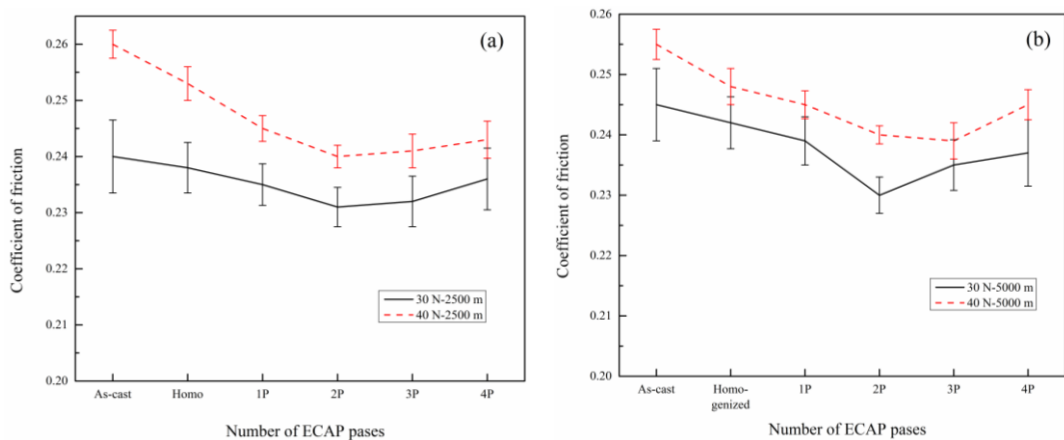


Figure 4.12 COF curves for samples under 30 N and 40 N load with sliding distance (a) 2500 m and (b) 5000 m

In case for 40 N load, no much fluctuation is observed for 2500 m and 5000 m. Variation in coefficient of friction is less for 40 N load compared to 30 N load condition. In figure 4.12, it can be seen that improved COF values are observed for ECAP processed samples compared to unprocessed (as-cast and homogenized) samples under 30 N load and 40 N load for sliding distance 2500 m and 5000 m. ECAP 2 pass sample showed lower coefficient of friction compared to other samples. So, the obtained results demonstrate that the ECAP processed samples showed improvement in COF values. Reduction in fluctuations was observed with higher load may be due to increased contact region between wear sample and steel disc (Li et al. 2010). Above results indicate that the ECAP process decreased the COF values because of their mechanical properties and the processed samples showed improvement in wear resistance.

4.1.4.2 Wear mass loss and wear morphology

Wear mass loss obtained for unprocessed and ECAP processed samples are as shown in figure 4.13. Test was conducted for two different loading (30 N and 40 N) and two different sliding distances (2500 m and 5000 m).

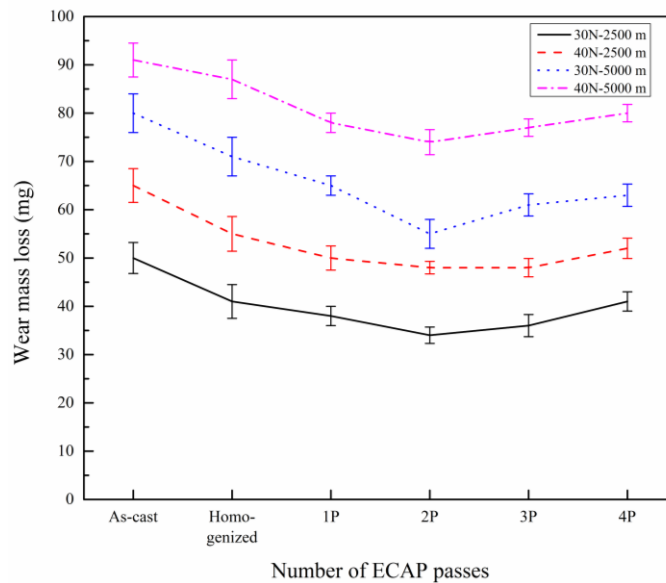


Figure 4.13 Wear mass loss versus number of ECAP passes

It can be observed from figure 4.13 that the wear mass loss decreased as ECAP pass increases as compared to initial condition (as-cast and homogenized) and this indicates increased wear resistance of ECAP processed samples. Wear mass loss is less in case of samples subjected to sliding distance 2500 m with comparison to 5000 m. It is also shown that wear mass loss increased with increasing load and sliding distance for both unprocessed and processed samples. Samples processed through ECAP 2 pass showed lowest wear mass loss as compared to unprocessed samples. The deviation in wear mass loss can be related to microhardness values. ECAP processed samples possess higher microhardness and causes lower wear mass loss compared to initial condition and this is related as explained by Archard equation 4.1 (Archard, 1953).

$$Q = KLF/H \dots\dots\dots (4.1)$$

Where, Q is the wear volume loss, K is the wear coefficient, L is the total sliding distance, F is the applied normal load in the wear test and H is the hardness of the wear surface. Figure 4.14 and 4.15 shows worn surfaces of unprocessed and processed samples for 30 N and 40 N load with sliding distance 2500 m. Figure 4.16 and 4.17 shows worn surfaces of unprocessed and processed samples for 30 N and 40 N load with sliding distance 5000 m.

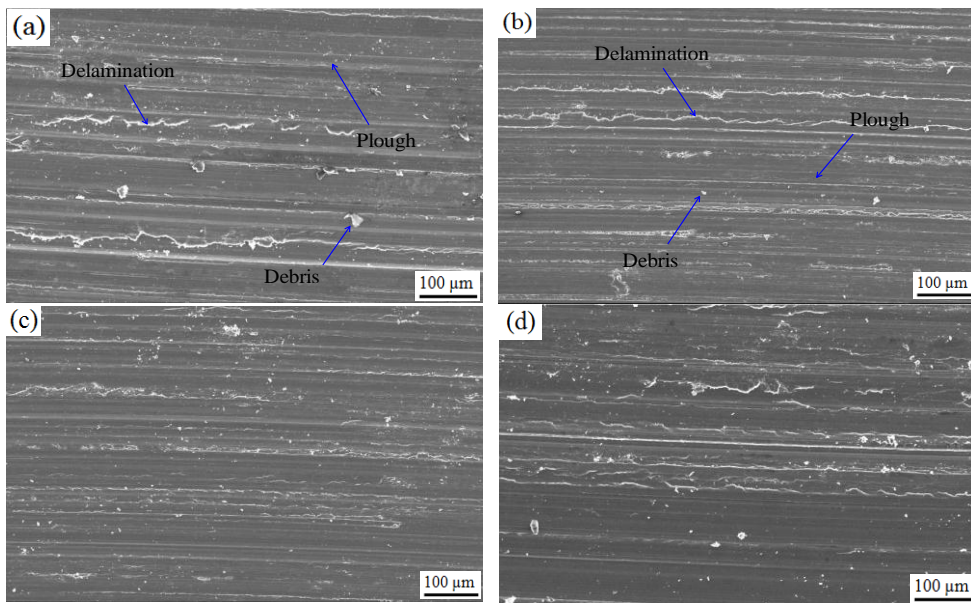


Figure 4.14 SEM images of worn surfaces of (a) Homogenized and ECAP processed (b) 1P, (c) 2P, and (d) 4P samples under 30 N load with sliding distance 2500 m

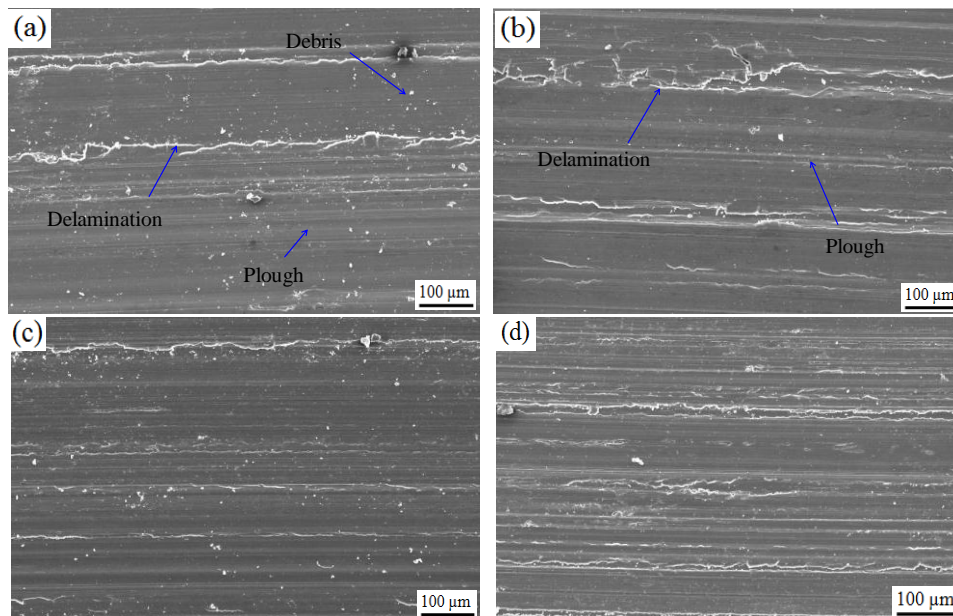


Figure 4.15 SEM images of worn surfaces of (a) Homogenized and ECAP processed (b) 1P, (c) 2P, and (d) 4P samples under 40 N load with sliding distance 2500 m

Delamination and wear debris were observed on the worn surfaces and small grooves were formed by ploughing, parallel to sliding direction which exhibits plastic deformation. From figure 4.14 to 4.17, it was observed that as the ECAP passes increases smooth wear surfaces can be observed, it may be because of enhanced microhardness distribution which hinders fatigue crack that occurred during cyclic sliding process and it reduces the creation of wear debris and also delamination (Xu et al. 2013). Variation of load has not shown much change on the surface morphology. But with the variation of sliding distance, the wear surface morphology is not smooth in case of samples subjected to sliding distance 5000 m (Figure 4.16 and 4.17). From figure 4.14 to 4.17, it is clear that the wear surface consists of delamination, debris and micro-ploughs down the sliding path. So the wear mechanism may be identified as abrasive wear (Xu et al. 2013). With the above discussion, it can be seen that ECAP processed samples possess wear resistance properties. Worn surfaces are also studied with EDS for homogenized and ECAP processed 2 pass samples as shown in figure 4.18 and 4.19 for different loads 30 N and 40 N respectively. EDS was conducted on the areas of delamination, debris and ploughs. From the EDS analysis, it was observed that along with magnesium peaks, oxygen peaks were visible in the areas of delamination, debris and also ploughs.

Magnesium alloys possess high tendency towards oxidation, so it plays major role in wear behavior (Taltavull et al. 2014). Similar chemical composition was observed on wear surfaces of both homogenized and ECAP processed 2 pass samples. So the wear mechanism from the above discussions can be identified as oxidation wear.

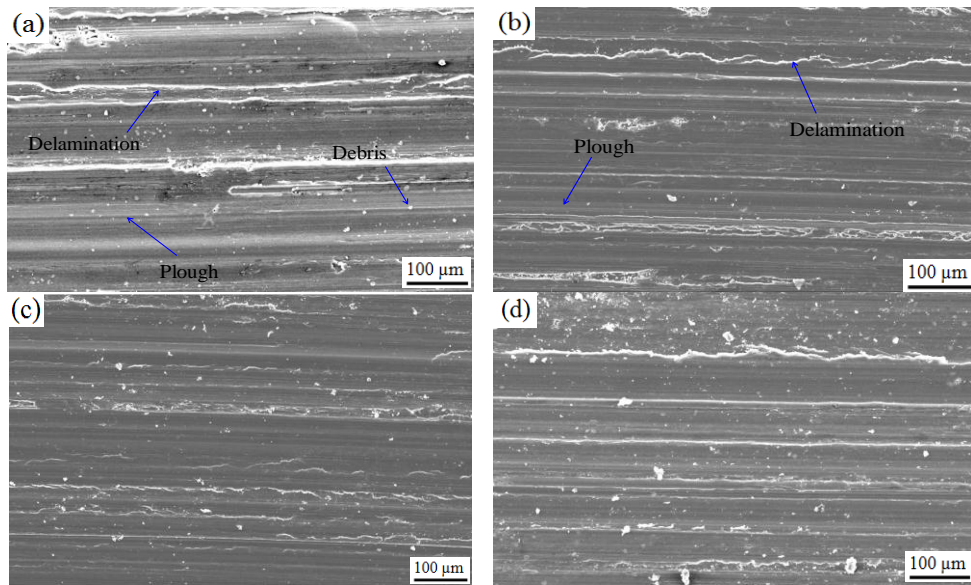


Figure 4.16 SEM images of worn surfaces of (a) Homogenized and ECAP processed (b) 1P, (c) 2P, and (d) 4P samples under 30 N load with sliding distance 5000 m

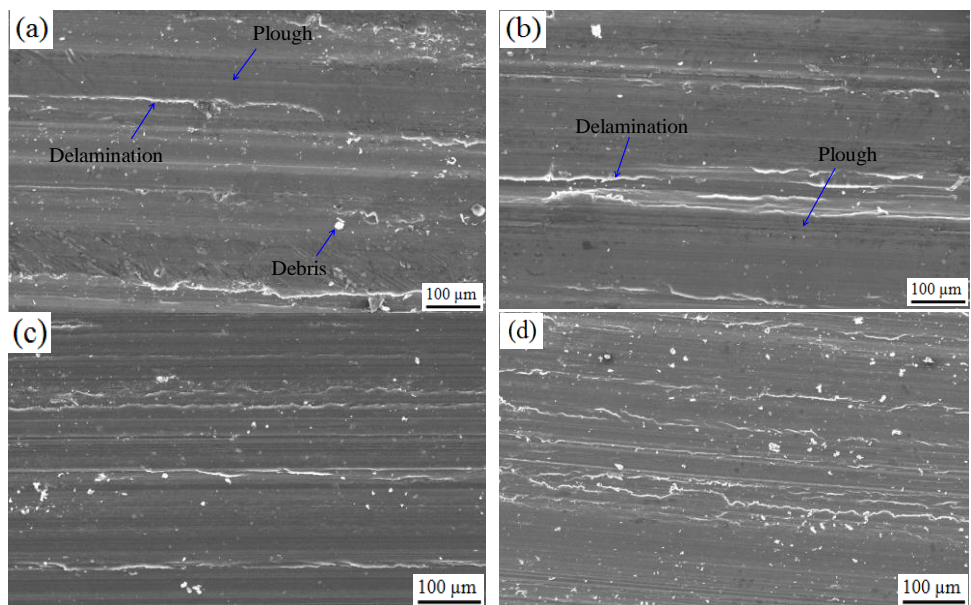


Figure 4.17 SEM images of worn surfaces of (a) Homogenized and ECAP processed (b) 1P, (c) 2P, and (d) 4P samples under 40 N load with sliding distance 5000 m

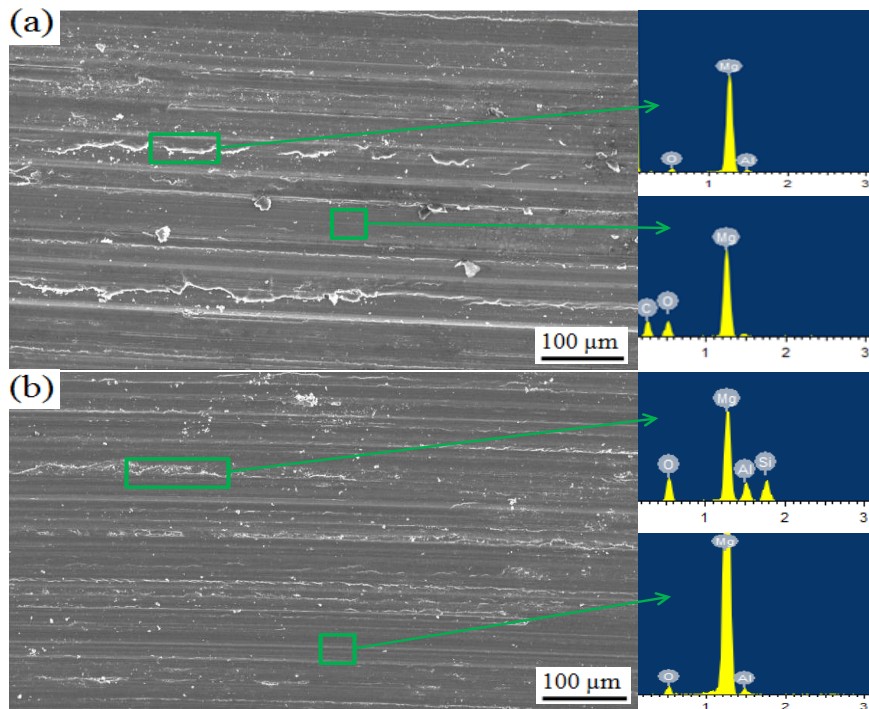


Figure 4.18 EDS analysis for (a) Homogenized and (b) ECAP processed 2P sample under 30 N load

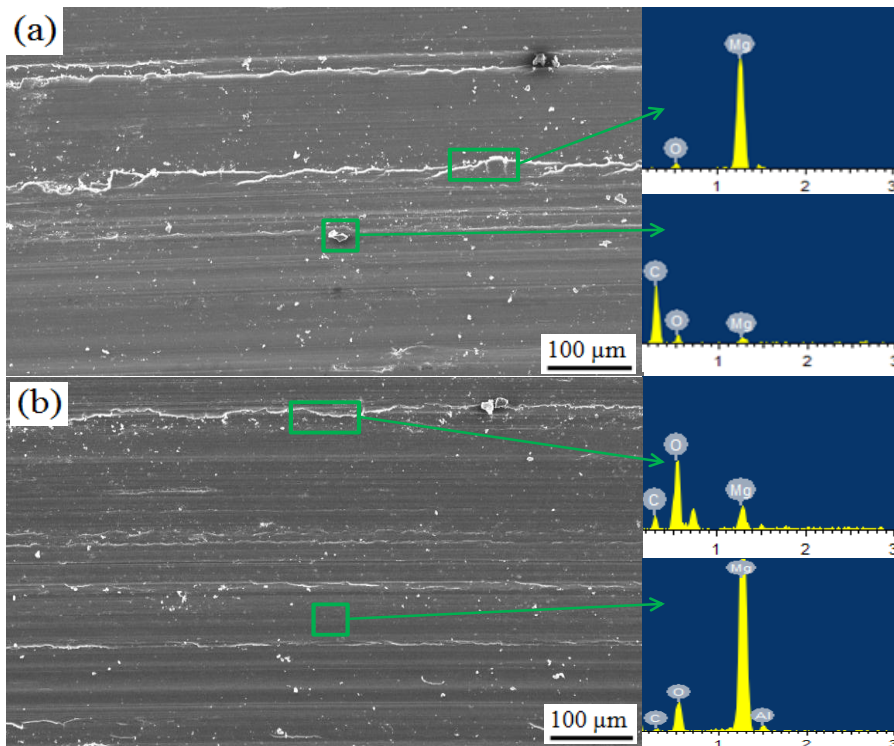


Figure 4.19 EDS analysis for (a) Homogenized and (b) ECAP processed 2P sample under 40 N load

4.1.5 Corrosion behavior

Electrochemical measurements were carried out using EC-biologic SP-150 workstation. Immersion test was conducted for 120 h for unprocessed and ECAP processed samples using 0.1 M NaCl solution.

4.1.5.1 Electrochemical measurements

(a) Potentiodynamic polarization study

Potentiodynamic polarization tests were performed to investigate the corrosion behavior of magnesium alloy and it gives various electrochemical information like corrosion potential (E_{corr}), corrosion current density (I_{corr}) and corrosion rate (mm/y). Tafel extrapolation method gives E_{corr} and I_{corr} values from the anodic part of polarization curves as shown in figure 4.20. Electrochemical kinetics parameters extracted from polarization plots such as E_{corr} , Tafel slopes (β_a & β_c), I_{corr} and corrosion rate (mm/y) are shown in table 4.2. From the figure 4.20, it can be observed that, as the number of ECAP passes increases, E_{corr} value shifted to nobler direction and causes a decrease in I_{corr} value as compared to initial condition. Lower I_{corr} value indicates high corrosion resistance. It can be observed that the corrosion rate and I_{corr} value decreases with increase in number of ECAP passes. But corrosion rate of ECAP 4 pass sample is increased compared to other ECAP processed (1 to 3 pass) samples with increment in I_{corr} value. Decrease in corrosion rate values were observed for ECAP processed samples due to presence of equiaxed ultrafine grains and homogeneously distributed secondary particles (Jiang et al. 2009). The main reason for enhancement in corrosion resistance of grain-refined materials is attributed to an improvement in passive film formation and adhesion due to increased grain boundary density (Ralston and Birbilis, 2010). Ultrafine grains provide better surface coverage which inhibits the rupture of outer $\text{Mg}(\text{OH})_2$ surface which slow down the corrosion rate (Orlov et al. 2011) and also the formation of β phases ($\text{Mg}_{17}\text{Al}_{12}$) which acts as a barrier for corrosion attack and also Al enrichment on the surface which forms the semi-protective Al-rich oxide layer which improves the corrosion resistance of the material (Song 2005 and Prado et al. 2008). Decrease in corrosion rate due to the increased cathodic kinetics attributed to the break-up and redistribution of the

intermetallics. Homogeneous solute distribution could have an effect on the protection of the surface film and presence of Al is beneficial in reducing the anodic reaction kinetics (Orlov et al. 2011). Decrease in corrosion resistance was observed for ECAP 4 pass may be due to increase in dislocations with more ECAP passes which resulted in dislocation accumulation which stores abundant internal energy.

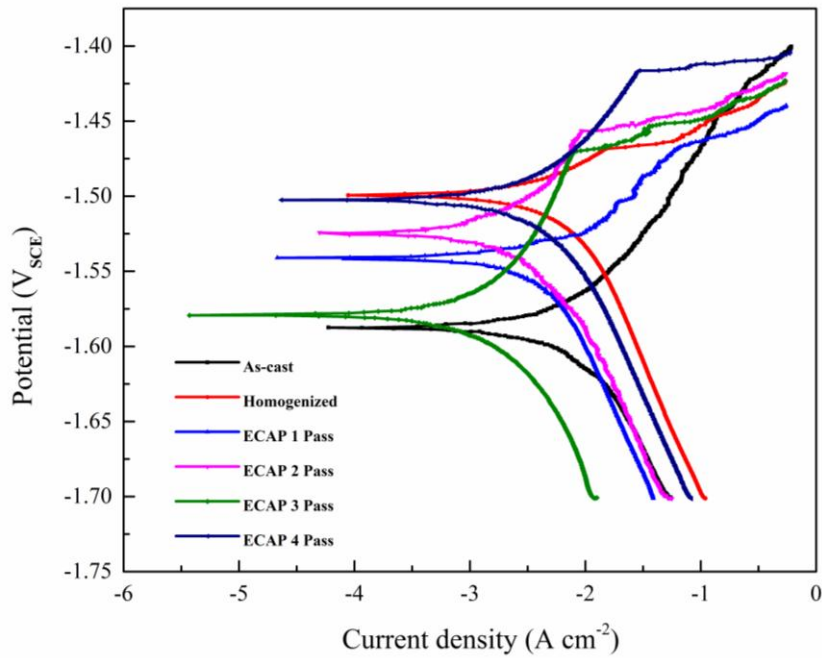


Figure 4.20 Electrochemical potentiodynamic polarization plots of unprocessed and ECAP processed samples

Table 4.2 Electrochemical kinetic parameters like corrosion potential, corrosion current density, Tafel slopes (β_a & β_c) and corrosion rate (mm/y).

Materials	$E_{corr}(V_{SCE})$	I_{corr} ($\mu A/cm^2$)	β_a (mV/decade)	β_c (mV/decade)	Corrosion rate (mm/y)
As-cast	-1.580±0.01	7.93±1	100.3±10	148.4±20	0.171±0.020
Homogenized	-1.495±0.005	7.53±1	39.6±7	171.6±20	0.162±0.020
ECAP 1 Pass	-1.540±0.01	3.51±0.5	36.6±5	178.7±10	0.075±0.010
ECAP 2 Pass	-1.525±0.01	2.97±0.5	33.2±5	181.5±10	0.064±0.010
ECAP 3 Pass	-1.575±0.005	2.16±0.5	32.6±5	186.1±10	0.046±0.010
ECAP 4 Pass	-1.500±0.02	5.59±1	41.3±15	171.8±15	0.120±0.015

Though, dynamic recrystallization occurs during ECAP process, abundant dislocations are still present in the higher ECAP passed samples. Porosity and stability of $\text{Mg}(\text{OH})_2$ protective film could not prevent the penetration of chloride ions and water molecules into the magnesium matrix which causes drastic corrosion reactions, because of the presence of large number of crystalline defects in higher ECAP pass samples. Hydrogen produced by corrosion reaction, further damages the $\text{Mg}(\text{OH})_2$ protective layer to a larger extent and more chloride and water molecules would penetrate and more corrosion reactions takes place (Song et al. 2010). From the above discussion, it can be concluded that increase in corrosion resistance may be because of equiaxed ultrafine grained structure and formation of β phases and corrosion activation of the ECAP 4 pass sample may be due to the presence of larger crystalline defects like energetic grain boundaries and dislocations.

(b) Electrochemical Impedance Spectroscopy (EIS)

Unprocessed and ECAP processed samples were subjected to EIS test to further study the corrosion behavior. Figure 4.21 shows Nyquist plots of samples which are immersed in 0.1 M NaCl solution. The arc represents the metal dissolution in the corrosion process, where diameter of the arc is associated with corrosion resistance (Cao et al. 1990; Pardo et al. 2008). It can be observed that, a second arc in the tail of every arc in the Nyquist plots reveals an inductive manner for all the samples, which relates to the breakage of corrosion protective film. The diameters of capacitive arcs of the ECAP processed samples are increasing with increase in number of ECAP passes. Increase in diameter of capacitive arcs corresponds to the increased corrosion resistance (Song et al. 2010). The first loop i.e., the capacitive arc represents the protective layer in the interface and the second loop i.e., the tail region or second arc represents the points where protective layer is damaged or cracked or separated from the surface and the interface is filled with electrolyte solution (Kral et al. 2011).

For better explanation of corrosion behavior, figure 4.22 shows the equivalent circuit of EIS characteristics. Randles circuit shows the electrochemical systems of metal/oxide layer/electrolyte, where R_s , R_t and C represent the electrolyte or solution resistance, the charge-transfer resistance of the corrosion reaction and the capacitance of oxide film, respectively. Since the inductive behavior is observed in lower

frequencies or tail region of the arc, an inductive element is considered in the Randles circuit. R_L represents the resistance of adsorbed intermediate products and L is the inductance. The inductive part is rather complicated and immaterial in electrochemical corrosion studies and the kinetics information is estimated from the capacitive arc (Song et al. 2011).

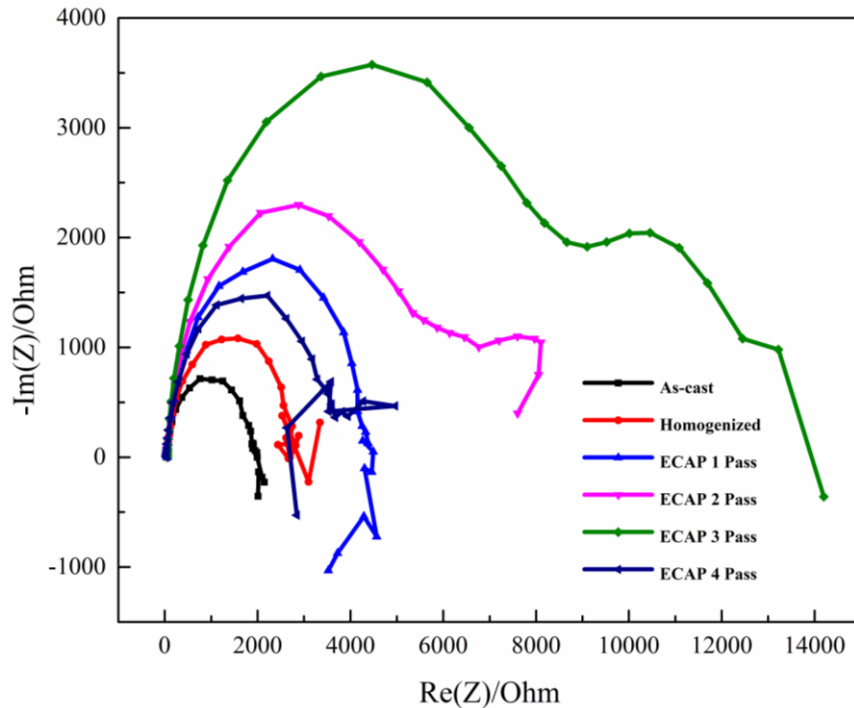


Figure 4.21 Nyquist plots of unprocessed and ECAP processed samples

Figure 4.22 shows the equivalent circuit, which was used to fit the experimental Nyquist plots of the samples by ZSimpwin commercial software to get the parameters of the capacitive arc i.e, the R_t values. Figure 4.23 shows the variation of R_t values versus the number of ECAP passes. Obtained R_t values showed the similar regularity to the variation of capacitive arc diameters. This indicates that the obtained R_t values of ECAP processed samples are larger than that of unprocessed samples and the corrosion resistance of ECAP processed samples was better than unprocessed samples (Minarik et al. 2013) and the values are tabulated in table 4.3. Presence of $Mg(OH)_2$, MgO and β phases ($Mg_{17}Al_{12}$) are observed in XRD of ECAP processed 3 pass corrosion sample as shown in figure 4.24 and it indicates the formation of protective layer on the surface of the sample.

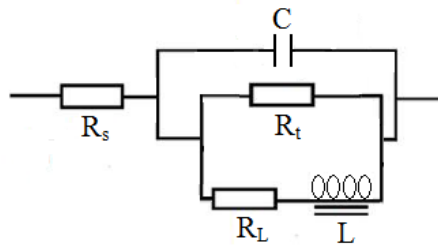


Figure 4.22 Equivalent circuit (Randles circuit) for analyzing of the EIS characteristics

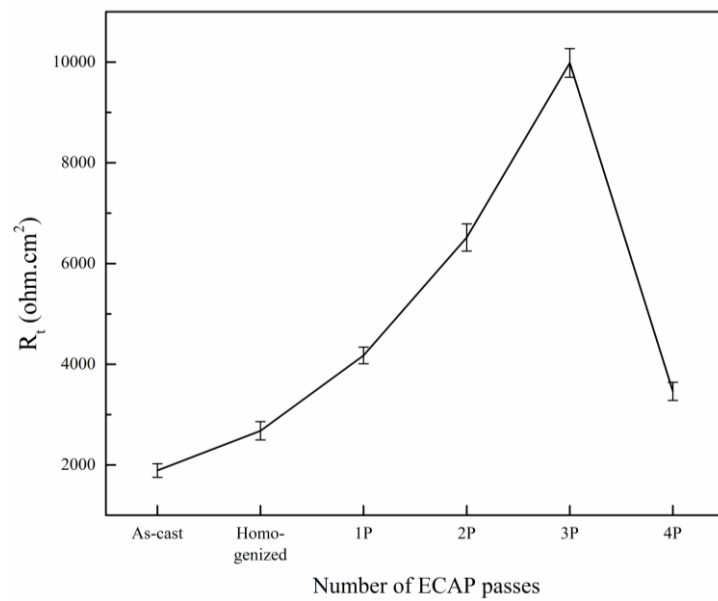


Figure 4.23 R_t verses number of ECAP passes

Table 4.3 Fitted R_t values for unprocessed and ECAP processed sample

Materials	R_t (ohm cm ²)
As-cast	1890±135
Homogenized	2678±182
ECAP 1 Pass	4175±165
ECAP 2 Pass	6517±270
ECAP 3 Pass	9984±285
ECAP 4 Pass	3462±180

SEM images of the corroded surfaces are as shown in figure 4.25. From the figure 4.25, it can be observed that pitting is more in case of unprocessed samples (as-cast

and homogenized) and deep pits are observed. ECAP processed samples constitute of less number of pits and are not deep. With increase in number of ECAP passes, number of pits reduces as shown in figure 4.25.

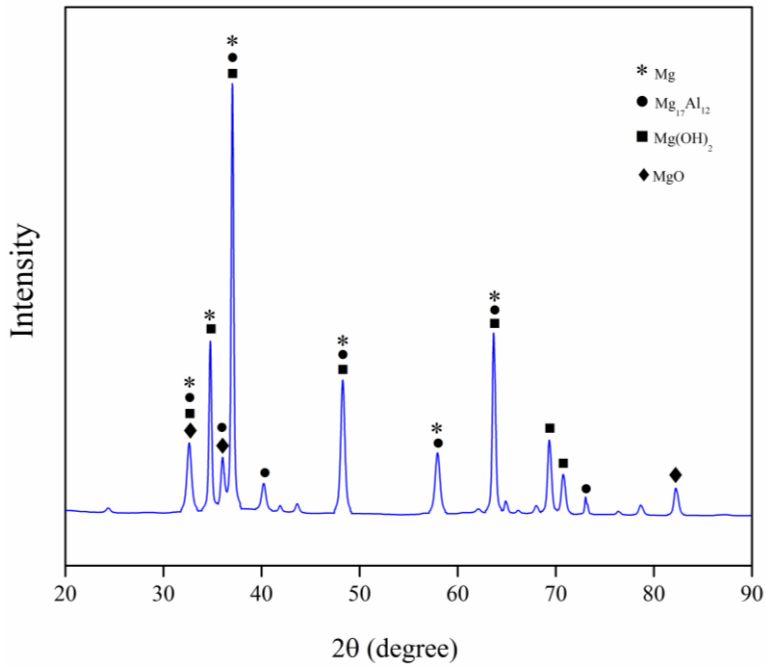


Figure 4.24 XRD of ECAP processed 3 pass corrosion sample

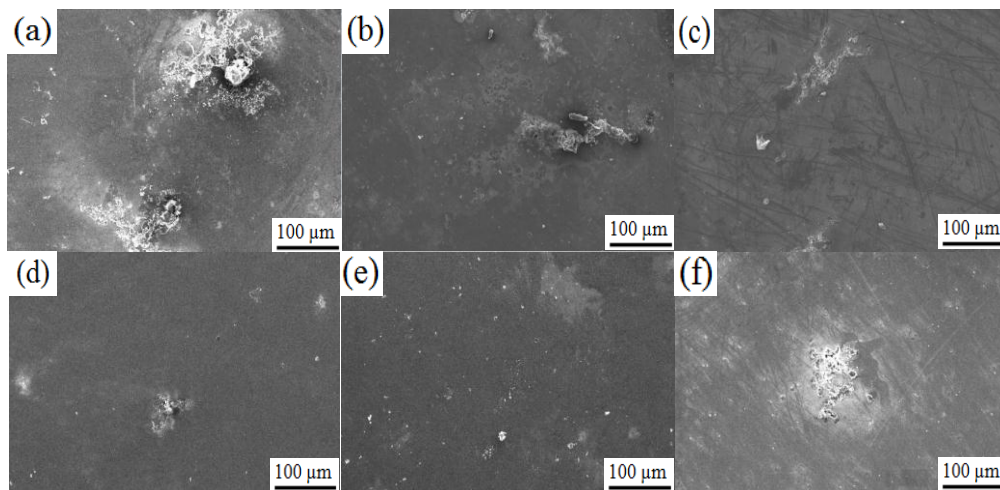


Figure 4.25 SEM images of corrosion samples for different ECAP passes

4.1.5.2 Immersion test

Corrosion resistance of the unprocessed and ECAP processed samples were also estimated by immersion test by hydrogen evolution. Corrosion rate obtained for different conditions is shown in table 4.4. Hydrogen evolution is directly proportional to the corrosion rate. It can be observed that ECAP processed samples showed lower corrosion rate with low hydrogen evolution. SEM images of corroded sample surfaces after immersion test for 120 h in 0.1 M NaCl solution are shown in figure 4.26. ECAP processed samples showed less pits and deeper pits are observed on unprocessed samples. Homogeneous and refined grains and the presence of β phases ($Mg_{17}Al_{12}$) helped in reducing the degradation of ECAP processed samples.

Table 4.4 Corrosion rate of immersed samples verses number of ECAP passes

Material	Corrosion Rate (mm/y)
As-cast	0.330±0.020
Homogenized	0.255±0.020
ECAP 1 Pass	0.135±0.020
ECAP 2 Pass	0.110±0.010
ECAP 3 Pass	0.070±0.010
ECAP 4 Pass	0.160±0.015

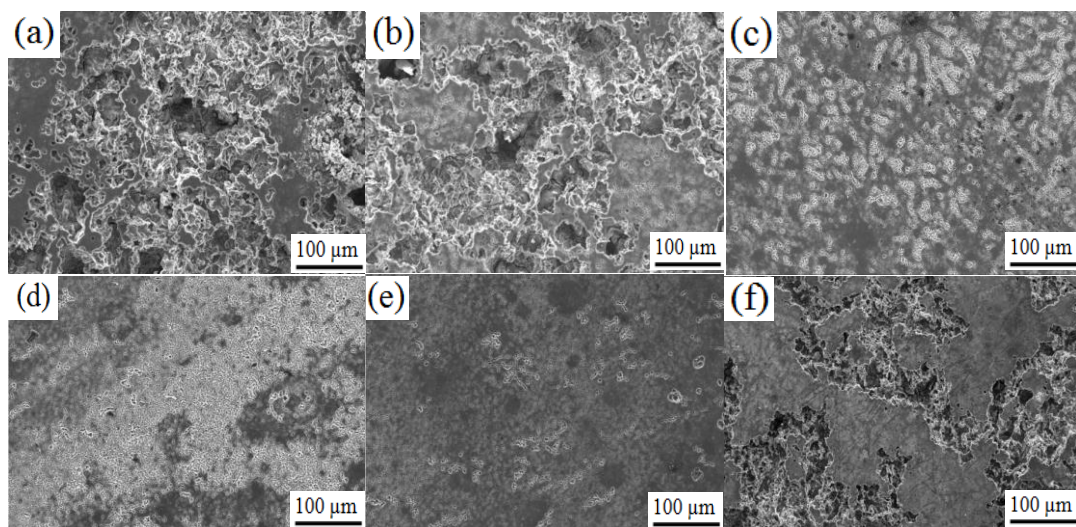


Figure 4.26 SEM images of immersed samples (a) as-cast (b) homogenized and ECAP processed (c) 1P, (d) 2P, (e) 3P, and (f) 4P samples

SEM image with EDS and elemental maps of the surface films after immersion test of ECAP 3 pass sample can be observed from figure 4.27. On the surface of magnesium alloy, including magnesium (Mg), oxygen (O) also present in the surface film and which implies that the surface film consists of magnesium oxide (MgO) and magnesium hydroxide (Mg(OH)₂) (Wang et al. 2009; Liao et al. 2012-a,b). These observations show that the passivity is enhanced and the corrosion on the surface is reduced as the grain size is decreased (Liao et al. 2012-a).

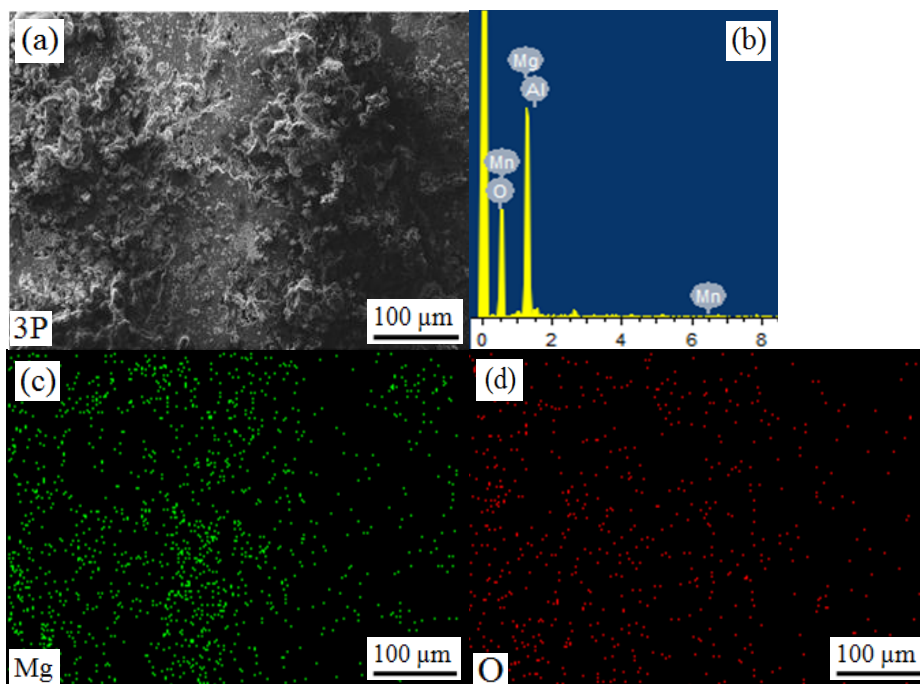


Figure 4.27 SEM images with EDS and elemental mapping of ECAP 3P sample

4.2 Summary

ECAP has been carried out on AM70 magnesium alloy to study microstructural changes, mechanical, wear and corrosion properties using route B_C. The obtained results are summarized as below:

1. AM70 alloy was successfully processed by ECAP up to 4 passes at 275 °C using route B_C. The grain size reduced to an average of 1 μm. Initially, the microstructure was bimodal and as the number of ECAP passes increased, homogeneous structure was observed. Dynamic recrystallization was

found to be the mechanism for grain refinement. EBSD results showed that frequency of HAGBs increased with increase in strain rate.

2. UTS increased up to 2 passes of ECAP processing, which came 112% and 34% larger as compared to that of as-cast and homogenized samples, respectively. Increase in UTS is attributed to grain boundary strengthening mechanism. YS increased up to 2 passes of ECAP processing, which came 188 and 79% larger as compared to that of as-cast and homogenized samples, respectively. Ductility for ECAP 2 pass sample came 20.7%, while it was just 3.1% for the as-cast sample. With further ECAP passes, strength and ductility reduced but the obtained results still held higher values as compared to that of as-cast condition. Fracture surface of ECAP-processed alloy showed fine and equiaxed dimples type of fracture, which signify ductile fracture behavior.
3. Hardness increased up to ECAP 2 pass and decreased with further passes. Hardness exhibited the same trend as UTS, thus, the two test results seemed to be interdependent on each other.
4. COF decreased for ECAP 2 pass sample as compared to unprocessed condition and lower fluctuation in COF values was found at 40 N load in comparison to 30 N load. Reduced COF values showed better wear resistance property for ECAP 2 pass sample.
5. ECAP 2 pass sample showed increased wear resistance properties as compared to unprocessed samples. Wear mass loss of ECAP processed samples reduced by ~1.47 (2500 m) and ~1.45 (5000 m) times under 30 N load and ~1.35 (2500 m) and ~1.22 (5000 m) times under 40 N load compared to as-cast condition.
6. SEM micrographs showed the occurrence of delamination, plowing, and wear debris on the wear surface. ECAP 2 pass sample exhibited smoother wear surface as compared to unprocessed condition due to uniform hardness distribution throughout the sample surface. EDS analysis identified the presence of oxygen peaks along with magnesium peaks on the sliding surface, and wear mechanism was identified as abrasion and oxidation wear.

7. Potentiodynamic polarization test showed reduced I_{corr} value for the ECAP processed samples. EIS plots showed better corrosion resistance properties of ECAP 3 pass sample and R_t values increased by ~5.28 and ~3.72 times in comparison to as-cast and homogenized samples due to refined microstructure and formation of β phases. Immersion test exhibited lower corrosion rate with low hydrogen evolution for ECAP processed samples compared to unprocessed condition.

CHAPTER 5

RESULTS AND DISCUSSION

5.1 Equal channel angular pressing of AM80 alloy

AM80 alloy was processed by ECAP at 275 °C up to 4 passes using route B_C. Microstructures of as-cast, homogenized and ECAP processed samples were characterized using OM, SEM and TEM. Samples are also analyzed by EBSD for grain structure and grain boundaries misorientation angles and XRD was conducted to identify the different phases in the samples. Tensile and microhardness test was carried out for samples up to 4 passes. Tribological properties were studied by pin-on-disc dry sliding wear test machine and corrosion test was conducted by electrochemical measurements and immersion test methods for unprocessed and ECAP processed samples. The obtained results are discussed in the following sections.

5.1.1 Microstructure analysis

Microstructure of as-cast, homogenized and ECAP processed samples from 1 to 4 ECAP passes was observed in optical microscope and is as shown in figure 5.1 (a-f). During first pass, coarse grains broke into many finer grains with some larger grains around the smaller grains appearing to be bimodal in structure. Bimodal grain structure is due to limited number of slip systems in magnesium and magnesium alloys. Therefore the grains which are oriented in favorable direction are initially deformed and gets refined during ECAP process and the grains which are less deformed or larger grains are present within the microstructure (Janecek et al. 2012). The rate of grain refinement was more during the first pass because of higher dislocation rate (Jahadi et al. 2014). Homogeneous and equiaxed microstructure was noticed after ECAP 2 pass and it may be due to dynamic recrystallization during ECAP or static recrystallization during initial heating of the sample for required temperature before ECAP pressing was done (Akbaripanah et al. 2013-b). ECAP

process leads to homogeneous grains and also produces small sub-grains which make microstructure finer and homogeneous with increase in ECAP passes up to a certain limit (Feng and Ai, 2009). Volume fraction of finer grains increases with higher ECAP passes with reduction in larger grains. Grain size of as-cast, homogenized and ECAP processed samples from 1 to 4 pass was measured and to be an average of 80, 100, 65, 45, 8 and 3 μm , respectively using linear intercept method. Reduction of grain size in the ECAP processed material shows that the current process with Φ of 110° and Ψ of 20° is effective.

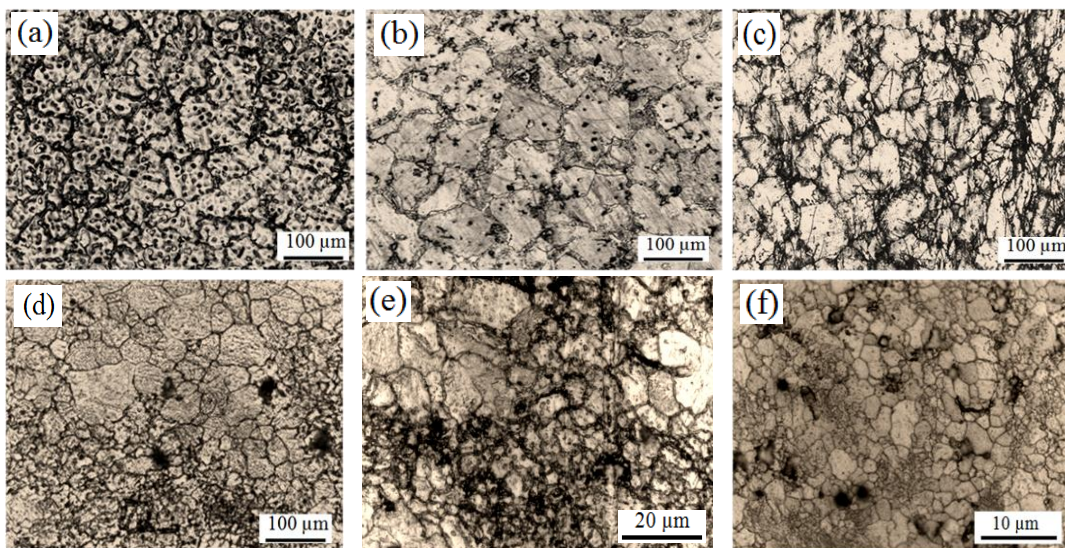


Figure 5.1 Microstructures of (a) as-cast (b) Homogenized (c) 1P (d) 2P (e) 3P and (f) 4P ECAP samples

SEM images of AM80 magnesium alloy samples of unprocessed (as-cast and homogenized) and ECAP processed up to 4 passes are as shown in figure 5.2. XRD profile shows the existence of different phases in as-cast and ECAP processed 2 and 4 pass samples. Grain sizes of unprocessed and ECAP processed samples are represented in figure 5.3. TEM images of ECAP processed 4 pass samples are as shown in figure 5.4 with selected area electron diffraction (SAED) patterns.

High dislocation density was observed in figure 5.4 (a). Larger strains lead to the generation of more number of dislocation walls which forms more sub-grains during DRX process (Feng and Ai, 2009). Spots which are observed on SAED patterns are diffraction spots arranged in form of circle that indicates large portion of high angle grain boundaries (HAGBs) as shown in figure 5.4 (b).

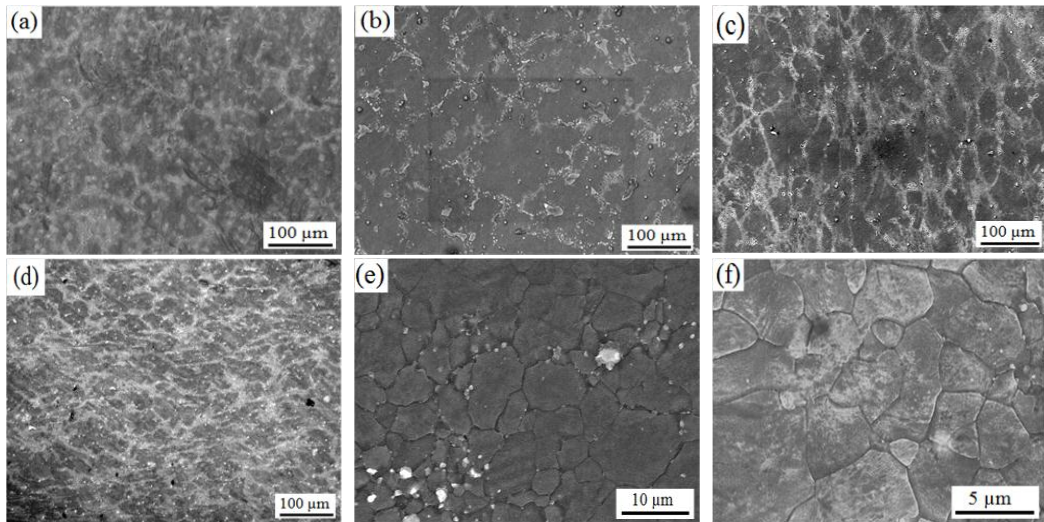


Figure 5.2 SEM micrographs of ECAP (a) as-cast (b) Homogenized (c) 1P (d) 2P (e) 3P and (f) 4P samples

Figure 5.5 shows Orientation Imaging Microscopy (OIM) of AM80 alloy for as-cast and ECAP processed 4 pass sample with inverse pole figure (IPF). IPF map shows the crystal orientations with different colors. Heterogeneous structure can be observed in as-cast sample and in case of ECAP processed 4 pass sample homogeneous microstructure with refined grains can be observed as shown in figure 5.5.

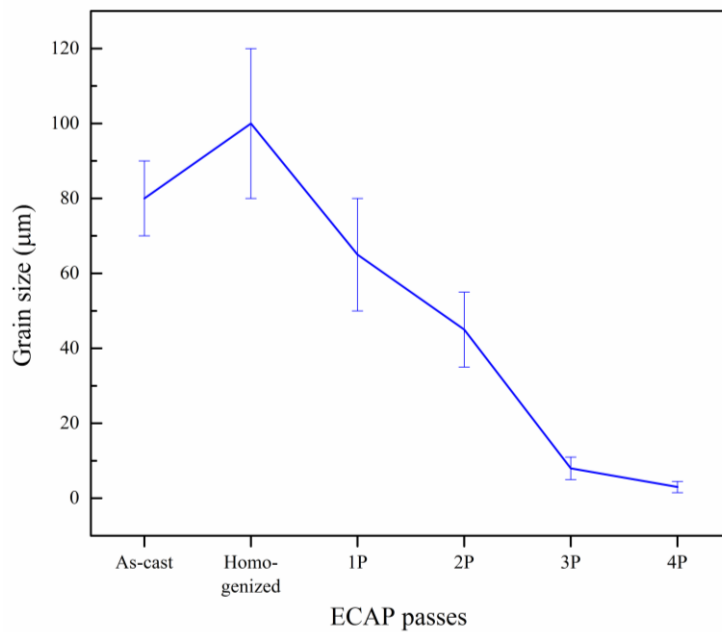


Figure 5.3 Grain size of as-cast, homogenized and ECAP processed samples

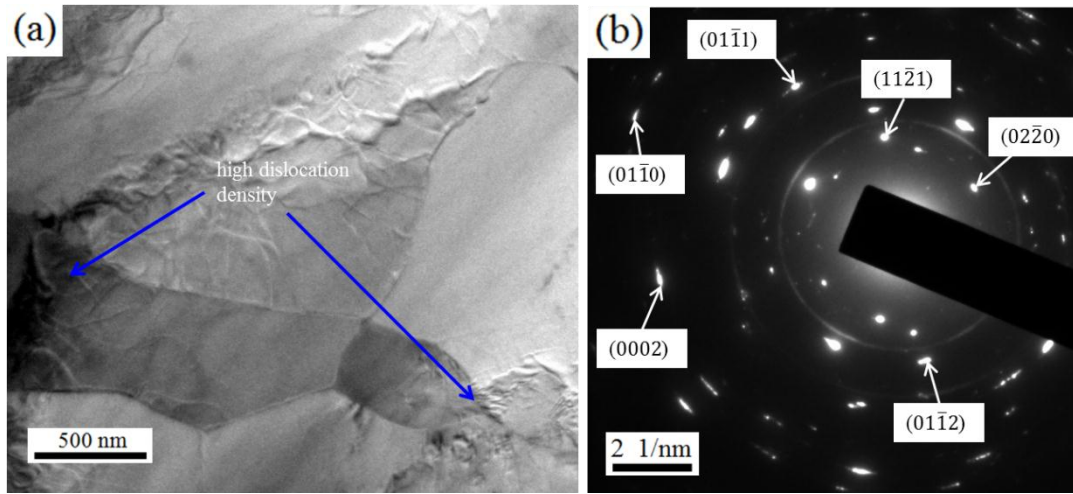


Figure 5.4 TEM images of ECAP 4 pass sample

Misorientation angles distribution for as-cast and processed samples are shown in figure 5.6. Growth of misorientation are identified in larger fraction at an angle of $\sim 40^\circ$ to $\sim 90^\circ$, i.e., with higher passes frequency of HAGBs increases ($>15^\circ$) as strain increases. The rate of misorientation is reduced below 20° for ECAP 4 pass sample when compared with as-cast sample as shown in figure 5.6.

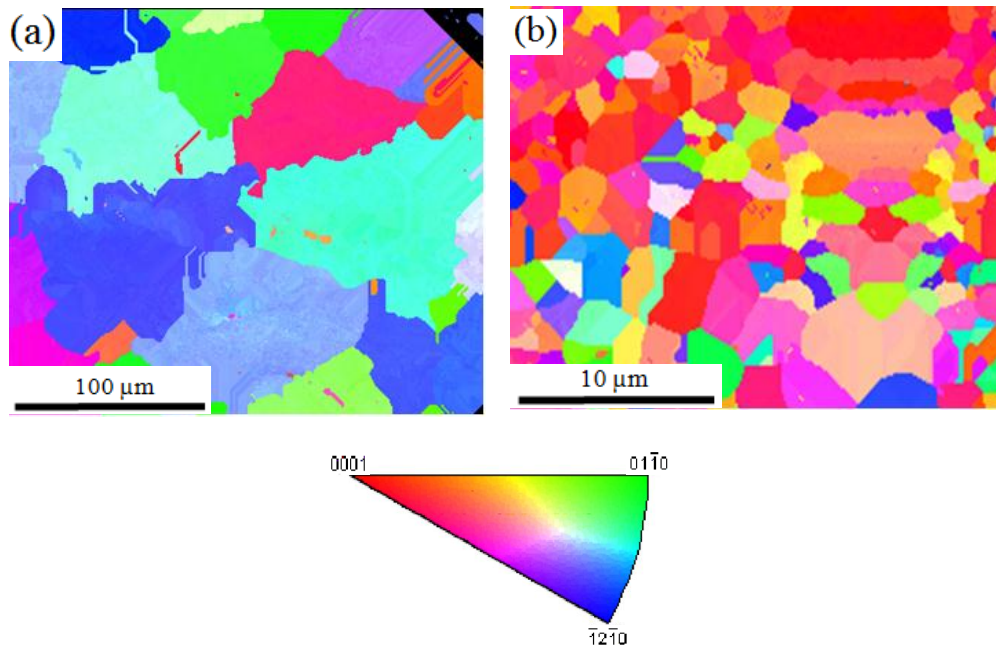


Figure 5.5 OIM with IPF image of (a) as-cast and (b) ECAP 4P samples

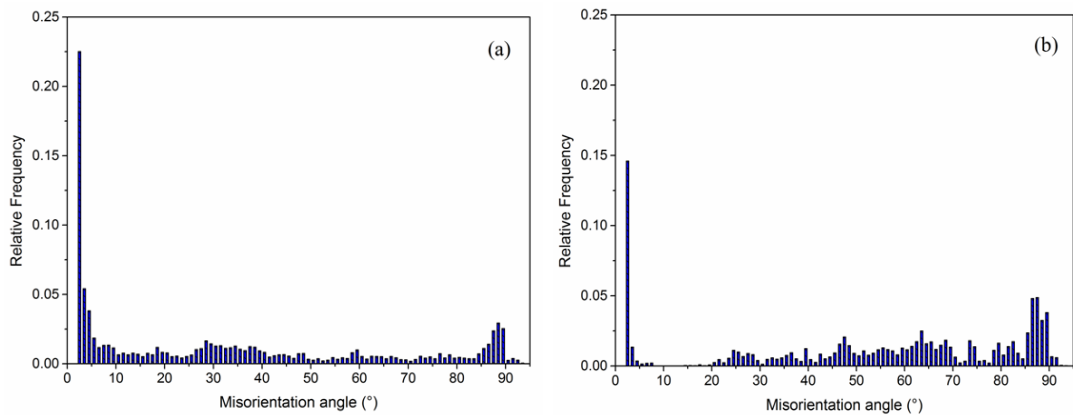


Figure 5.6 Misorientation angle grain distribution of (a) as-cast and (b) ECAP 4 pass sample

It was observed from figure 5.1 (e) and (f), grain refinement rate was reduced at higher passes and also as strain increases, an evolution from LAGBs to HAGBs takes place, leading to a stable microstructure, because of the occurrence of dynamic recrystallization (Dumitru et al. 2014). As the rate of LAGBs has declined with the increment in HAGBs during higher ECAP passes, there was no much drastic change in grain size. Small portion of recrystallized grains increases as strain increases during recrystallization because of higher rate of nucleation, which leads to relatively homogeneous microstructure with finer grains as represented in figure 5.1 (f) and 5.2 (f). Attained results indicates that refinement rate is more during initial stages of ECAP and further ECAP passes results in more HAGBs rather than grain refinement (Biswas et al. 2010; Jin et al. 2006).

5.1.2 X-ray diffraction analysis

X-ray diffraction of as-cast and ECAP processed 2 and 4 pass samples are as shown in figure 5.7. Variation of intensities of peaks can be observed with increase in number of ECAP passes along with the intermetallic phases ($Mg_{17}Al_{12}$, Mg_2Al_3 and $MnAl_6$). Increase in precipitation of $Mg_{17}Al_{12}$ and $MnAl_6$ is observed at $\sim 58^\circ$ and $\sim 70^\circ$ for ECAP 2 pass sample. Therefore increase in mechanical properties is observed in ECAP 2 pass sample. Plane (10 $\bar{1}$ 1) is showing similar intensity for unprocessed and ECAP processed samples. It can be observed that for plane (0002), high intensity was witnessed for ECAP 4 pass in comparison to as-cast sample.

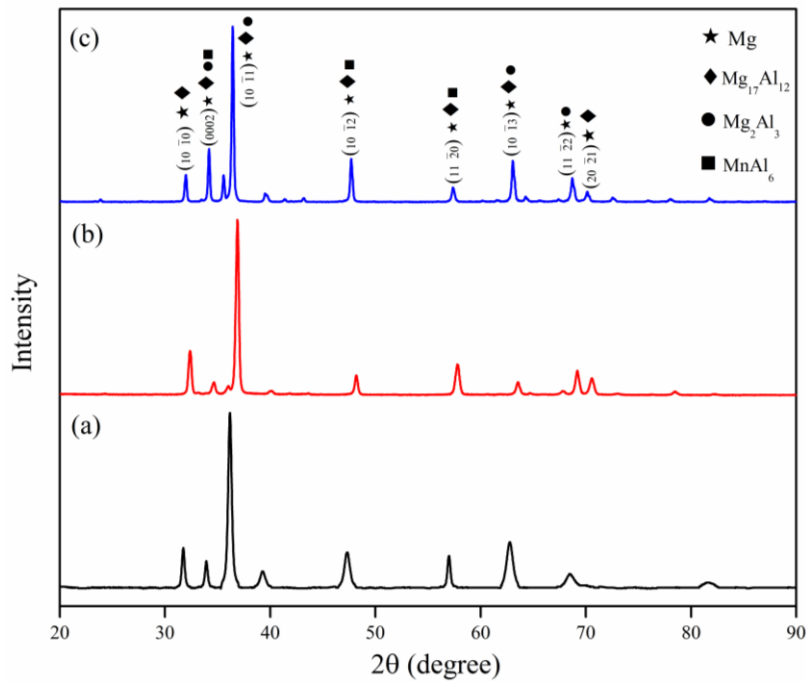


Figure 5.7 XRD profile of (a) as-cast (b) ECAP 2 pass and (c) ECAP 4 pass samples

This may be due to increase in ECAP passes and as the ECAP passes increases intensity of peaks appears to be increased showing strong intensity for processed samples as shown in figure 5.7. Along with the basal plane, more fluctuations are observed for $(10\bar{1}0)$, $(10\bar{1}1)$, $(10\bar{1}2)$, $(11\bar{2}0)$, $(10\bar{1}3)$, $(11\bar{2}2)$ and $(20\bar{2}1)$ planes. These variations may be due to grain refinement and also texture modifications during the process of ECAP. It has happened due to activation of prismatic and pyramidal slip, which is caused by the influence of grain boundaries (Dumitru et al. 2014). Generally, crystallographic texture is very important in case of HCP materials (Feng and Ai, 2009). This factor changes during ECAP process due to plastic deformation. Shear deformation eliminates the existing texture and forms the new texture during the ECAP process (Kim et al. 2003).

5.1.3 Mechanical properties

5.1.3.1 Tensile behavior

Tensile tests are conducted for as-cast, homogenized and ECAP processed samples up to 4 pass and the results are represented in figure 5.8 and the summary of the mechanical properties are shown in table 5.1. Maximum ultimate tensile strength

obtained for ECAP 2 pass sample was 310 MPa as compared to UTS of as-cast (138 MPa) and homogenized (144 MPa) samples. UTS increased up to 2 pass and decreased with further ECAP passes i.e., for 3 pass (246 MPa) and 4 pass (205 MPa). Yield strength (YS) obtained for ECAP 2 pass sample was 160 MPa, which is 100% and 45.5% larger as compared to as-cast (80 MPa) and homogenized (110 MPa) samples. YS obtained for 3 pass and 4 pass samples are 140 MPa. Increase in strength may be due to grain boundary strengthening mechanism, where the size of the grains gets reduced as explained by Hall-Petch equation (Valiev et al. 2006; Figueiredo and Langdon, 2010). Variation in ductility may be due to strain hardening occurred in the material with different passes (Kim and Kim, 2004). Decrease in strength after 2 passes is because of weak texture. ECAP process increases the tensile strength with reduction in grain size at room temperature with increase in dislocation density. But at high temperature, the recovery process plays a major role where the tensile strength reduces with ECAP process (Feng and Ai, 2009). Higher ECAP passes leads to the formation of new basal texture due to which basal planes of most of the grains will tilt towards extrusion direction along with higher basal slip Schmid factor value, which results in lower strength properties (Mostaed et al. 2015).

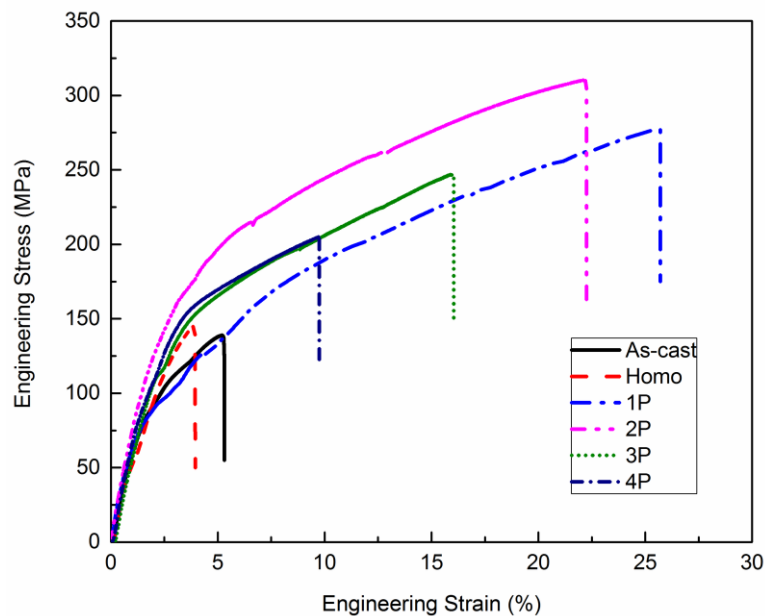


Figure 5.8 Tensile properties for as-cast, homogenized and ECAP processed samples

Table 5.1 Mechanical properties of AM80 alloy processed by ECAP up to 4 passes.

ECAP passes	UTS (MPa)	YS (MPa)	% Elongation
As-cast	138±7.5	80±5.5	5.3±0.10
Homogenized	144±5.2	110±7.2	3.9±0.08
1 Pass	277±8.5	80±8.7	26.5±0.10
2 Pass	310±7.3	160±5.4	22.2±0.08
3 Pass	246±5.7	140±4.5	16±0.12
4 Pass	205±12.2	140±6.3	9.7±0.10

5.1.3.2 Vickers Microhardness

Samples were subjected to microhardness test to find the distribution of hardness. Figure 5.9 illustrates the relationship between microhardness and number of ECAP passes. With increase in ECAP passes, microhardness value increased from 68 Hv for homogenized samples to 91 Hv for 2 pass sample. Large increase in hardness during initial stages of ECAP passes could be directly attributed to strain hardening rather than grain refinement (Shaarbaaf and Toroghinejad, 2008).

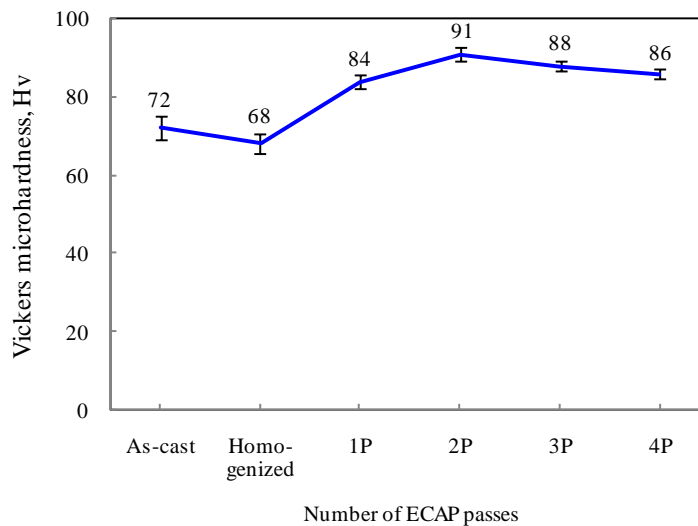


Figure 5.9 Microhardness values of homogenized and ECAP processed samples

With increase in ECAP passes, microhardness values enter into a steady state, where it reduces marginally with decrease in grain size. Stabilization of hardness is because

of nucleation of new recrystallized grains, which hinders strain hardening effects (Su et. al 2008). Hardening behavior showing saturation was reported by Nakashima et. al (2000), Xing et. al (2002), Shaarbaaf and Toroghinejad (2008).

5.1.3.3 Fractography

Figure 5.10 illustrates the fracture surfaces of as-cast, homogenized and ECAP processed at 1, 2, 3 and 4 pass samples. Fracture surfaces become smoother with increase in number of ECAP passes with grain size reduction. Tearing ridges are visible on fractured surface of unprocessed and ECAP 1 pass sample (Figure 5.10 (a-c)) and may be due to plastic deformation at grain boundaries. In hcp metals, like magnesium cleavage arise on basal plane (0002) and it appears as quasi-cleavage fracture in which tear ridges appear (Akbaripanah et al. 2013-a). At higher ECAP passes, cleavage planes are observed (Figure 5.10 (d) and (e)) and frequency of tearing ridges and cleavage planes decreases as grain size gets refined with higher passes. Fewer cleavage planes were observed on fracture surfaces for ECAP 4 pass sample. Initially, surface looks like mixed mode of fracture of ductile-brittle type. After ECAP 2 pass, fracture surface with high fraction of fine and equiaxed dimples was observed nearly homogeneous in size and increased abundantly, which represents the feature of ductile fracture behavior.

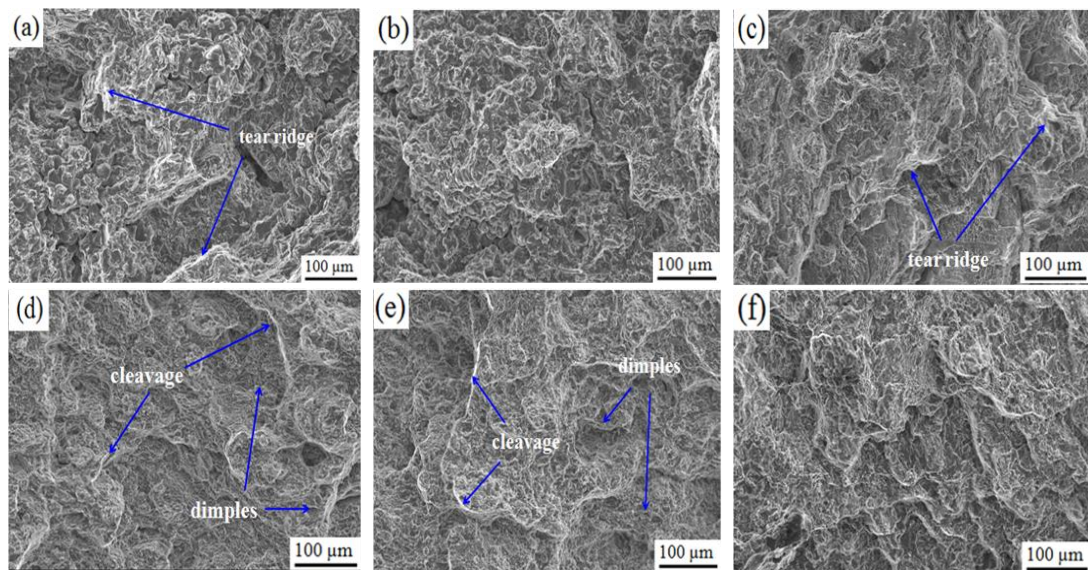


Figure 5.10 SEM micrographs of fractured surfaces (a) as-cast (b) homogenized and ECAP (c) 1P (d) 2P (e) 3P and (f) 4P samples

5.1.4 Wear behavior

5.1.4.1 Coefficient of friction (COF) during wear test

Samples are subjected to wear test under two different loading conditions 30 N and 40 N, with two sliding distance of 2500 m and 5000 m at a constant speed of 3 m/s and track diameter 110 mm. Figure 5.11 (a) and (b) shows the variation of COF with number of ECAP passes for sliding distances of 2500 m and 5000 m. More fluctuation in COF is seen in case of samples subjected to 30 N load compared to samples subjected to 40 N load. Lower COF values were observed in ECAP 2 pass samples. Fluctuations reduced with 40 N load due to increase in surface contact between sample and steel disc during wear test (Li et al. 2010). With the above discussion it can be concluded that ECAP process leads to the decrement of COF values due to their hardness properties and exhibited wear resistance properties.

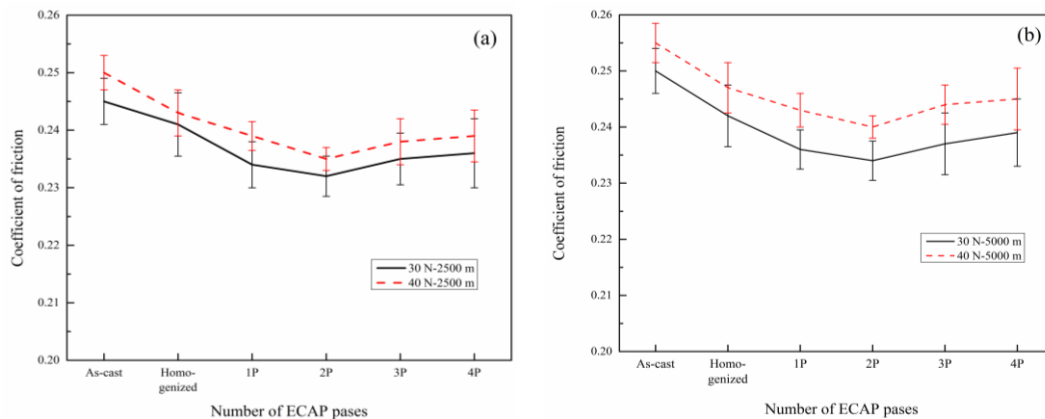


Figure 5.11 COF curves for samples under 30 N and 40 N load with sliding distance (a) 2500 m and (b) 5000 m

5.1.4.2 Wear mass loss and wear morphology

Figure 5.12 shows the relationship between wear mass loss and number of ECAP passes for different load conditions. ECAP processed samples showed minimum wear mass loss which indicates the increased wear resistance property of ECAP processed samples. With increase in load and sliding distance the wear rate increases for unprocessed and processed samples as shown in figure 5.12.

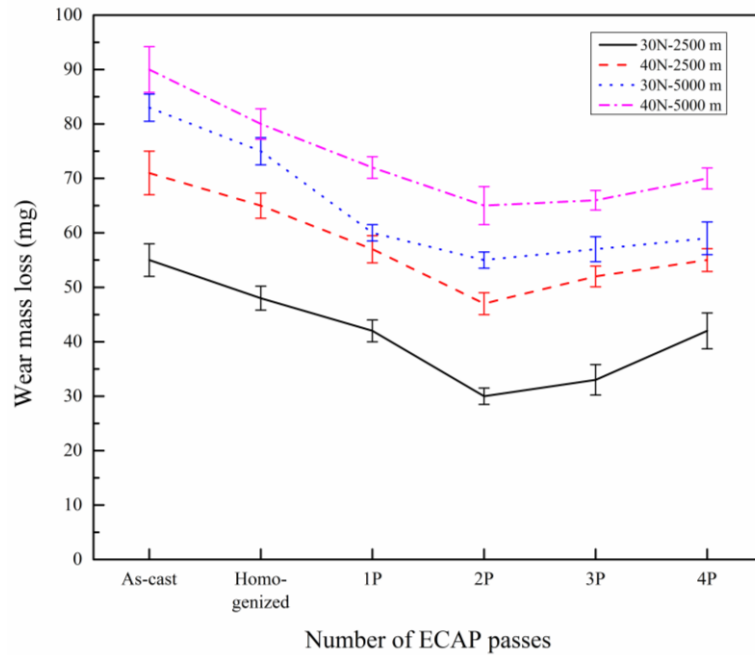


Figure 5.12 Wear mass loss versus number of ECAP passes

As ECAP pass increases the wear mass loss reduced up to ECAP 2 pass but increased with further passes (ECAP 3 and 4 pass) due to decrease in hardness of the sample. Increase in wear mass loss after ECAP 2 pass is related to hardness of the processed samples and is related by Archard equation. Decrease in hardness of the ECAP processed sample after 2 pass is due to nucleation of new grains during higher ECAP passes (Gopi et al. 2016). Worn surfaces showed the features of delamination, ploughing and wear debris in the sliding direction. Delaminations are caused due to initiation and propagation of subsurface cracks, resulted during removal of material in the form of flakes or wear debris as shown in figure 5.13 to 5.16. Ploughing is caused due to the interaction of hard particles between disc and the sample surfaces, which cause wear by removing material in the form of small fragments. It can be observed that the delamination, ploughing and wear debris are reduced on the samples processed by ECAP up to two passes. During cyclic sliding process, it avoids the formation of wear debris and delamination, where material gets detached due to crack formation in perpendicular to sliding direction (Xu et al. 2013). Variation of load has not shown much change on the surface morphology. The above results showed the wear mechanism may be identified as abrasive wear due to formation of delamination and wear debris and the processed samples have better wear resistance properties.

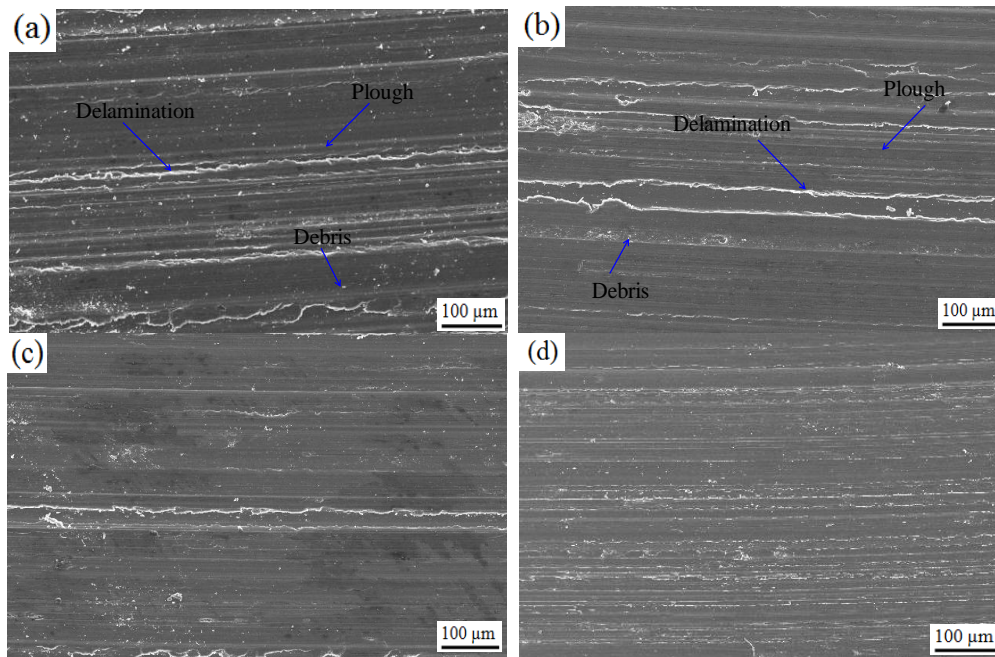


Figure 5.13 SEM images of worn surfaces of (a) Homogenized and ECAP processed (b) 1P, (c) 2P, and (d) 4P samples under 30 N load with sliding distance 2500 m

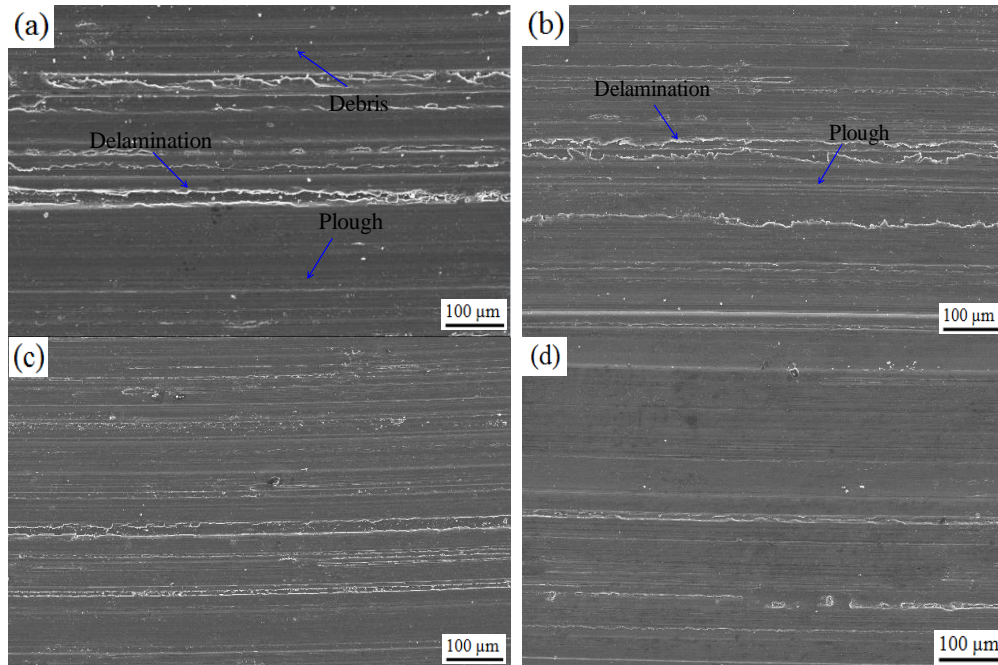


Figure 5.14 SEM images of worn surfaces of (a) Homogenized and ECAP processed (b) 1P, (c) 2P, and (d) 4P samples under 40 N load with sliding distance 2500 m

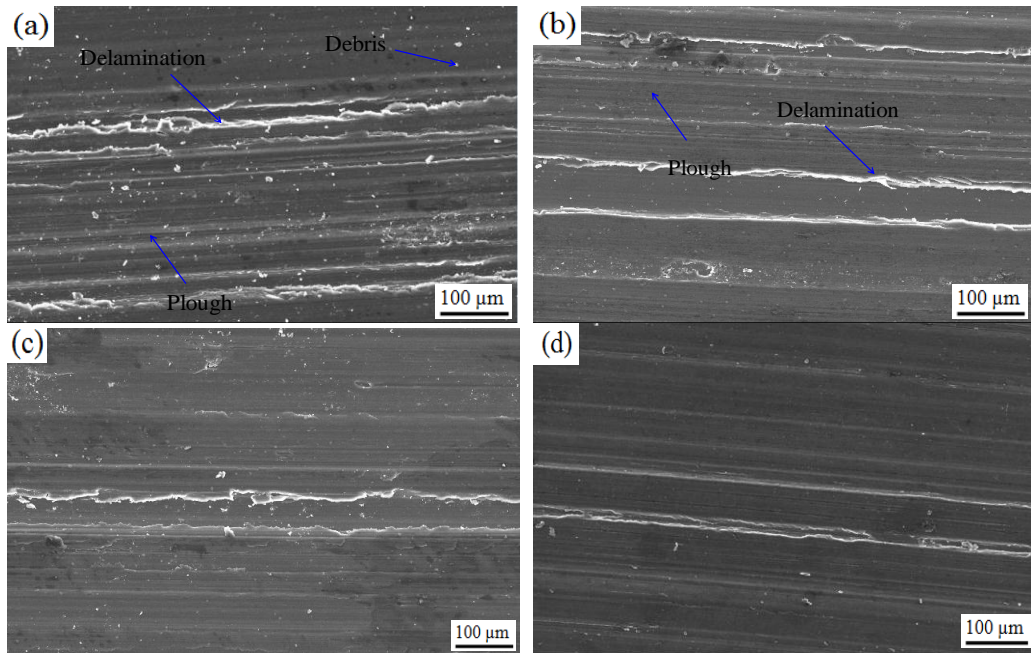


Figure 5.15 SEM images of worn surfaces of (a) Homogenized and ECAP processed (b) 1P, (c) 2P, and (d) 4P samples under 30 N load with sliding distance 5000 m

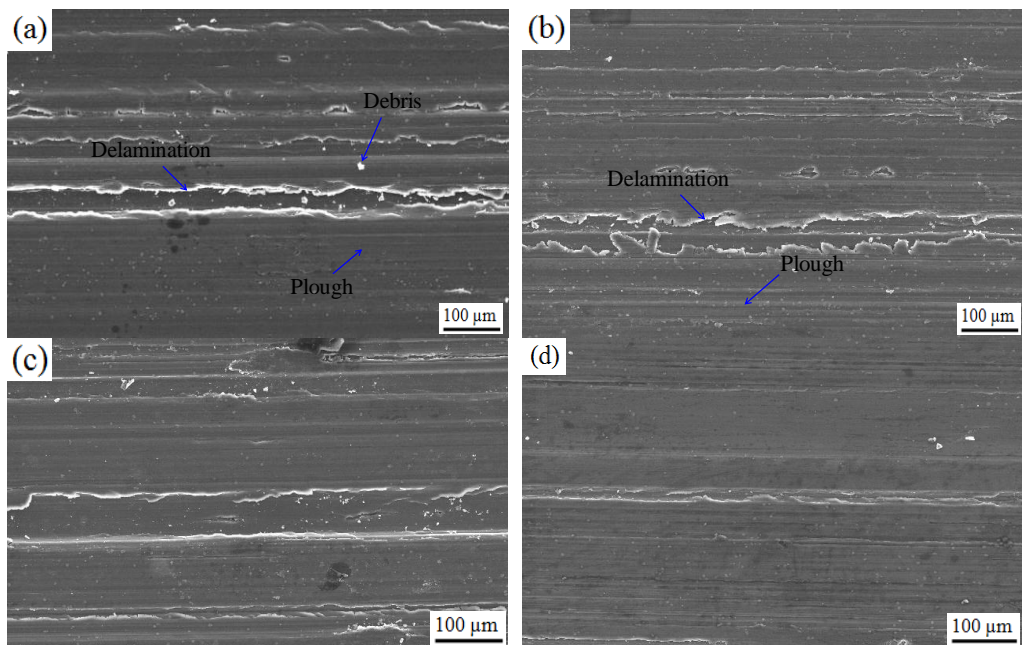


Figure 5.16 SEM images of worn surfaces of (a) Homogenized and ECAP processed (b) 1P, (c) 2P, and (d) 4P samples under 40 N load with sliding distance 5000 m

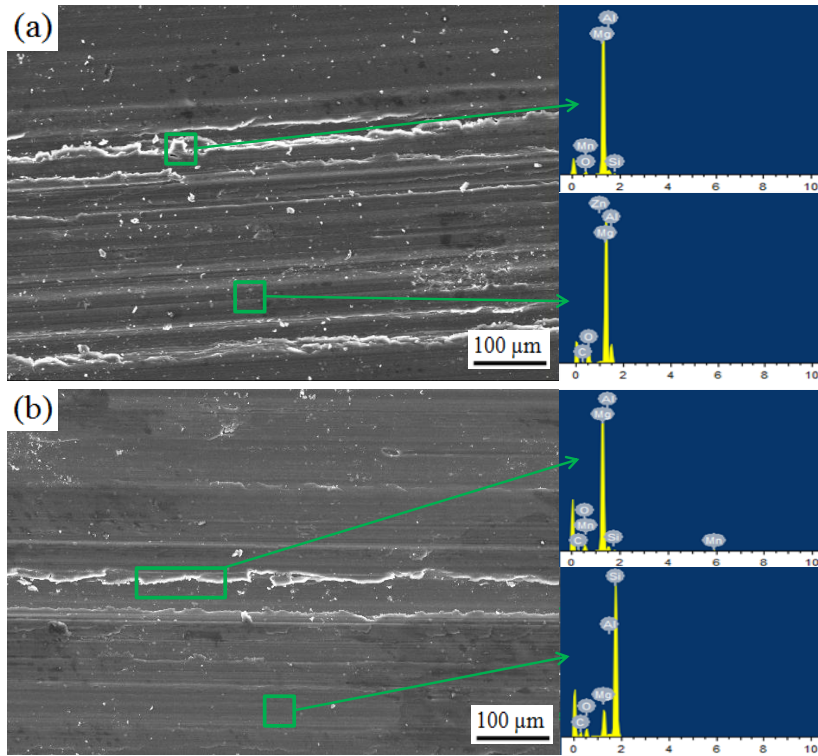


Figure 5.17 EDS analysis for (a) Homogenized and (b) ECAP processed 2P sample under 30 N load

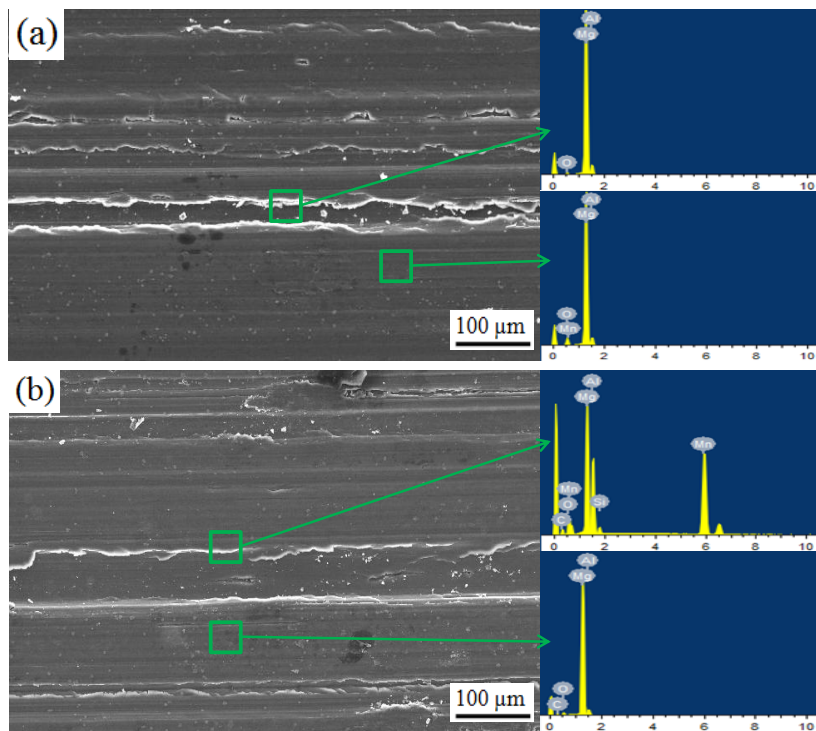


Figure 5.18 EDS analysis for (a) Homogenized and (b) ECAP processed 2P sample under 40 N load

Delamination, debris and ploughing areas were analyzed by EDS for homogenized and ECAP processed 2 pass samples as shown in figure 5.17 and 5.18. Oxygen peaks were visible in the region of delamination, debris and ploughing along with magnesium peaks. Surface oxidation was found on the samples in both unprocessed and ECAP processed conditions, under 30 and 40 N load. Since magnesium and its alloys possess high affinity to oxidation, it plays a key role in wear behavior (Taltavull et al. 2014). So the wear mechanism can be identified as oxidation wear and it revealed that the processed samples have better wear resistance. These results are supported with reported data on AZ31 magnesium alloy (Xu et al. 2013).

5.1.5 Corrosion behavior

Corrosion test was conducted by electrochemical measurements like potentiodynamic polarization and electrochemical impedance spectroscopy. Immersion test was also carried out to study the corrosion behavior of unprocessed and ECAP processed samples with 0.1 M NaCl solution.

5.1.5.1 Electrochemical measurements

(a) Potentiodynamic polarization study

Electrochemical potentiodynamic polarization plot is shown in figure 5.19 and the parameters like corrosion potential (E_{corr}), corrosion current density (I_{corr}) and corrosion rate (mm/y) are extracted from Tafel extrapolation method and values are shown in table 5.2. Corrosion rate is mainly dependent on corrosion current density (I_{corr}). Decrease in I_{corr} value decreases the corrosion rate. It was found that ECAP processed samples possess lower I_{corr} value with increase in number of ECAP passes and so the increase in corrosion resistance was observed for the processed samples.

In case of ECAP 4 pass sample, the corrosion resistance is decreased. Improvement in corrosion resistance is due to ultrafine grained microstructure and uniform distribution of secondary particles which helped in passive film formation ($\text{Mg}(\text{OH})_2$) and adhesion due to increased grain boundary density which increases the corrosion resistance. Small and refined grains increase the grain boundary area which in turn increases the surface protective film area (Ralston and Birbilis, 2010).

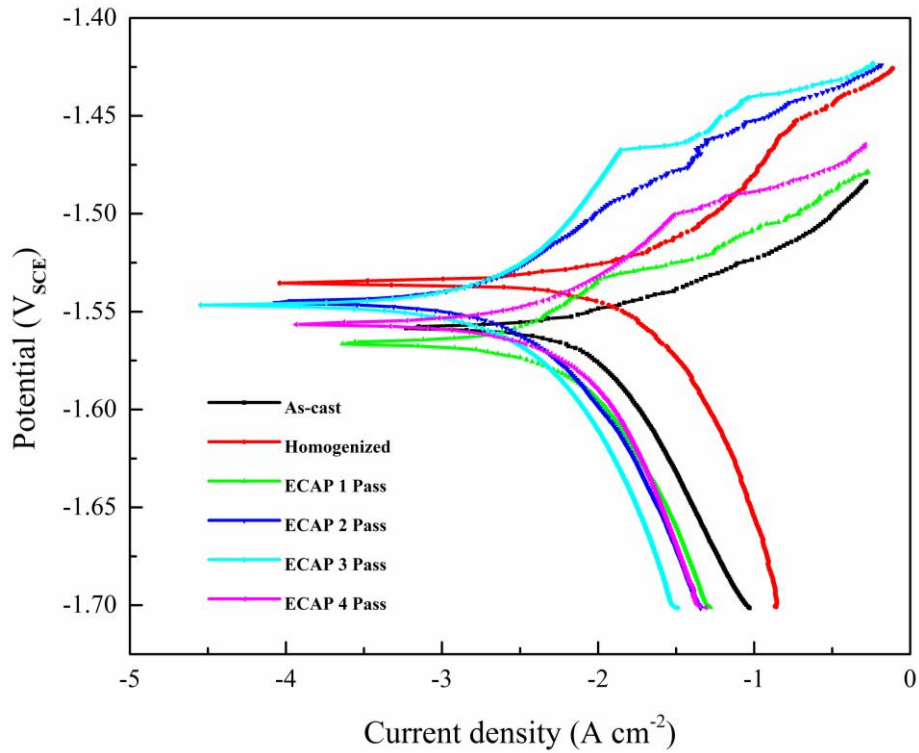


Figure 5.19 Electrochemical potentiodynamic polarization plots of unprocessed and ECAP processed samples

Table 5.2 Electrochemical kinetic parameters like corrosion potential, corrosion current density, Tafel slopes (β_a & β_c) and corrosion rate (mm/y).

Materials	$E_{\text{corr}}(\text{V}_{\text{SCE}})$	I_{corr} ($\mu\text{A}/\text{cm}^2$)	β_a (mV/decade)	β_c (mV/decade)	Corrosion rate (mm/y)
As-cast	-1.565 ± 0.005	10.38 ± 1	82.7 ± 10	135.8 ± 15	0.223 ± 0.030
Homogenized	-1.535 ± 0.005	5.65 ± 1	77.1 ± 10	141.4 ± 10	0.191 ± 0.020
ECAP 1 Pass	-1.570 ± 0.004	2.79 ± 0.5	75.9 ± 6	165.8 ± 10	0.060 ± 0.015
ECAP 2 Pass	-1.545 ± 0.003	2.27 ± 0.5	55.8 ± 5	173.4 ± 8	0.048 ± 0.020
ECAP 3 Pass	-1.548 ± 0.003	2.15 ± 0.5	45.9 ± 5	180.5 ± 6	0.035 ± 0.010
ECAP 4 Pass	-1.560 ± 0.003	2.89 ± 0.5	78.9 ± 5	161.4 ± 10	0.070 ± 0.015

ECAP 4 pass samples showed decreased corrosion resistance because of dislocation accumulation with increased ECAP passes which gives rise to abundant internal energy and more prone to corrosion.

(b) Electrochemical impedance spectroscopy (EIS)

EIS test for unprocessed and ECAP processed samples were carried out to further study the corrosion behavior. Figure 5.20 shows Nyquist plots of samples immersed in 0.1 M NaCl solution. Arc diameters of capacitive arcs of the ECAP processed samples increase with increase in number of ECAP passes. This is due to increased corrosion resistance which shows the protective layer in the interface. Second arc represents the damaged protective layer. Decrease in corrosion rate was observed for ECAP processed samples due to presence of equiaxed ultrafine grains and homogeneously distributed secondary particles (Jiang et al. 2009). The main reason for enhancement in corrosion resistance of grain-refined materials is attributed to an improvement in protective layer formation and adhesion because of increased grain boundary density (Ralston and Birbilis, 2010). EIS plots are fitted with Randles circuit using ZSimpwin commercial software to extract the values of charge-transfer resistance (R_t).

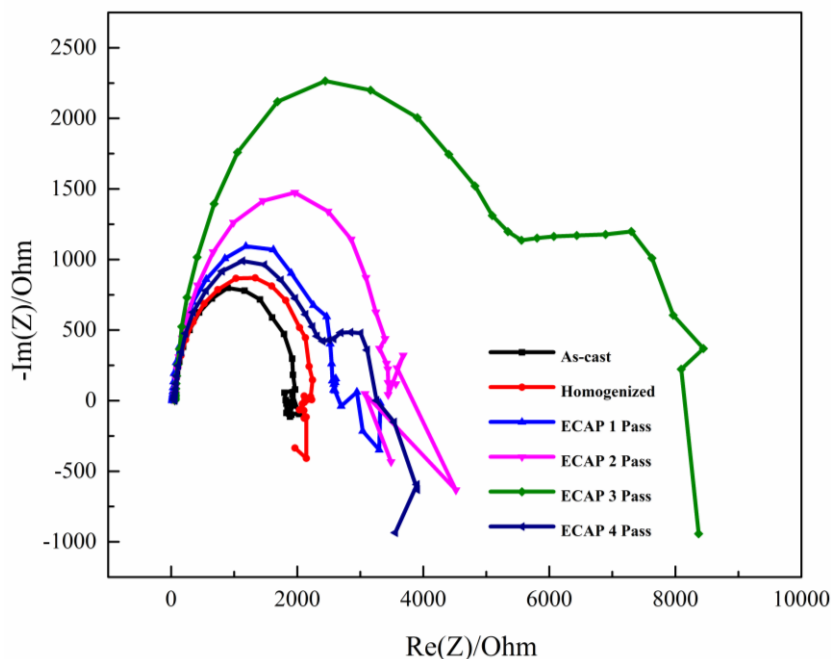


Figure 5.20 Nyquist plots of unprocessed and ECAP processed samples

Variation of capacitive arc indicates that the obtained R_t values of ECAP processed samples are increased and the corrosion resistance of ECAP processed samples was better than unprocessed samples as shown in figure 5.21 and table 5.3. R_t value for ECAP 4 pass is reduced because more dislocations are introduced into the materials with increase in ECAP passes and these dislocations get accumulated and act as energetic sites which are more prone to corrosion. The porosity and stability of $Mg(OH)_2$ protective film could not prevent the diffusion of chloride ions with water molecules into the magnesium matrix which cause severe corrosion reactions because of the presence of large number of crystalline defects in higher ECAP pass samples. Hydrogen evolved by corrosion reaction further damages the $Mg(OH)_2$ protective layer to a larger extent and more chloride and water molecules would diffuse and further corrosion process takes place (Song et al. 2010). Ultrafine grains provide better surface coverage which inhibits the rupture of outer $Mg(OH)_2$ surface which reduces the corrosion rate (Orlov et al. 2011) and also the formation of β phases ($Mg_{17}Al_{12}$) which acts as a barrier for corrosion occurrence and which improves the corrosion resistance of the material (Pardo et al. 2008; Song, 2005).

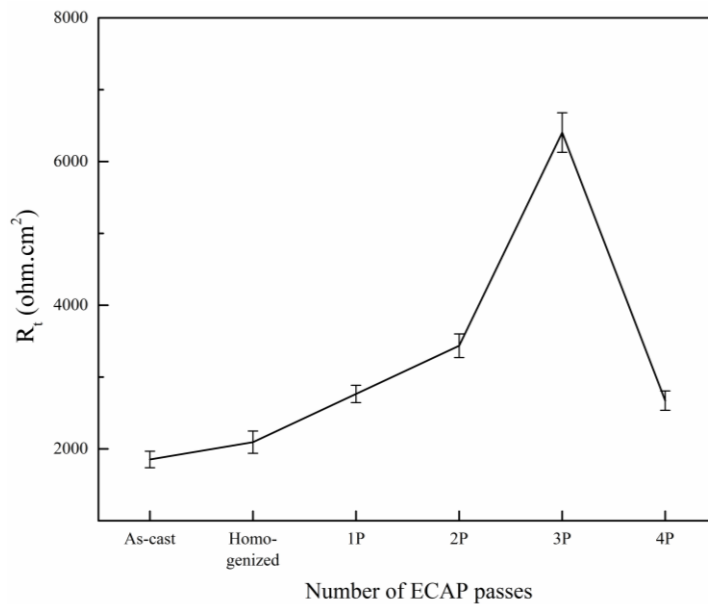


Figure 5.21 R_t verses number of ECAP passes

ECAP 4 pass sample showed decreased corrosion resistance due to increase in dislocations (Gopi et al. 2016) with more ECAP passes which resulted in dislocation accumulation which stores abundant internal energy like energetic grain boundaries.

The passive protective films are more prone to nucleation at the crystalline defect regions which leads to corrosion (Song et al. 2010; Johansen et al. 1957).

Table 5.3 Fitted R_t values for unprocessed and ECAP processed sample

Materials	$R_t(\text{ohm cm}^2)$
As-cast	1853±115
Homogenized	2094±155
ECAP 1 Pass	2765±120
ECAP 2 Pass	3436±165
ECAP 3 Pass	6404±275
ECAP 4 Pass	2672±135

X-ray diffraction of ECAP processed 3 pass sample is shown in figure 5.22 to identify $\text{Mg}(\text{OH})_2$, MgO and β phases ($\text{Mg}_{17}\text{Al}_{12}$). Presence of $\text{Mg}(\text{OH})_2$ and MgO shows the formation of passivation layer which reduces the corrosion process (Wang et al. 2009) and also $\text{Mg}_{17}\text{Al}_{12}$ phase acts as barrier for the occurrence of corrosion.

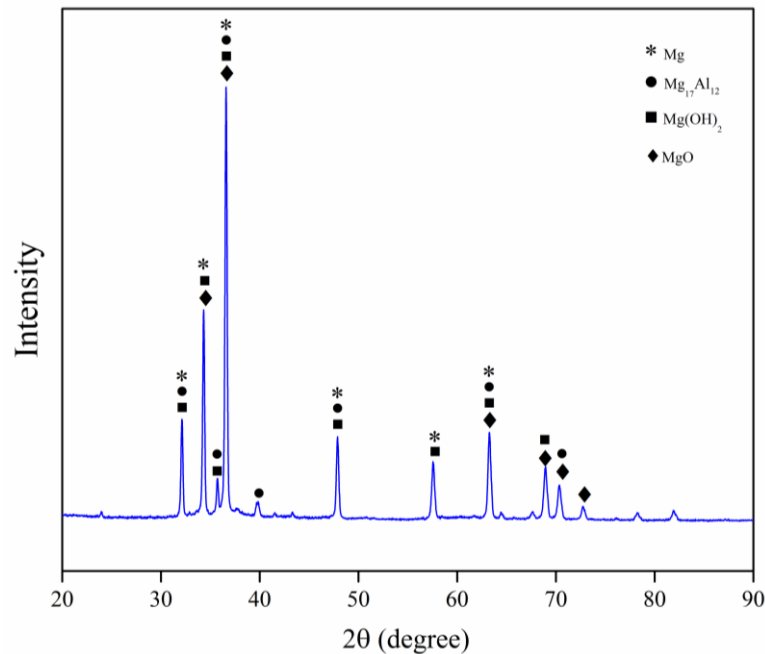


Figure 5.22 XRD of ECAP processed 3 pass corrosion sample

Microstructural images of corroded surfaces of unprocessed and ECAP processed samples are shown in figure 5.23. More pitting is seen in case of as-cast and homogenized samples and is shown in figure 5.23 (a) and (b). ECAP Processed

samples showed less pits. With increase in number of ECAP passes, number of pits are reduced, because of grain refinement and are shown in figure 5.23 (c-f).

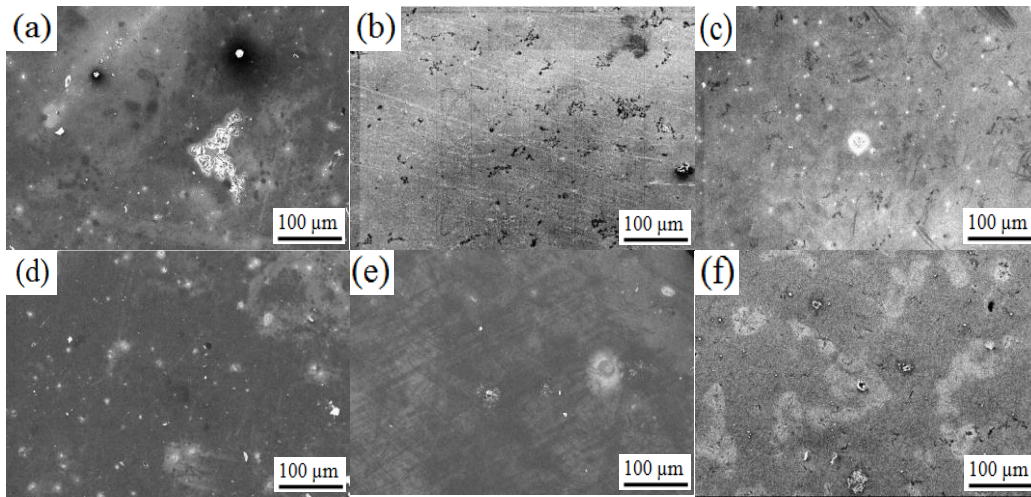


Figure 5.23 SEM images of corrosion samples for different ECAP passes

5.1.5.2 Immersion test

Immersion test is carried out to estimate the corrosion resistance of unprocessed and ECAP processed samples by hydrogen evolution. Corrosion rate based on hydrogen evolution is shown in table 5.4. Hydrogen evolution experienced by the samples during constant immersion is proportional to the corrosion rate of the materials. It can be observed that ECAP processed samples showed lower corrosion rate with low hydrogen evolution compared to unprocessed condition and are shown in table 5.4. SEM images of sample surfaces after immersion test for 120 h in 0.1 M NaCl solution are shown in figure 5.24.

Table 5.4 Corrosion rate of immersed samples verses number of ECAP passes.

Material	Corrosion Rate (mm/y)
As-cast	0.352±0.030
Homogenized	0.290±0.030
ECAP 1 Pass	0.156±0.020
ECAP 2 Pass	0.115±0.015
ECAP 3 Pass	0.078±0.010
ECAP 4 Pass	0.185±0.015

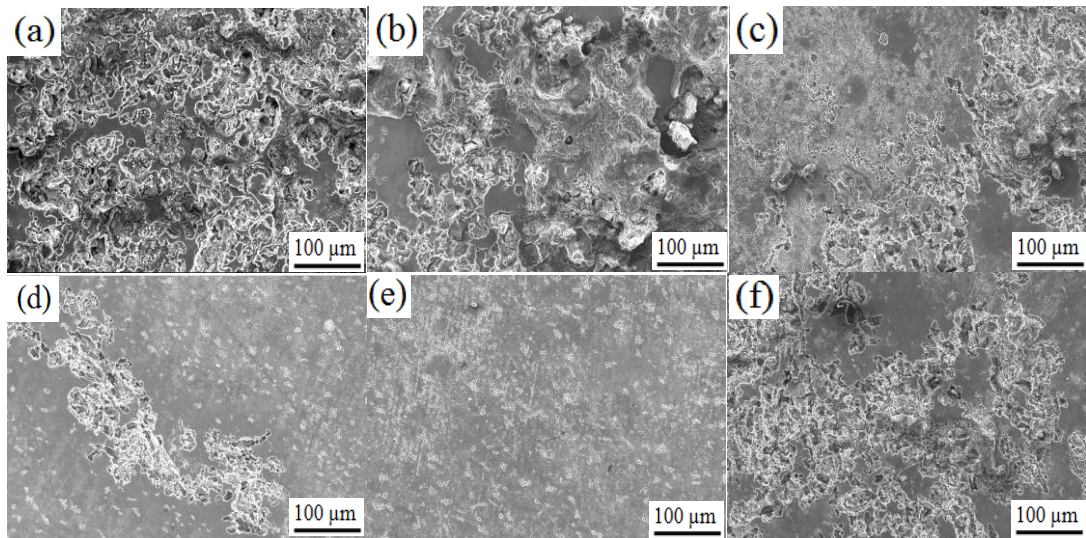


Figure 5.24 SEM images of immersed samples (a) as-cast (b) homogenized and ECAP processed (c) 1P, (d) 2P, (e) 3P, and (f) 4P samples

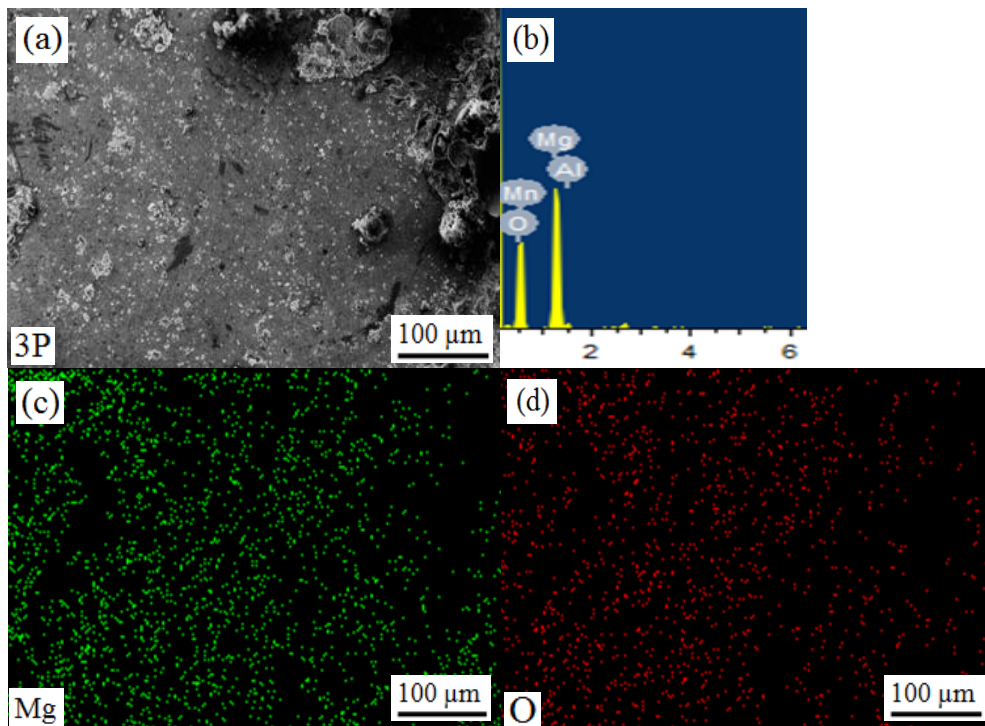


Figure 5.25 SEM images with EDS and elemental mapping of ECAP 3P sample

Less corrosion pits are observed on the ECAP processed samples compared to unprocessed condition. With the increase in number of ECAP passes the number of pits decreases. Larger and deeper pits are observed on unprocessed samples. Degradation of ECAP processed samples is very slow, due to refined microstructure

and the presence of secondary phases. This shows that ECAP processed samples have more corrosion resistance compared to unprocessed condition. Elemental mapping showed the distribution of magnesium and oxygen on the corroded surface after immersion test of ECAP 3 pass sample and is shown in figure 5.25. Presence of oxygen indicates the possibility of formation of magnesium oxide and magnesium hydroxide, which indicate the formation of passivity layer that has been formed, hence improved corrosion resistance (Liao et al. 2012-a,b).

5.2 Summary

ECAP was conducted on AM80 magnesium alloy and its effect on microstructure, mechanical, wear properties was investigated and corrosion behavior was observed by electrochemical measurements and immersion test. Obtained outcome was summarized as below:

1. ECAP was carried out for AM80 magnesium alloy up to four passes. Grain size was found to reduce to an average of $\sim 3 \mu\text{m}$.
2. ECAP 2 pass sample showed increased mechanical properties compared to unprocessed condition. UTS increased by 124 and 115% and YS increased by 100 and 45% as compared to as-cast and homogenized condition, respectively. Elongation increased from 5.3 to 22.2% after ECAP 2 passes. Fracture surface showed fine dimples with increase in ECAP passes representing ductile fracture behavior.
3. Hardness of ECAP processed samples increased up to 2 passes and reduced with further passes due to texture softening or texture modification.
4. ECAP processed samples were subjected to dry sliding wear test to know the wear resistance of processed samples in comparison with unprocessed samples. The average coefficient of friction values decreased with ECAP processed samples compared to homogenized condition, and fluctuations were reduced with increased load of 40 N as compared to 30 N load.
5. Wear mass loss reduced for ECAP processed samples compared to homogenized condition, and the results are related to hardness of the processed material. ECAP 2 pass sample showed reduced wear mass loss

of ~1.83 (2500 m) and ~1.5 (5000 m) times under 30 N load and ~1.51 (2500 m) and ~1.38 (5000 m) times under 40 N load compared to initial condition.

6. Worn surfaces showed, delamination, ploughing and wear debris. Oxygen peaks were also observed on both surfaces of homogenized and ECAP-processed samples and the wear mechanism was recognized as abrasive wear and oxidation wear.
7. Potentiodynamic polarization test showed increased corrosion resistance due to reduced I_{corr} value for the ECAP processed samples up to 3 passes compared to initial condition. EIS plots represented reduced corrosion rate for ECAP processed samples with increase in diameter of the capacitive arcs in the Nyquist plots compared to initial condition. R_t values increased by ~3.45 and ~3.05 times compared to as-cast and homogenized condition.
8. Immersion test showed results similar to electrochemical measurements with lower corrosion rate with low hydrogen evolution for ECAP processed samples compared to initial condition.

CHAPTER 6

RESULTS AND DISCUSSION

6.1 Equal channel angular pressing of AM90 alloy

AM90 alloy samples were processed by ECAP at 275 °C up to 4 passes using route B_C. Microstructures of the processed samples were characterized using OM, SEM and TEM. EBSD was also carried out on samples to study the grain structure and grain boundaries misorientation angles. XRD analysis was performed to identify the different phases in the samples. Tensile and microhardness test were carried out for ECAP processed samples to study the mechanical properties. Wear and corrosion test was conducted to know the wear and corrosion behavior of unprocessed and ECAP processed samples and the obtained results are discussed.

6.1.1 Microstructure analysis

Microstructure of the unprocessed and ECAP processed samples were analyzed using OM, SEM, TEM and EBSD. Figure 6.1 shows the optical micrographs of unprocessed and ECAP processed samples. Average grain size of as-cast sample was found to be 80 μm. The as-cast samples were subjected to homogenization at a temperature of 400 °C for 24 hours to ensure uniform distribution of secondary particles into the magnesium matrix. Homogenized sample possessed an average grain size of 100 μm. Homogenized samples were subjected to ECAP up to 4 passes. During the first and second passes, larger grains were broken down to small grains, and these small grains were surrounded by larger grains forming bimodal structure as represented in figure 6.1 (c) and (d). Bimodal grain structure is due to limited slip systems in Mg alloy in which only favorably oriented grains are refined and deformed initially and less deformed or coarse grains are left in the microstructure (Janecek et al. 2012). Refinement rate is more during 1 and 2 pass which may be due to higher dislocation rate (Jahadi et.al. 2014). Bimodal grain structure is clearly seen during 2 pass which

consists of larger grains of size varying between 20 to 25 μm surrounded with 4 to 6 μm smaller grains and the average grain size was found to be 20 μm .

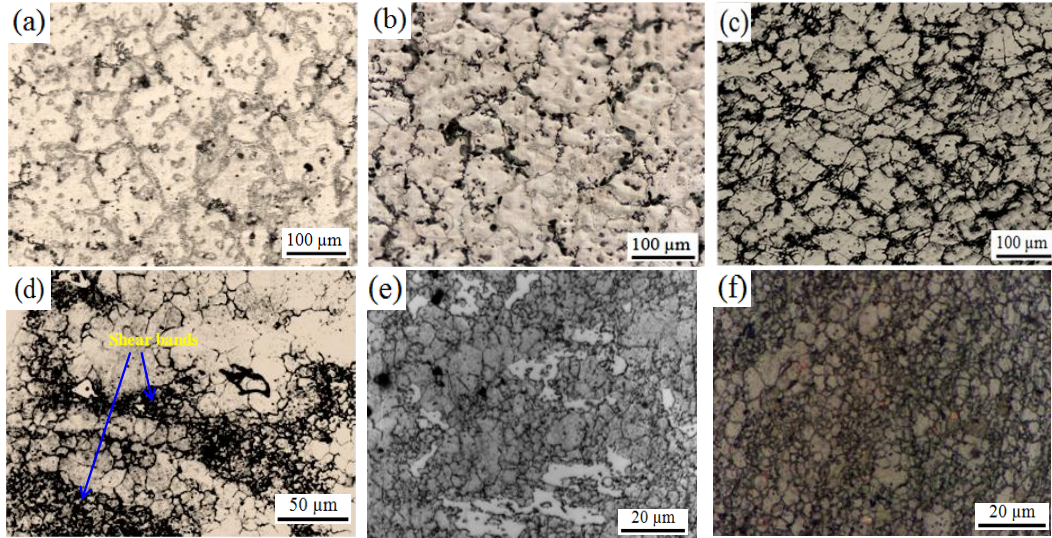


Figure 6.1 Optical micrographs of (a) as-cast (b) homogenized and ECAP (c) 1P, (d) 2P, (e) 3P and (f) 4P samples

In 2 pass ECAP sample it can be observed that there are large areas (Figure 6.1(d)) which shows non uniform grain deformation with combination of deformed fine grains and coarse grains. Inhomogeneous deformation is due to strain localization of shear bands in the form of stripes which is attributed by the presence of refined grains. This is due to various factors like variation in grain size, grain orientation and fine precipitates, these sites of strain localization were considered as weak areas in the samples. This flow or strain localization leads to the formation of shear bands, under plain strain loading condition due to flow softening. Flow softening in shear bands is due to dynamic recovery, recrystallization and reversal effect of strengthening mechanisms (Semiatin and Jonas, 1984). Shear bands are also formed due to dynamic recrystallization (DRX) (Ion et al. 1982). Slip systems in HCP structured materials is less compared to cubic materials, so the Schmid factors varies significantly in grains with different orientations. Grains with hard orientations with small Schmid factors find difficult to deform whereas the soft grains which possess large Schmid factors can deform easily (Feng and Ai, 2009). Lin et al. (2005) reported that high Schmid factor value of 0.27 for magnesium alloy of ECAP processed condition and zero Schmid factor for unprocessed condition leads to non-uniform microstructure. Homogeneity of microstructure can be improved by increasing the deformation with

increase in ECAP passes. Homogeneity in microstructure increased with increase in number of ECAP passes and it was clear from figure 6.1 (e) and (f). Average grain size obtained after 3 pass and 4 ECAP passes was 7 μm and 3 μm , respectively. Homogeneous and equiaxed microstructure may be due to dynamic recrystallization (DRX) which occurred during ECAP or may be because of static recrystallization before ECAP, when the die was heated to the required temperature (Akbaripanah et al. 2013-b). Extensive plastic deformation that took place in the samples with higher ECAP passes lead to grain refinement.

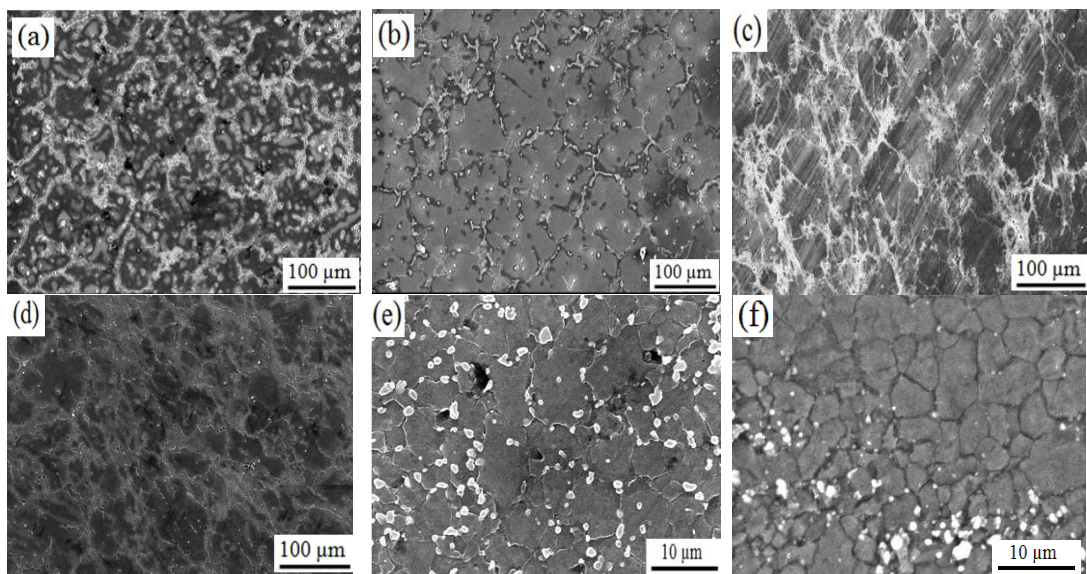


Figure 6.2 SEM images of (a) As-cast (b) Homogenized and ECAP (c) 1P (d) 2P (e) 3P and (f) 4P samples

SEM micrographs of unprocessed and ECAP processed samples are shown in figure 6.2. Secondary particles were found in higher percentage in ECAP processed 3 and 4 pass samples, as represented in figure 6.2 (d) and (e). Grain sizes of unprocessed and ECAP processed samples are represented in figure 6.3. TEM images of ECAP processed 4 pass samples with grain size of around 800 nm to 1 μm as shown in figure 6.4 along with selected area electron diffraction (SAED) patterns inset. High dislocation density was observed in figure 6.4 (a) and (b) indicating the formation of fine grained structure. During ECAP process, high strain causes subdivision of grains due to formation of planar dislocation boundaries and incidental dislocation boundaries.

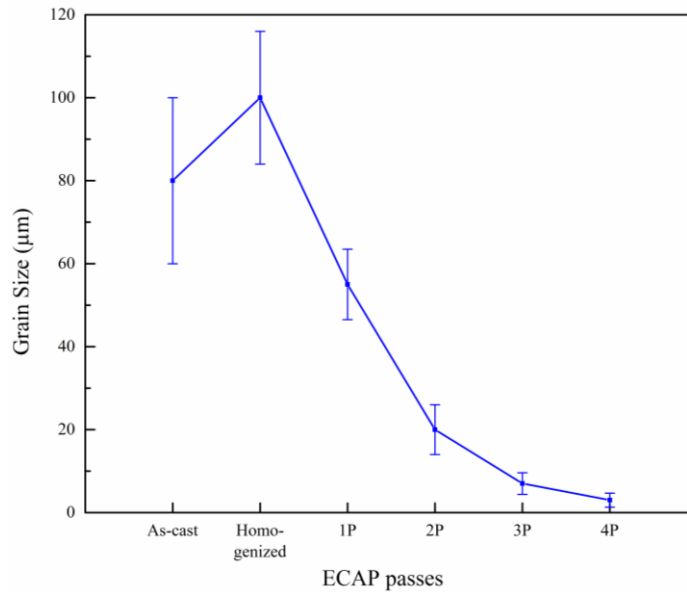


Figure 6.3 Grain size of as-cast, homogenized and ECAP processed samples

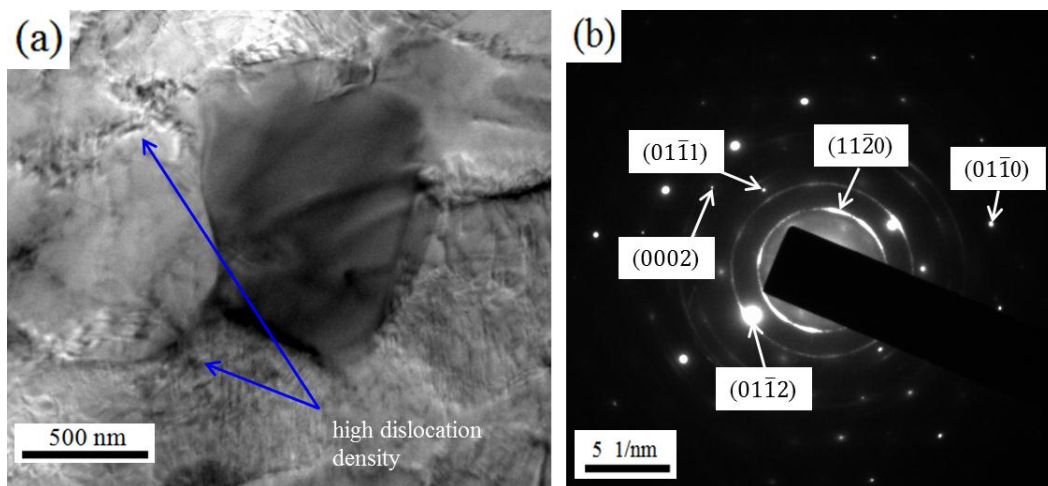


Figure 6.4 TEM micrographs of ECAP 4 pass sample

High misorientations are formed across dislocation boundaries and reduces the space between boundaries and leads to the formation of fine grain (Chino et al. 2008). TEM confirms the presence of coarse and fine grains as shown in figure 6.4 (a) and it is in good agreement with the optical micrographs having bimodal microstructure. Grains with nanometer size are also visible as observed from the figure 6.4 (a) along with coarser grains. Spots which are observed on SAED patterns are diffraction spots arranged in form of circle that indicates large portion of fine grains with high angle grain boundaries (HAGBs) as shown in figure 6.4 (b). Some diffraction spots are not

continues and they look separated may be because of the presence of coarse grains with low angle grain boundaries (LAGBs). Few spots are expanded which indicates the presence of high internal stress, which may be because of grain boundaries diffusion and they are said to be in high energy states (Stolyarov et al. 2001). Figure 6.5 shows OIM micrographs of AM90 alloy for as-cast and ECAP processed sample with inverse pole figure (IPF). IPF map shows the crystal orientations with different colors. Heterogeneous structure can be observed in as-cast sample whereas homogeneous and fine grains are observed in ECAP processed 4 pass sample.

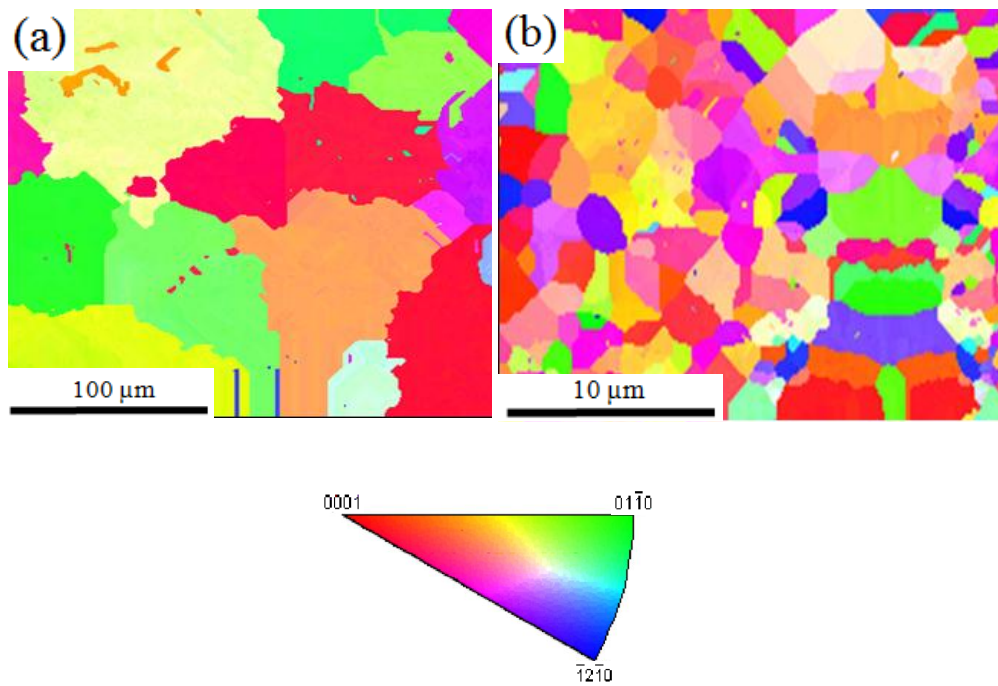


Figure 6.5 OIM micrographs with IPF image (a) as-cast and (b) ECAP 4 pass samples

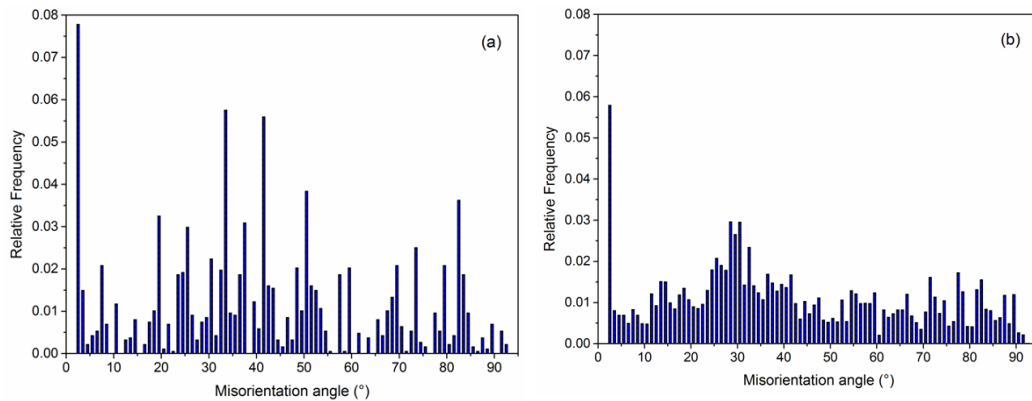


Figure 6.6 Misorientation angle grain distribution of (a) as-cast and (b) ECAP 4 pass sample

Distribution of grain misorientation angles is shown in figure 6.6. In unprocessed samples, high intensity peaks are distributed over wide range of misorientation angle. But in ECAP 4 pass sample, intensity peak height is restricted and grains are distributed in the range of $\sim 10^\circ$ to $\sim 50^\circ$ misorientation angle. It was observed from figure 6.1 (e) and (f), grain refinement rate was reduced at higher passes and LAGBs evolved to HAGBs, leading to a stable microstructure because of DRX (Dumitru et al. 2014). With higher ECAP passes, equiaxed fine grains were formed within the coarse grains by dislocation accumulation and tangling which is known as dislocation subdivision mechanism (Valiev et al. 2006). Small segment of recrystallized grains increases, as strain increases during recrystallization because of higher rate of nucleation, which leads to relatively homogeneous microstructure with finer grains as represented in figure 6.1 (f) and 6.2 (d). Achieved results indicates that refinement rate is more during initial stages of ECAP and further ECAP passes results in more HAGBs rather than grain refinement (Biswas et al. 2010; Jin et al. 2006). With increase in number of ECAP passes, misorientation of grain boundaries increases and leads to the formation of fine grained structures (Zhan et al. 2008).

6.1.2 X-ray diffraction analysis

X-ray diffraction (XRD) profile of as-cast and ECAP processed samples are as shown in figure 6.7. Presence of different intermetallic phases with variation in intensities for different ECAP passes are observed from the figure. Increase in precipitation of phases ($Mg_{17}Al_{12}$, Mg_2Al_3 and $MnAl_{16}$) is represented by increase in the intensity of peaks in the XRD plot. Increment in phases is due to the increase in number of ECAP passes which influences the mechanical properties of the material. The intensity of plane (0002) which was observed in as-cast sample was initially decremented and as the ECAP pass increases the plane (0002) shows strong intensity for ECAP 4 pass using route B_C. In Mg and Mg alloys, basal planes lie parallel to the direction of extrusion, which indicate that the slip on the basal plane is difficult and increase in strength occurs with partial non-basal slip actions (Kim et al. 2005). Basal slip system (0002) was operated more after ECAP passes and no much variation is seen in plane (10 $\bar{1}$ 1). Also it can be observed that as the ECAP pass increases, fluctuations in the intensities was seen and strong intensities can be identified for planes (10 $\bar{1}$ 0), (10 $\bar{1}$ 2),

(11 $\bar{2}$ 0), (10 $\bar{1}$ 3), (11 $\bar{2}$ 2) and (20 $\bar{2}$ 1). These above variations may be because of refinement of grains during ECAP and also shows change in texture that are created during ECAP process which may be due to the activation of prismatic and pyramidal slip, which are caused by the influence of grain boundaries (Dumitru et al. 2014).

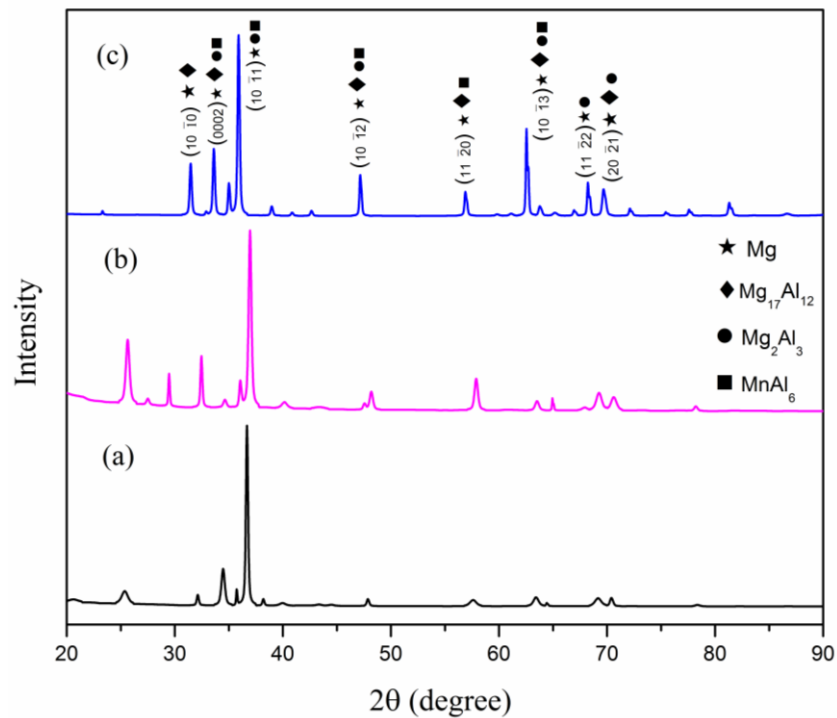


Figure 6.7 XRD profile of (a) as-cast, (b) ECAP 2 pass and (c) ECAP 4 pass samples

It was observed from the figure 6.7, that the material changes their texture when processed through ECAP with strong variations in the intensities. Shear deformation eliminates the existing texture during the ECAP process and because of that variation in the intensities was observed. With the increase in ECAP passes, the initial texture was removed and new texture was formed (Feng and Ai, 2009).

6.1.3 Mechanical properties

6.1.3.1 Tensile behavior

Figure 6.8 illustrates the tensile test results for unprocessed and ECAP processed samples. Summary of the mechanical properties are shown in table 6.1. UTS obtained for 1 to 4 pass ECAP processed samples are 198 MPa, 255 MPa, 221 MPa and 202 MPa respectively. The percentage increase for UTS of about 85%, 138%, 106% and

89% was obtained for ECAP processed 1 to 4 pass samples with comparison to as-cast (107 MPa) condition. Yield strength (YS) achieved for 1 to 4 pass ECAP processed condition are 160 MPa, 170 MPa, 135 MPa and 100 MPa respectively. YS increased for about 255%, 278%, 200% and 122% was obtained for ECAP processed 1 to 4 pass samples, respectively as compared to as-cast (45 MPa) sample.

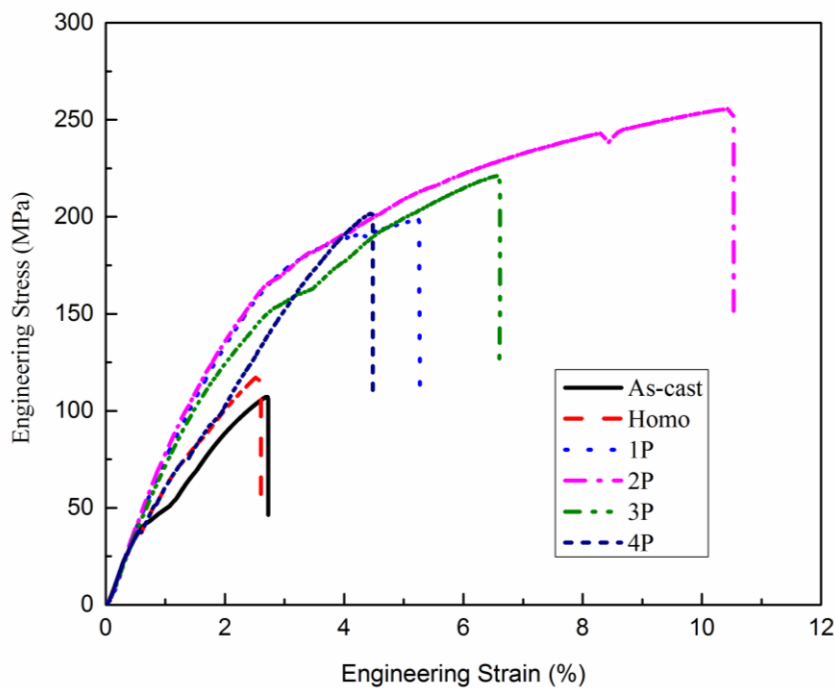


Figure 6.8 Tensile properties of initial condition and ECAP processed samples

During ECAP process, intermetallics were broken into smaller segments and are uniformly distributed over the matrix which strengthens the alloy by increasing the density of dislocations (Janecek et al. 2012). Maximum UTS was obtained for ECAP 2 pass sample and elongation was 10.5% compared with 2.8% for the as-cast sample but for further ECAP passes decrease in UTS was observed in figure 6.8. Strength decreased for ECAP 3 pass and 4 pass samples due to texture modification that takes place in HCP structure of the material. Along with grain size reduction, initial texture was changed by the ECAP process and it was observed with the intensities which are varying with the ECAP process as shown in figure 6.7 for as-cast and ECAP processed sample.

Table 6.1 Mechanical properties of AM90 alloy processed by ECAP up to 4 passes.

ECAP passes	UTS (MPa)	YS (MPa)	% Elongation
As-cast	107±8.5	45±6.5	2.8±0.11
Homogenized	112±6.5	80±5.3	2.7±0.09
1 Pass	198±7.3	160±8.5	5.2±0.10
2 Pass	255±8.2	170±5.5	10.5±0.15
3 Pass	221±6.1	135±7.2	6.5±0.12
4 Pass	202±8.5	100±6.5	4.45±0.10

6.1.3.2 Vickers Microhardness

Vickers microhardness (Hv) was conducted using omni-tech hardness tester by subjecting the sample to a load of 25 g for 15s. Test was carried out throughout the cross section of the sample to know the consistency of hardness that has distributed over the surface of deformed sample. Variations of microhardness for unprocessed and different ECAP passes are as shown in figure 6.9. Hardness value of as-cast sample obtained was 83 Hv and as the ECAP passes increases hardness increased to 88 Hv for 1 pass and 98 Hv for 2 pass ECAP processed sample. An enhancement in hardness could be due to high dislocation density and also formation of sub microcrystalline structures that occurred during severe plastic deformation. With refined microstructure, hardness increased due to the restriction of dislocation movement imposed by high dislocation density, misorientation of grains and LAGBs (Panigrahi and Jayaganthan, 2008). As the ECAP passes increases after ECAP 2 pass, hardness decreases because of the development of new grains which hinders the strain hardening effect. With further increase in ECAP passes, microhardness values slightly reduces to 89 Hv, which may be due to variation in texture. Similar trend was observed in UTS and YS. Decrease in hardness after 3 pass could be also due to decrease in dislocation density because of dynamic recrystallization and grain growth (Kapoor et al. 2013). Variation in microhardness relates to UTS and they appear to be mutually dependent with each other. Homogeneity of microhardness increased as the ECAP passes increases. It can be observed from the figure 6.9, microhardness of ECAP processed 1 and 2 pass samples are less homogeneous compared to 3 and 4

pass condition. Enhancement in homogeneity of hardness during 3 pass and 4 pass may be due to microstructural uniformity which had improved with higher ECAP passes (Shaarbaaf and Toroghinejad, 2008).

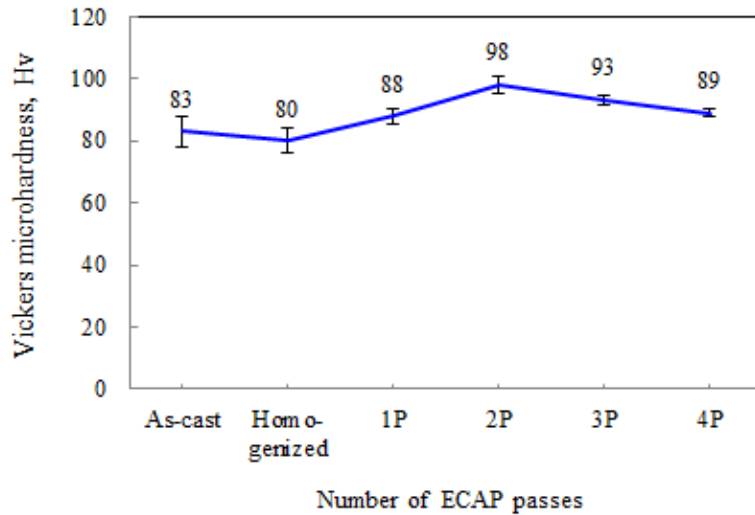


Figure 6.9 Vickers microhardness values of homogenized and ECAP processed samples

6.1.3.3 Fractography

Fractography provides the information regarding the nature of fracture occurred in the sample. Figure 6.10 shows SEM images of tensile fractured surfaces of unprocessed and ECAP processed samples from 1 to 4 passes. From the figure, it can be seen that the fractured surfaces appears to be smoother as the ECAP pass increases and the samples are fractured in ductile manner, which consists of well-established dimples over the fractured surface. In ECAP processed materials, rougher and deeper surfaces are visible within the dimples indication considerable deformation energy expended by the process of void coalescence. Tear ridges or striation were observed on as-cast and also ECAP 1 pass sample as identified in figure 6.10 (a) and (c). This may be because of plastic deformation at the grain boundaries and fracture appeared to be mixed mode of brittle type. As the ECAP passes increases cleavage planes are observed in ECAP 2 and 3 pass samples but with further higher ECAP passes, the rate of cleavage planes reduces as grain size decreases. Initially, appears like a mixed mode of ductile and brittle fracture. After ECAP 2 pass, it can be observed from figure 6.10 (d-f), high portion of equiaxed and fine dimples are almost uniform in

size, which reveals the state of ductile fracture behavior. Dimple size reduces with increase in number in ECAP passes due to grain refinement and strain hardening (Fang et al. 2007).

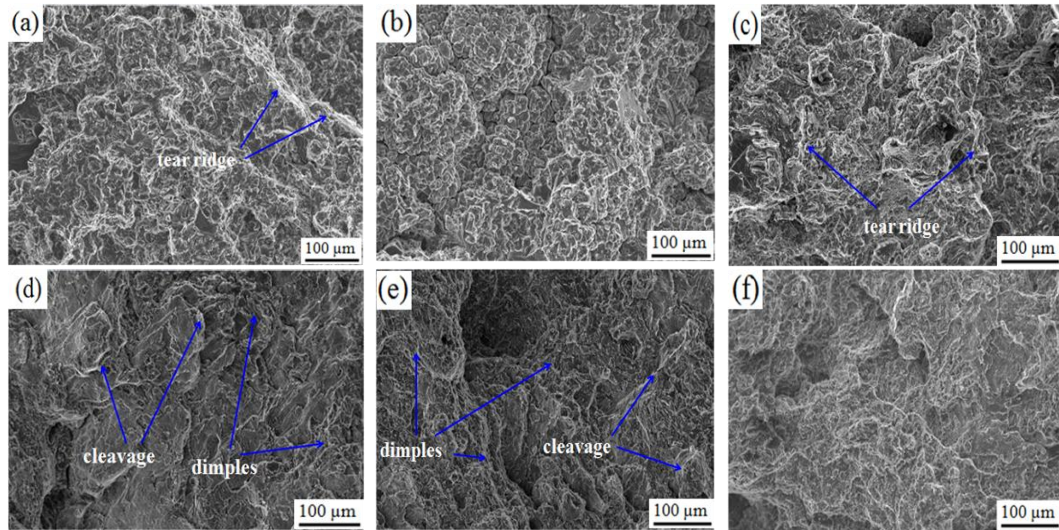


Figure 6.10 SEM micrographs of fractured surfaces (a) as-cast (b) homogenized and ECAP (c) 1P (d) 2P (e) 3P and (f) 4P samples

6.1.4 Wear behavior

6.1.4.1 Coefficient of friction (COF) during wear test

Two loads and two sliding distances were selected as varying parameters to conduct wear test using DUCOM pin-on-disc wear testing machine.

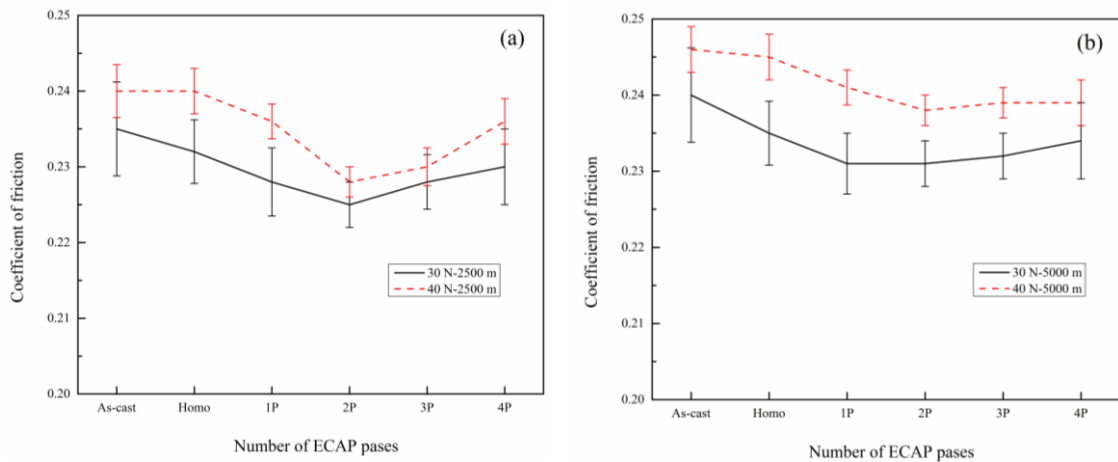


Figure 6.11 COF curves for samples under 30 N and 40 N load with sliding distance (a) 2500 m and (b) 5000 m

Load of 30 and 40 N and sliding distance of 2500 m and 5000 m were selected. For each condition, 3 trials were conducted and the average COF values obtained for different conditions are plotted and are shown in figure 6.11. In as-cast and homogenized samples, there is no much change in COF, but as the ECAP passes increase, COF starts reducing indicating wear resistance properties of processed samples. Fluctuation in COF value for 40 N load is less compared to 30 N as shown in figure 6.11. Reduced fluctuation shows increased wear resistance property of the ECAP processed material.

6.1.4.2 Wear mass loss and wear morphology

Wear mass loss follows the similar trend of COF. Samples are subjected to different loads and sliding distances for evaluating the wear behavior. ECAP processed samples showed reduced wear mass loss when compared to unprocessed condition. This is due to enhanced microhardness distribution which avoids loss of material due to sliding motion of the sample with the disc preventing the formation of delamination and wear debris. Wear mass loss for different condition are shown in figure 6.12. ECAP 2 pass sample showed high wear resistance because of higher hardness value due to grain refinement. Grain refinement due to ECAP process has increased the hardness of the material which in turn increased the wear resistance property of the material which is related by Archard equation (Archard et al. 1953).

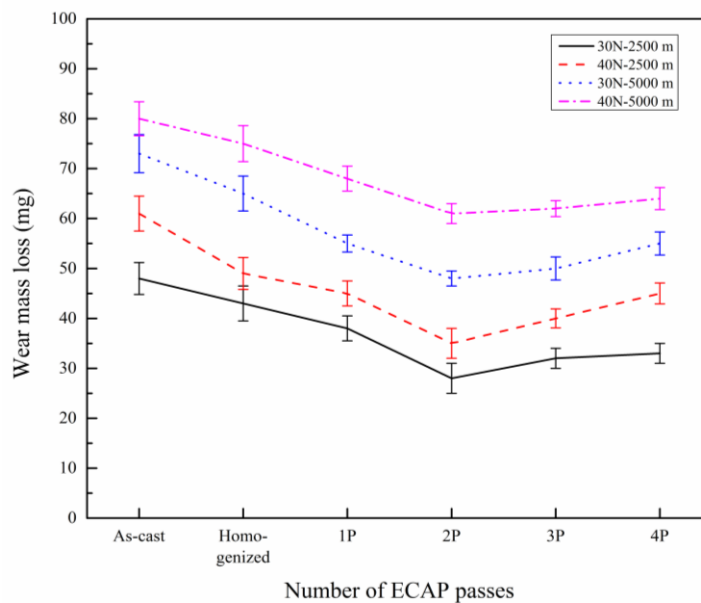


Figure 6.12 Wear mass loss versus number of ECAP passes

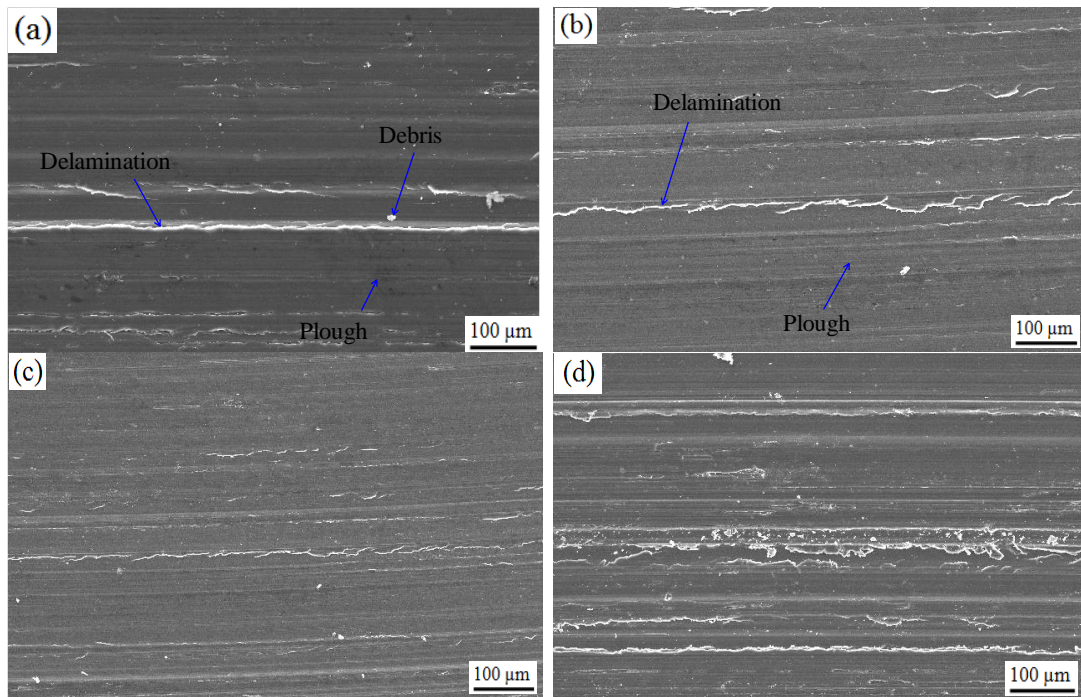


Figure 6.13 SEM images of worn surfaces of (a) Homogenized and ECAP processed (b) 1P, (c) 2P, and (d) 4P samples under 30 N load with sliding distance 2500 m

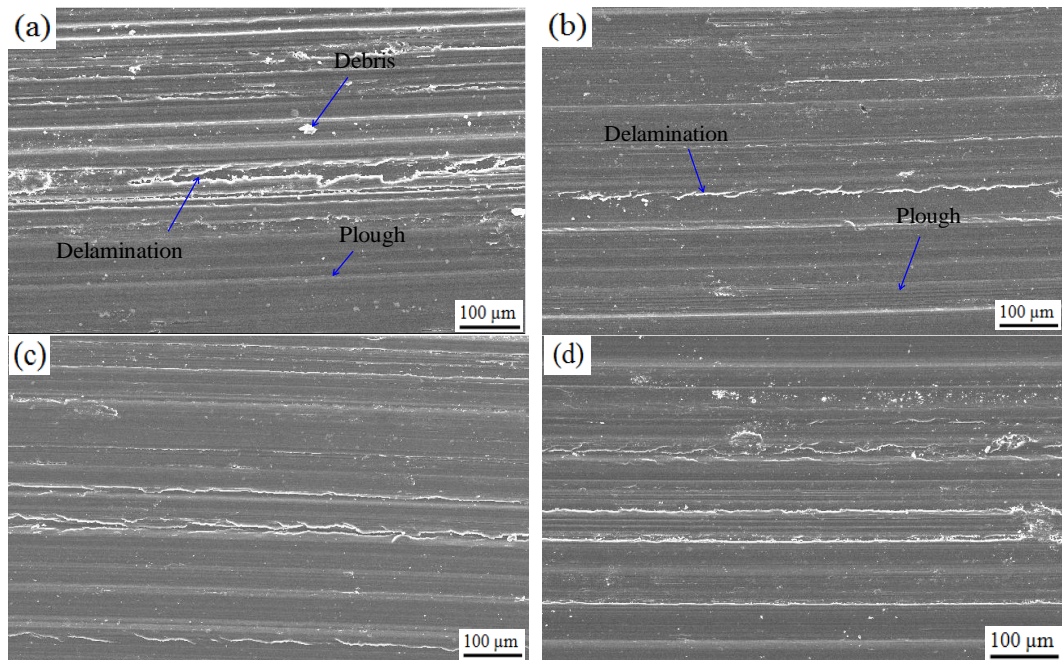


Figure 6.14 SEM images of worn surfaces of (a) Homogenized and ECAP processed (b) 1P, (c) 2P, and (d) 4P samples under 40 N load with sliding distance 2500 m

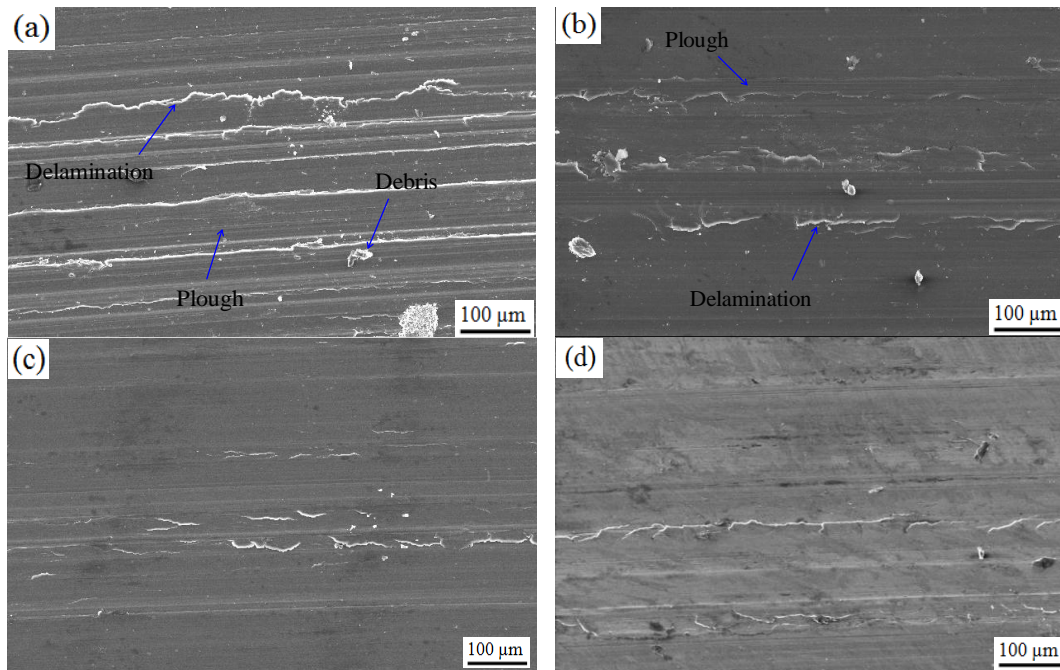


Figure 6.15 SEM images of worn surfaces of (a) Homogenized and ECAP processed (b) 1P, (c) 2P, and (d) 4P samples under 30 N load with sliding distance 5000 m

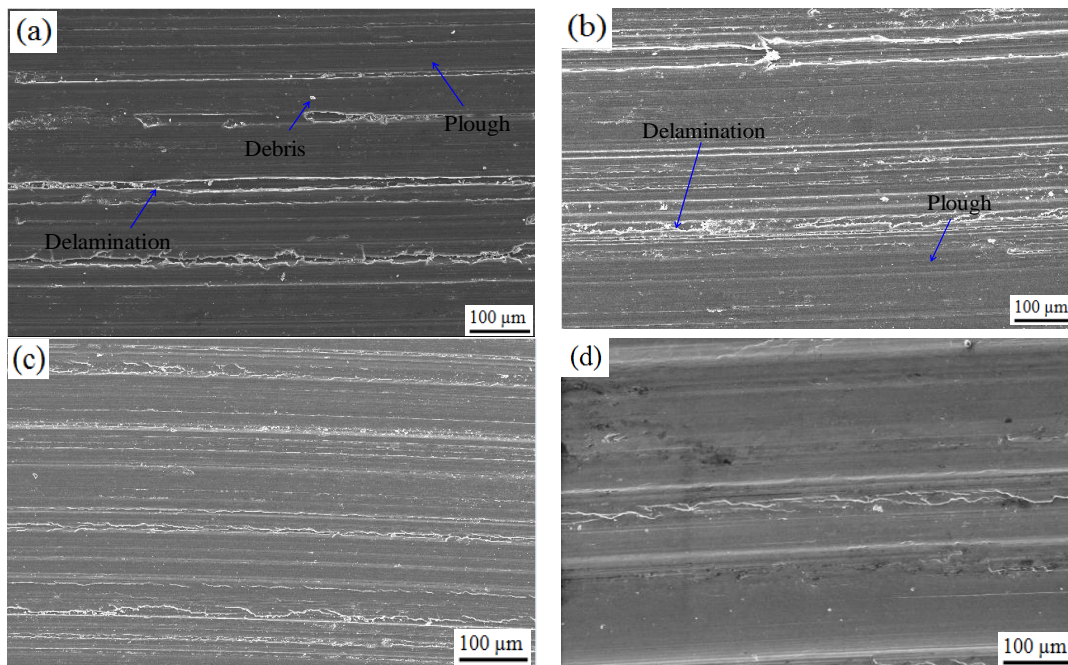


Figure 6.16 SEM images of worn surfaces of (a) Homogenized and ECAP processed (b) 1P, (c) 2P, and (d) 4P samples under 40 N load with sliding distance 5000 m

Delamination and wear debris were observed and small grooves were formed by ploughing parallel to sliding direction are observed on the worn surface as shown in figure 6.13 to 6.16. Due to increased hardness property, the formation of delamination and wear debris is reduced during sliding thus by increasing the wear resistance property. With these surface morphologies the mechanism of wear is noted to be abrasive wear. EDS analysis revealed the presence of oxygen element along with magnesium. Since magnesium is more prone to oxidation when comes in contact with oxygen it can be considered as one of the reason for wear rate. Magnesium and oxygen elements are identified on the wear surface in the areas of delamination, ploughing and wear debris as shown in figure 6.17 and 6.18. Based on the above discussion we can also consider the possibility of oxidation wear.

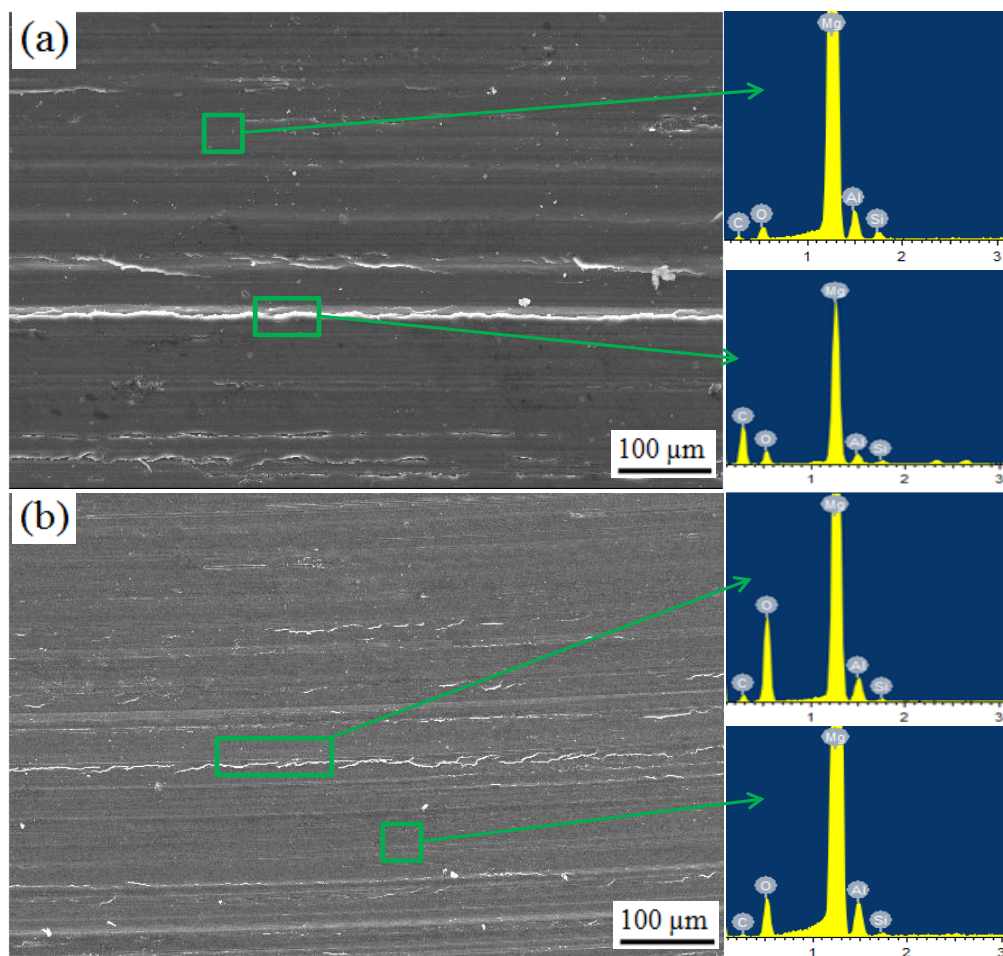


Figure 6.17 EDS analysis for (a) Homogenized and (b) ECAP processed 2P sample under 30 N load

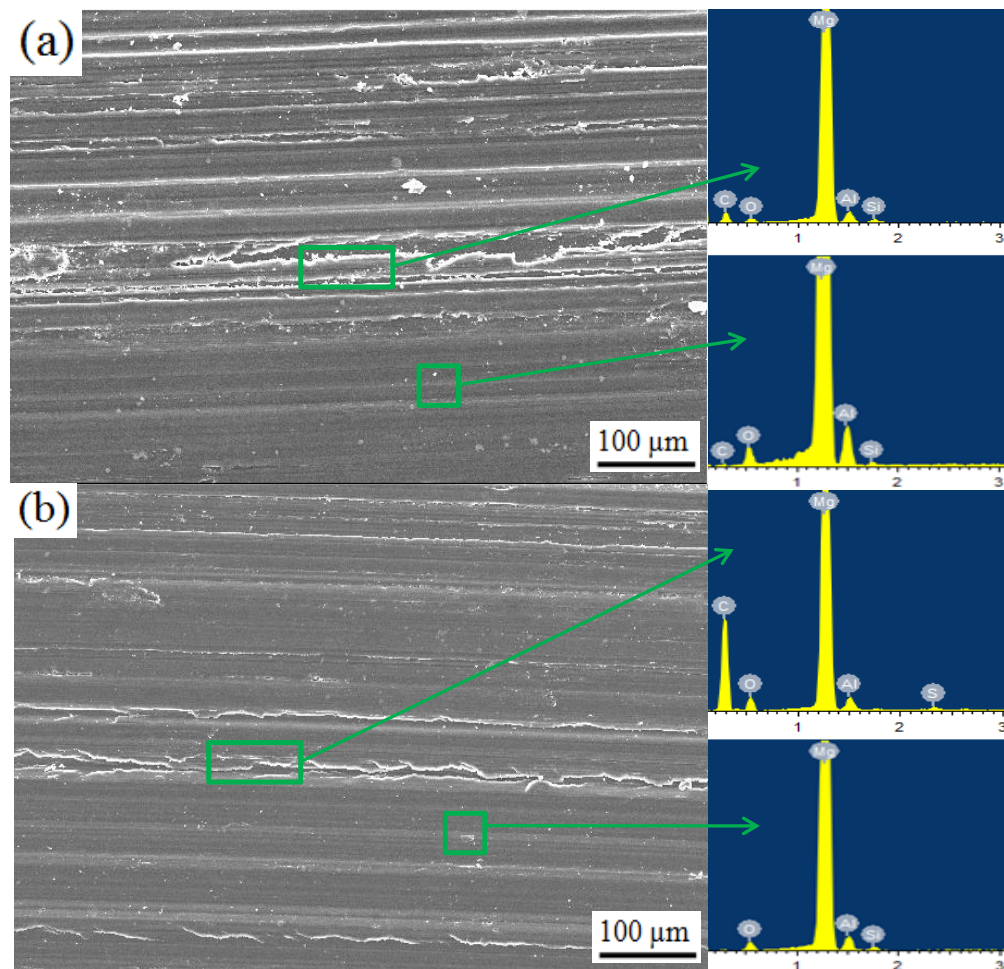


Figure 6.18 EDS analysis for (a) Homogenized and (b) ECAP processed 2P sample under 40 N load

6.1.5 Corrosion behavior

AM90 magnesium alloy samples were subjected to corrosion tests to know the corrosion behavior by conducting electrochemical measurement test and immersion test.

6.1.5.1 Electrochemical measurements

(a) Potentiodynamic polarization study

Unprocessed and ECAP processed samples were subjected to potentiodynamic polarization tests to study the corrosion behavior. Polarization curves are shown in figure 6.19. Corresponding parameters like E_{corr} , I_{corr} , Tafel slopes (β_a & β_c) and corrosion rate (mm/y) are tabulated in table 6.2. The vertical axis is electrical

potential and the horizontal axis is the logarithm of absolute current. The use of a logarithmic axis is necessary because of the wide range of current values that must be recorded during a corrosion experiment.

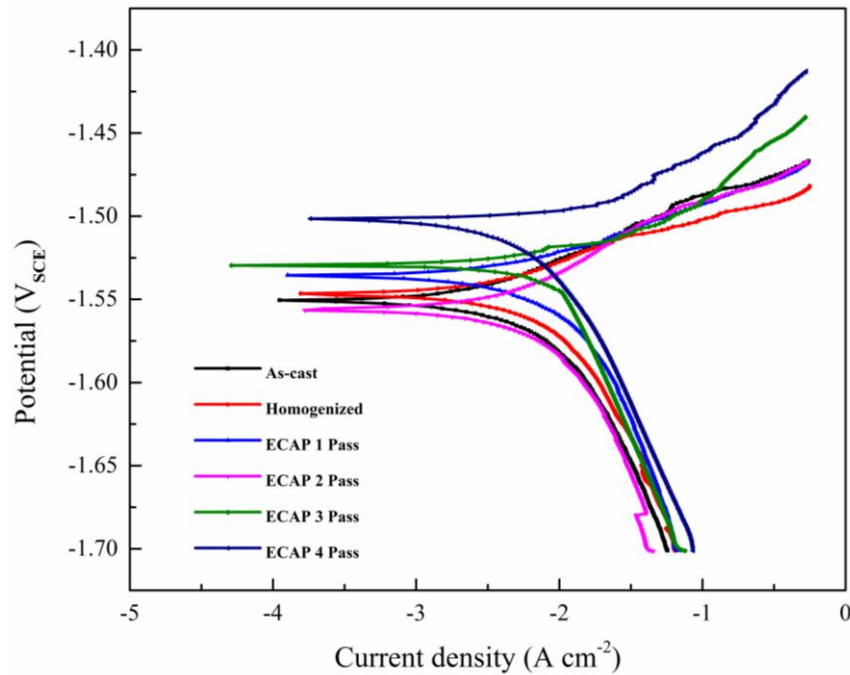


Figure 6.19 Electrochemical potentiodynamic polarization plots of unprocessed and ECAP processed samples

I_{corr} cannot be measured directly. However, it can be estimated using Tafel extrapolation method by EC-biologic software. Because of the phenomenon of passivity, current often change during a corrosion experiment. With increase in ECAP passes, I_{corr} value decreases which indicate high corrosion resistance of the processed samples. Decreased corrosion rate may be because of the presence of fine grained microstructure and uniformly distributed secondary particles which help to get good adhesion property for the passive film due to increased grain boundary density. Refined microstructure showed better surface coverage avoiding the damage to protective passive film ($\text{Mg}(\text{OH})_2$) and also the intermetallics slows down the corrosion reaction. ECAP 4 pass sample experiences decreased corrosion resistance due to increase large crystalline defects like energetic grain boundaries and dislocations. These variations are occurring during the corrosion process because the potential of the metal is the means by which the anodic and cathodic reactions are

kept in balance. If the anodic reaction releases too many electrons into the metal, excess electrons thus shift the potential of the metal more negative, which slows the anodic reaction and speeds up the cathodic reaction where increase in reduction of hydrogen takes place which intern affects the corrosion resistance.

Table 6.2 Electrochemical kinetic parameters like corrosion potential, corrosion current density, Tafel slopes (β_a & β_c) and corrosion rate (mm/y).

Materials	$E_{\text{corr}}(V_{\text{SCE}})$	I_{corr} ($\mu\text{A}/\text{cm}^2$)	β_a (mV/decade)	β_c (mV/decade)	Corrosion rate (mm/y)
As-cast	-1.550±0.005	6.37±1	83.4±10	126.6±15	0.298±0.010
Homogenized	-1.545±0.005	4.50±1	62.6±10	134.0±10	0.183±0.010
ECAP 1 Pass	-1.530±0.008	3.31±0.5	57.4±10	158.5±15	0.080±0.010
ECAP 2 Pass	-1.560±0.005	3.20±0.5	43.6±5	167.1±8	0.074±0.015
ECAP 3 Pass	-1.530±0.004	3.05±0.5	36.7±5	173.7±5	0.062±0.015
ECAP 4 Pass	-1.500±0.01	4.40±1	44.2±10	150.5±20	0.162±0.010

(b) Electrochemical impedance spectroscopy (EIS)

Corrosion behavior was also studied using EIS test with frequency ranges from 100 kHz to 10 mHz and the amplitude of sinusoidal potential signal is 5 mV. EIS plots obtained for different conditions, shown in figure 6.20, represents the Nyquist plots. First arc is the capacitance arc which represents the protective film formation and the second arc or tail region represents the degradation or damage of protective layer formed on the surface. Diameter of the arc is proportional to the variation of corrosion rate. Diameters of capacitive arcs of the ECAP processed samples increases with ECAP passes, which implies increased corrosion resistance. Randles circuit is used to fit the EIS plots to measure the charge-transfer resistance using ZSimpwin software. Obtained R_t values are plotted against number of ECAP passes are shown in figure 6.21 and in table 6.3. R_t values increases with increase in ECAP passes up to 3 passes. In the 4 pass ECAP sample, R_t value reduced indicating reduction on corrosion resistance.

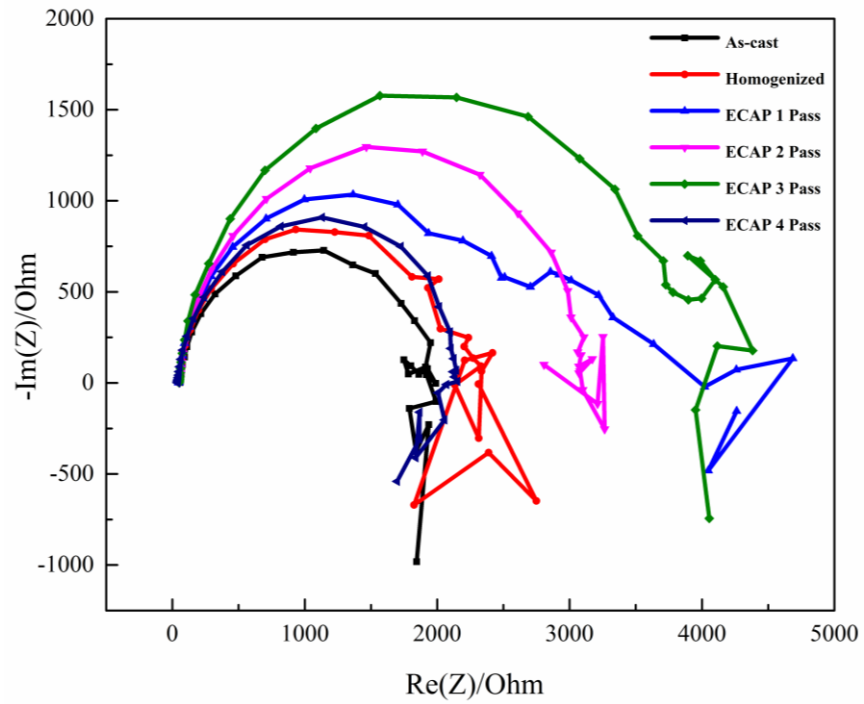


Figure 6.20 Nyquist plots of unprocessed and ECAP processed samples

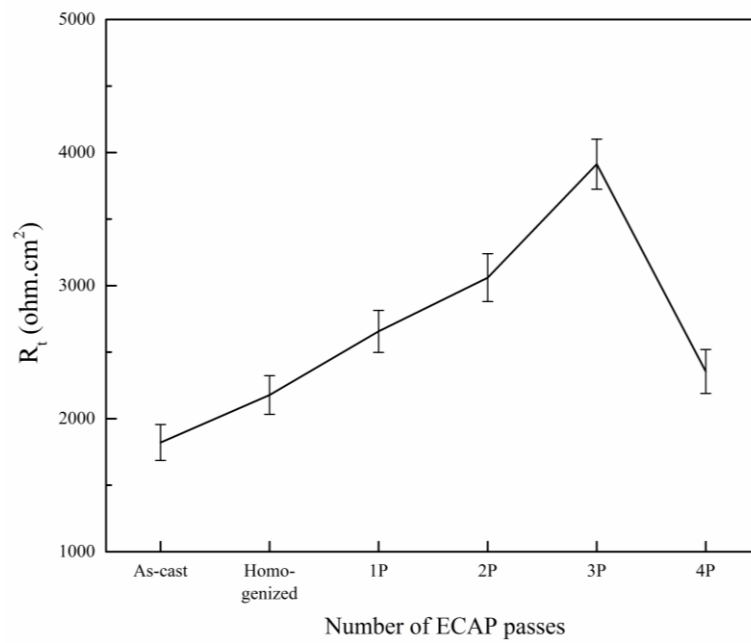


Figure 6.21 R_t verses number of ECAP passes

Table 6.3 Fitted R_t values for unprocessed and ECAP processed sample

Materials	R_t (ohm cm^2)
As-cast	1821±135
Homogenized	2178±145
ECAP 1 Pass	2656±158
ECAP 2 Pass	3060±180
ECAP 3 Pass	3913±188
ECAP 4 Pass	2355±165

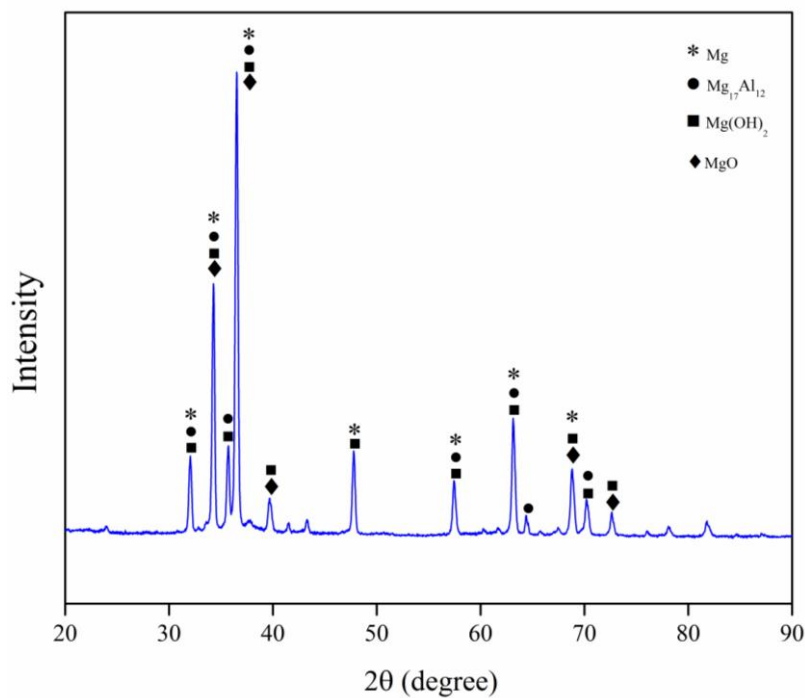


Figure 6.22 XRD of ECAP processed 3 pass corrosion sample

XRD was conducted on the corroded ECAP 3 pass sample to identify the phases present on the corroded surface as shown in figure 6.22. Mg(OH)_2 , MgO and $\text{Mg}_{17}\text{Al}_{12}$ are visible on the surface and this indicates the presence of protective passivation layer on the sample which hinders the corrosion attack (Wang et al. 2009). SEM micrograph shows the corroded surface of unprocessed and ECAP processed samples as shown in figure 6.23. Pits are more visible on as-cast and homogenized conditions which are large and deep. Pits tend to decrease with the ECAP processed samples as compared to unprocessed condition. Reduction in pits is due to the refined

microstructure and uniform distribution of secondary particles, which avoids the process of corrosion to occur on the surface.

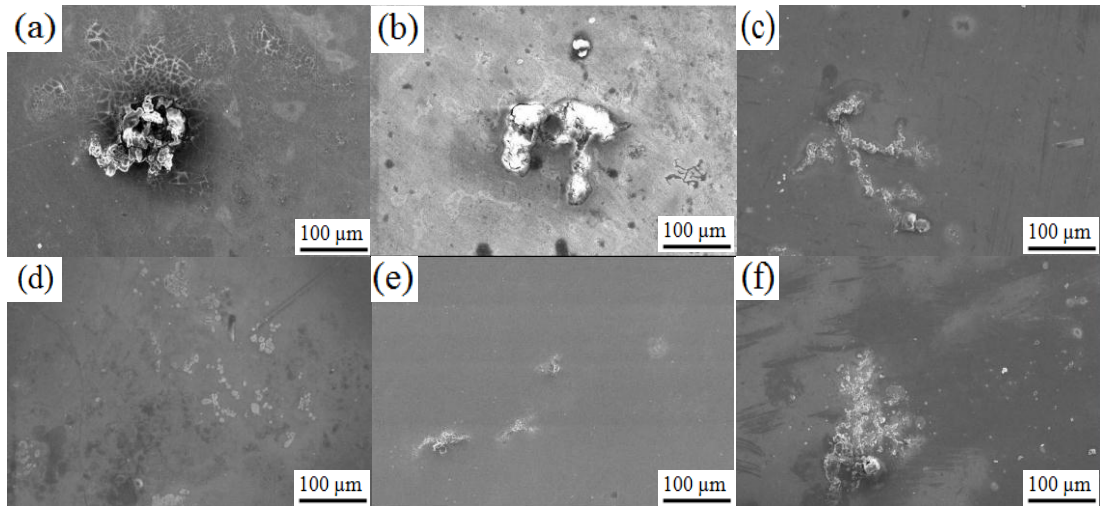


Figure 6.23 SEM images of corrosion samples for different ECAP passes

6.1.5.2 Immersion test

Immersion corrosion test is like a natural corrosion process which occurs by keeping the samples in 0.1 M NaCl solution for longer period of time (120 h). But in case of electrochemical measurements current is induced to corrode the sample. Corrosion rate is dependent on the evolution rate of hydrogen and the obtained values are tabulated in table 6.4. ECAP processed samples show increased corrosion resistance as shown in table compared to unprocessed condition. Figure 6.24 (a-f) show the surface morphology of samples. Figures show pit formation on corroded surface of immersed samples.

Table 6.4 Corrosion rate of immersed samples verses number of ECAP passes

Material	Corrosion Rate (mm/y)
As-cast	0.388±0.020
Homogenized	0.295±0.030
ECAP 1 Pass	0.170±0.015
ECAP 2 Pass	0.135±0.015
ECAP 3 Pass	0.085±0.010
ECAP 4 Pass	0.195±0.015

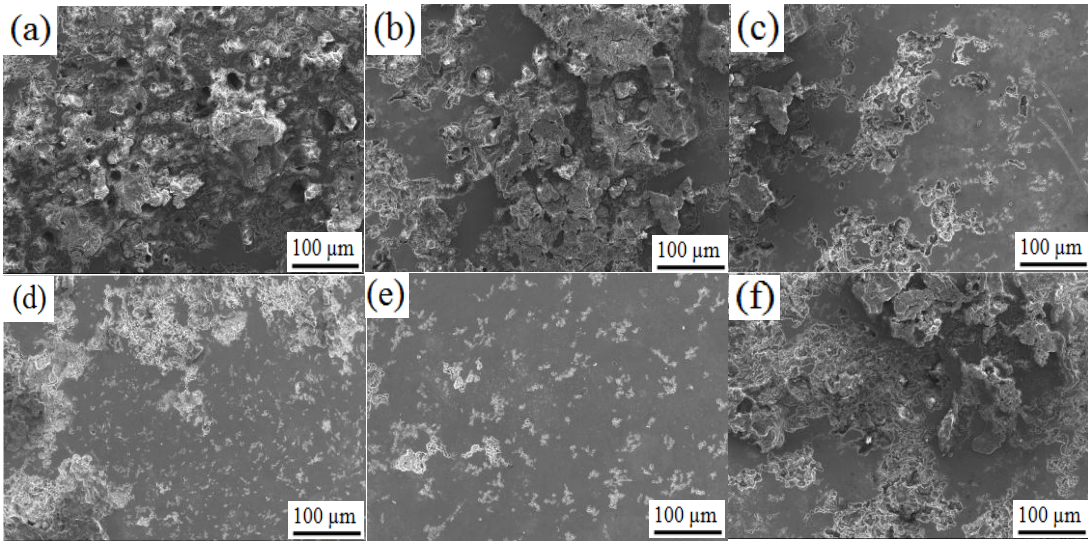


Figure 6.24 SEM images of immersed samples (a) as-cast (b) homogenized and ECAP processed (c) 1P, (d) 2P, (e) 3P, and (f) 4P samples

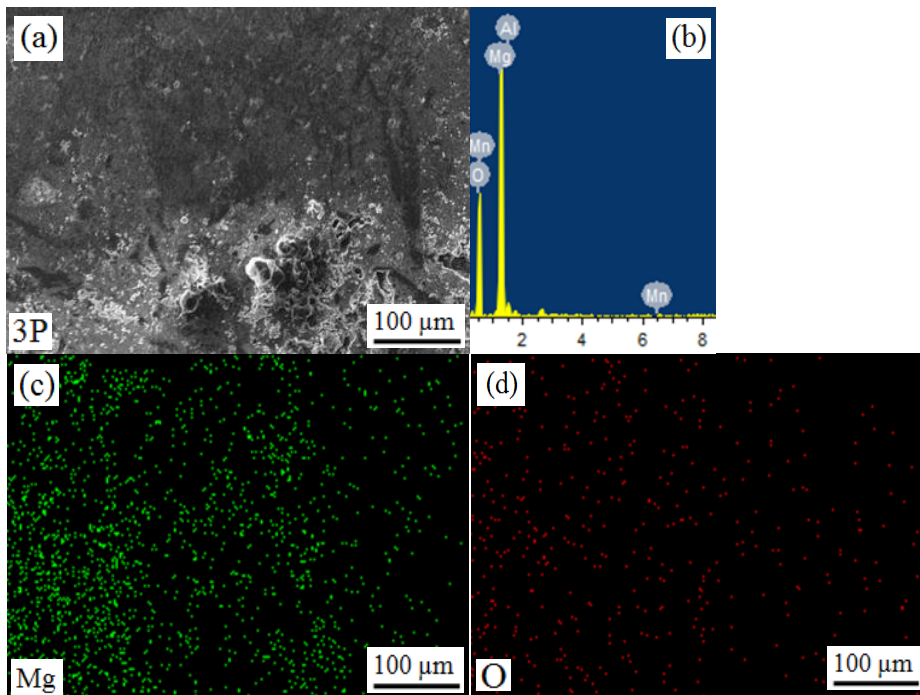


Figure 6.25 SEM images with EDS and elemental mapping of ECAP 3P sample
 Intensity of pits reduces with increase in ECAP passes up to 3 passes. But in ECAP 4 pass sample, pits increase because of the presence of large crystalline defects in higher ECAP pass samples that are more prone to corrosion, which causes increased corrosion reaction. EDS and elemental mapping shows the presence of oxygen on the surface. Distribution of magnesium and oxygen can be seen in figure 6.25. With these results,

it shows the formation of magnesium oxide and magnesium hydroxide on the corroded surface which improves the corrosion resistance properties.

6.2 Summary

ECAP was performed on AM90 magnesium alloy at a temperature of 275 °C using processing route B_C up to four passes. Microstructure, mechanical, wear and corrosion behavior of ECAP-processed samples were examined and the achieved results are summed up as mentioned below:

1. ECAP was carried out on AM90 Mg alloy using route B_C. Grain size decreased to ~3 μm average grain size for ECAP-processed 4-pass sample. With higher ECAP passes, a homogeneous and stable microstructure developed due to the dynamic recrystallization happening during ECAP processing or static recrystallization which might have occurred during preheating the sample before the ECAP process. EBSD result showed that the microstructure in ECAP 4 pass sample had grain boundaries of covering almost all the misorientation range rather than peaks at some definite misorientation values as in the as-cast sample.
2. UTS increases to ~77, 128, 97, 80% and YS increases to ~100, 113, 69, 25% for ECAP-processed 1 pass to 4 pass samples, respectively, as compared to homogenized condition. Maximum UTS was obtained for ECAP-processed 2 pass sample, and also, the elongation of this sample was 10.5% which is quite higher as compared to that of homogenized condition, viz. just 2.7%. Increase in the strength is because of grain boundary strengthening mechanism. During further ECAP passes, a decrease in strength and ductility is observed. However, obtained UTS, YS and elongation values were still quite higher in comparison with that of the as-cast and homogenized condition.
3. ECAP processed samples at higher passes show dimple kind of fracture revealing the state of ductile fracture behavior, whereas for homogenized condition and ECAP 1 pass sample, the surface appears to be of ductile-brittle type of fracture.

4. Increment in hardness was observed up to two passes (98Hv) and decrement with further passes. Deviation in microhardness and ultimate tensile strength is related to each other, and they appear to be mutually dependent and the variation is due to strain hardening.
5. The coefficient of friction values decreased with ECAP processed samples compared to unprocessed condition, and fluctuations were reduced with increased load of 40 N. Wear mass loss of ECAP processed samples reduced by ~1.71 (2500 m) and ~1.52 (5000 m) times under 30 N load and ~1.74 (2500 m) and ~1.31 (5000 m) under 40 N load in comparison to as-cast condition.
6. Wear surfaces showed delamination, plowing and wear debris. Oxygen peaks were also observed on both surfaces of homogenized and ECAP processed samples and the wear mechanism was recognized as abrasive and oxidation wear.
7. Potentiodynamic polarization test showed reduced corrosion current density (I_{corr}) which indicates higher corrosion resistance for the ECAP processed samples due to the presence of equiaxed fine grain microstructure and homogeneously distributed secondary phase particles ($\text{Mg}_{17}\text{Al}_{12}$). The charge-transfer resistance (R_t) values extracted from EIS plots showed increased values for ECAP processed samples compared to unprocessed condition. Increase in R_t values represents increased corrosion resistance.
8. Immersion corrosion test showed lower corrosion rate with low hydrogen evolution for ECAP processed samples due to the formation of protective surface layer $\text{Mg}(\text{OH})_2$ which controls the corrosion rate.

6.3 Comparison of properties in ECAP processed AM70, AM80 and AM90 alloys

ECAP was conducted on AM70, AM80 and AM90 alloys at 275 °C. Microstructural studies, mechanical testing, wear and corrosion behavior were observed on ECAP processed samples. The obtained results are summarized and discussed in chapters 4, 5 and 6, respectively for AM70, AM80 and AM90 alloys.

Effect of aluminium and manganese content in the alloys

Aluminium and manganese are the major alloying elements in AM70, AM80 and AM90, where Al improves strength and hardness of the material and addition of Mn improves the corrosion resistance by removing iron and other heavy metal elements (Avedessian and Baker, 1999). AM70, AM80 and AM90 alloys contains aluminium (Al) content of 7.1%, 8.22% and 9.06% followed by manganese (Mn) content of 0.35%, 0.39%, 0.42%, respectively. These alloys were subjected to ECAP at 275 °C up to 4 passes using route B_C.

Variation in Al content played major role in terms of strength properties rather than grain refinement. UTS obtained for AM80 is more compared to AM70 for ECAP 2 passes because of high Al content. But UTS of AM90 alloy is less compared to AM80 for ECAP 2 passes and the reason may be because of texture modification or texture softening in the early stages of ECAP process. Strength increases up to certain limit, if texture remains constant (Akbaripanah et al. 2013-a). As the Al content increased in the alloy, the microhardness values increased. AM90 alloy has the highest values of microhardness after each ECAP passes.

In wear analysis, COF and wear mass loss is reduced for AM90 compared to AM70 and AM80 alloy. Increase in aluminium content has decreased the COF and wear mass loss, which is interdependent on hardness values of the alloys. This implies increased wear resistance property of the alloy. Increase in aluminium content increased the intermetallic phases in the microstructure and improved the hardness of the alloy.

In corrosion studies, increase in Al and Mn content increased the corrosion resistance up to ECAP 3 passes for AM70 and AM80 but reduced for AM90 alloy. The reason may be because AM90 alloy possesses large crystalline defects energetic grain

boundaries after ECAP 3 pass where more corrosion reaction takes place (Song et al. 2010; Johansen et al. 1957). Corrosion properties are increased with increase in Al and Mn content due to the formation of intermetallic phases which acts as a barrier for corrosion occurrence and which improves the corrosion resistance of the material (Pardo et al. 2008; Song, 2005) by forming protective passivation layer on the surface of the material.

CHAPTER 7

CONCLUSIONS

Equal channel angular pressing was performed on AM70, AM80 and AM90 magnesium alloy at a temperature of 275 °C using route B_C. Effects of ECAP process on microstructure, mechanical properties, wear behavior and corrosion studies were investigated. Microstructural studies were conducted using SEM, TEM, EBSD and XRD to study the grain structure, grain size, grain misorientation angles and presence of intermetallics in the microstructure. Tensile and hardness tests were carried out to know the strength and hardness of ECAP processed samples. Unprocessed and ECAP processed samples were subjected to wear studies to identify the wear resistance properties. Electrochemical measurements and immersion tests were conducted to measure the corrosion resistance of unprocessed and ECAP processed samples and the conclusions are summed up based on the achieved outcome.

Microstructural studies of as-cast and ECAP processed magnesium alloys

- ECAP was carried out on AM70, AM80 and AM90 magnesium alloy using route B_C and average grain size decreased to 1 μm for AM70 and 3 μm for both AM80 and AM90 for ECAP 4 passes.
- Increase in ECAP passes lead to homogeneous microstructure due to dynamic recrystallization which occurred during ECAP process or because of static recrystallization before ECAP process.
- EBSD was conducted to know the misorientation angles of as-cast and ECAP processed samples. It was observed that, with higher ECAP passes the occurrence of HAGBs increased as strain increases during ECAP process.

Mechanical properties of as-cast and ECAP processed magnesium alloys

- Maximum UTS was obtained for ECAP processed 2 pass sample and also elongation was maintained. Increase in the strength is because of grain boundary strengthening mechanism. During further ECAP passes, decrement in strength and ductility was observed but achieved results holds good with comparison to as-cast condition. This reduction is due to dynamic recrystallization (DRX) that happened during ECAP process which is responsible for the removal of dislocations and also static recrystallization prior to ECAP processing.
- Increase in hardness was observed up to 2 pass and decremented with further passes. Variation in microhardness relates to ultimate tensile strength and they appear to be mutually dependent with each other. The reason may be because of strain hardening. As the ECAP passes increases, decrease in hardness value was observed and it is due to the development of new grains which hinders the strain hardening effect.
- Fracture surface of ECAP processed sample shows dimpled appearance suggesting ductile fracture behavior. Whereas for as-cast sample, it appears to be brittle type of fracture.

Wear behavior of as-cast and ECAP processed magnesium alloys

- Coefficient of friction (COF) values decreased for ECAP processed samples compared to unprocessed condition. Lower fluctuation was observed in COF values at 40 N load samples compared to 30 N load samples. Reduced COF values showed better wear resistance.
- Wear mass loss reduced for ECAP processed samples compared to unprocessed condition and the variation in wear mass loss is related to hardness of the material and this represents the improved wear resistance of the processed material.
- Microstructure of the worn surfaces showed delamination, ploughing and wear debris. Oxygen peaks were also observed on both surfaces of

unprocessed and ECAP processed samples. So the wear mechanism was recognized as abrasive wear and oxidation wear.

Corrosion behavior of as-cast and ECAP processed magnesium alloys

- Potentiodynamic polarization test showed reduced corrosion current density (I_{corr}) which indicates higher corrosion resistance for the ECAP processed samples due to the presence of equiaxed fine grain microstructure and homogeneously distributed secondary particles ($\text{Mg}_{17}\text{Al}_{12}$).
- The charge-transfer resistance (R_t) values extracted from EIS plots showed increased values for ECAP processed samples compared to unprocessed condition. Increase in R_t values represents increased corrosion resistance.
- Immersion test showed lower corrosion rate with low hydrogen evolution for ECAP processed samples compared to unprocessed condition. Lower hydrogen evolution is due to the formation of protective surface layer $\text{Mg}(\text{OH})_2$ which controls the corrosion rate.

Scope for Future Work

AM series magnesium alloys were processed through equal channel angular pressing (ECAP) up to four passes using route B_C . ECAP processed samples showed significant grain refinement and increased strength and hardness properties were achieved by ECAP process. Improvement in wear and corrosion resistance was achieved for ECAP processed samples. Apart from these features, the following various aspects can be considered for future work and its applications can be expanded in different areas of engineering.

- Microstructural studies can be conducted still further by texture analysis using pole figures to study in depth behavior of material after ECAP.
- Annealing studies can be conducted for ECAP processed samples to know the behavior of ECAP processed material at different annealing temperatures, when samples are subjected to practical applications.

- Fatigue behavior of ECAP processed samples can be studied to determine the behavior of material under fluctuating loads.
- Interface related mechanical behavior of ECAP processed material can be studied.

References

- Aghion, E., Bronfin, B., Von Buch, F., Schumann, S. and Friedrich, H. (2003). "Newly developed magnesium alloys for powertrain applications." *JOM*, 55(11), 30-33.
- Akbaripannah, F., Fereshteh-Saniee, F., Mahmudi, R. and Kim, H. K. (2013-a). "Microstructural homogeneity, texture, tensile and shear behavior of AM60 magnesium alloy produced by extrusion and equal channel angular pressing." *Mater. Des.*, 43, 31-39.
- Akbaripannah, F., Fereshteh-Saniee, F., Mahmudi, R. and Kim, H. K. (2013-b). "The influences of extrusion and equal channel angular pressing (ECAP) processes on the fatigue behavior of AM60 magnesium alloy." *Mater. Sci. Eng., A*, 565, 308-316.
- Argade, G. R., Panigrahi, S. K. and Mishra, R. S. (2012). "Effects of grain size on the corrosion resistance of wrought magnesium alloys containing neodymium." *Corros. Sci.*, 58, 145-151.
- Archard, J. (1953). "Contact and rubbing of flat surfaces." *J. Appl. Phys.*, 24(8), 981-988.
- ASM Handbook (1992). "Vol. 3-Alloy Phase Diagrams." *ASM International Materials*, Ohio, 2-173.
- ASM International, Metals Handbook, Corrosion, ninth ed., vol. 13, *ASM International*, 1987.
- Avedessian, M. M. and Baker, H. (1999). "Magnesium and Magnesium alloys." *ASM International, Materials Park*, OH, 14-16.
- Azushima, A., Kopp, R., Korhonen, A., Yang, D. Y., Micari, F., Lahoti, G. D. and Yanagida, A. (2008). "Severe plastic deformation (SPD) processes for metals." *CIRP Ann.-Manuf. Technol.*, 57(2), 716-735.
- Beygelzimer, Y., Varyukhin, V., Synkov, S. and Orlov, D. (2009). "Useful properties of twist extrusion." *Mater. Sci. Eng., A*, 503(1), 14-17.
- Biswas, S., Dhinwal, S. S. and Suwas, S. (2010). "Room-temperature equal channel angular extrusion of pure magnesium." *Acta mater.*, 58(9), 3247-3261.
- Callister, W. D. and Rethwisch, D. G. (2011). *Mater. Sci. Eng.* (Vol. 5), NY: John Wiley & Sons.
- Chino, Y., Kimura, K. and Mabuchi, M. (2008). "Twinning Behavior and Deformation Mechanisms of Extruded AZ31 Mg Alloy." *Mater. Sci. Eng. A*, 486 (1), 481-488.

- Choi, I.C., Lee, D.H., Ahn, B., Durst, K., Kawasaki, M., Langdon, T.G. and Jang, J.i. (2015). "Enhancement of strain-rate sensitivity and shear yield strength of a magnesium alloy processed by high-pressure torsion." *Scripta Mater.*, 94, 44-47.
- Chen, Y. J., Wang, Q. D., Roven, H. J., Liu, M. P., Karlsen, M., Yu, Y. D. and Hjelen, J. (2008). "Network-shaped fine-grained microstructure and high ductility of magnesium alloy fabricated by cyclic extrusion compression." *Scripta Mater.*, 58(4), 311-314.
- Chen, Y. J., Chai, Y. C., Roven, H. J., Gireesh, S. S., Yu, Y. D. and Hjelen, J. (2012). "Microstructure and mechanical properties of Al-xMg alloys processed by room temperature ECAP." *Mater. Sci. Eng. A*, 545, 139-147.
- Cheng, X., Li, Z. and Xiang, G. (2007). "Dry sliding wear behavior of TiNi alloy processed by equal channel angular extrusion." *Mater. Des.*, 28(7), 2218-2223.
- Chegini, M., Fallahi, A. and Shaeri, M. H. (2015). "Effect of Equal Channel Angular Pressing (ECAP) on Wear Behavior of Al-7075 Alloy." *Procedia Mater. Sci.*, 11, 95-100.
- Czerwinski, F. (2011). "Magnesium Alloys-Design." *Processing and Properties (InTech, Rijeka)*, 13.
- Darras, B. M., Khraisheh, M. K., Abu-Farha, F. K. and Omar, M. A. (2007). "Friction stir processing of commercial AZ31 magnesium alloy." *J. Mater. Process. Technol.*, 191(1), 77-81.
- Del Valle, J. A., Perez-Prado, M. T. and Ruano, O. A. (2005). "Accumulative roll bonding of a Mg-based AZ61 alloy." *Mater. Sci. Eng. A*, 410, 353-357.
- Ding, R., Chung, C., Chiu, Y. and Lyon, P. (2010). "Effect of ECAP on microstructure and mechanical properties of ZE41 magnesium alloy." *Mater. Sci. Eng. A*, 527(16), 3777-3784.
- Dumitru, F. D., Higuera-Cobos, O. F. and Cabrera, J. M. (2014). "ZK60 alloy processed by ECAP: Microstructural, physical and mechanical characterization." *Mater. Sci. Eng. A*, 594, 32-39.
- Djavanroodi, F. and Ebrahimi, M. (2010). "Effect of die parameters and material properties in ECAP with parallel channels." *Mater. Sci. Eng. A*, 527(29), 7593-7599.
- El Aal, M.I.A., El Mahallawy, N., Shehata, F.A., El Hameed, M.A., Yoon, E.Y. and Kim, H.S. (2010). "Wear properties of ECAP-processed ultrafine grained Al-Cu alloys." *Mater. Sci. Eng., A*, 527(16), 3726-3732.

- Eto, M., Sasaki, T., Fukushima, S., Shibahara, T., Miyata, K. and Wakita, M. (2006). "Development of super short interval multi-pass rolling technology for ultra fine-grained hot strip." *Rev. Met. Paris*, 103(7-8), 319-325.
- Etou, M., Fukushima, S., Sasaki, T., Haraguchi, Y., Miyata, K., Wakita, M., Tomida, T., Imai, N., Yoshida, M. and Okada, Y. (2008). "Super Short Interval Multi-pass Rolling Process for Ultrafine-grained Hot Strip." *ISIJ Int.*, 48(8), 1142-1147.
- Fatemi-Varzaneh, S. M. and Zarei-Hanzaki, A. (2009). "Accumulative back extrusion (ABE) processing as a novel bulk deformation method." *Mater. Sci. Eng., A*, 504(1), 104-106.
- Faraji, G. and Jafarzadeh, H. (2012). "Accumulative Torsion Back (ATB) Processing as a New Plastic Deformation Technique." *Mater. Manuf. Processes*, 27(5), 507-511.
- Fang, D.R., Duan, Q.Q., Zhao, N.Q., Li, J.J., Wu, S.D. and Zhang, Z.F. (2007). "Tensile properties and fracture mechanism of Al-Mg alloy subjected to equal channel angular pressing." *Mater. Sci. Eng., A*, 459(1), 137-144.
- Feng, X. M. and Ai, T. T. (2009). "Microstructure evolution and mechanical behavior of AZ31 Mg alloy processed by equal-channel angular pressing." *Trans. Non-Ferrous Met. Soc. China*, 19(2), 293-298.
- Figueiredo, R. B. and Langdon, T. G. (2010). "Grain refinement and mechanical behavior of a magnesium alloy processed by ECAP." *J. Mater. Sci.*, 45(17), 4827-4836.
- Figueiredo, R.B. and Langdon, T.G. (2009). "Principles of grain refinement and superplastic flow in magnesium alloys processed by ECAP." *Mater. Sci. Eng., A*, 501(1), 105-114.
- Figueiredo, R. B. and Langdon, T. G. (2006). "The development of superplastic ductilities and microstructural homogeneity in a magnesium ZK60 alloy processed by ECAP." *Mater. Sci. Eng., A*, 430(1), 151-156.
- Fintova, S. and Kunz, L. (2015). "Fatigue properties of magnesium alloy AZ91 processed by severe plastic deformation." *J. Mechanical Behavior of Biomed. Mater.*, 42, 219-228.
- Fleischer, R. L. and Peckner, D. (1964). "Strengthening of metals." *Reinhold*, New York, 29.
- Furukawa, M., Horita, Z., Nemoto, M. and Langdon, T.G. (2001). "Review: Processing of metals by equal-channel angular pressing." *J. Mater. Sci.* 36(12), 2835-2843

Furuno, K., Akamatsu, H., Oh-ishi, K., Furukawa, M., Horita, Z. and Langdon, T. G. (2004). "Microstructural development in equal-channel angular pressing using a 60° die." *Acta Mater.*, 52(9), 2497-2507.

Furukawa, M., Iwahashi, Y., Horita, Z., Nemoto, M. and Langdon, T. G. (1998). "The shearing characteristics associated with equal-channel angular pressing." *Mater. Sci. Eng., A*, 257(2), 328-332.

Furukawa, M., Horita, Z. and Langdon, T. G. (2002). "Factors influencing the shearing patterns in equal-channel angular pressing." *Mater. Sci. Eng., A*, 332(1), 97-109.

Friedrich, H. E. and Mordike, B. L. (2006). "Magnesium Technology: Metallurgy, Design Data, Automotive Applications." *Springer publications*, Verlag Berlin Heidelberg, Germany.

Furui, M., Kitamura, H., Anada, H. and Langdon, T. G. (2007). "Influence of preliminary extrusion conditions on the superplastic properties of a magnesium alloy processed by ECAP." *Acta Mater.*, 55(3), 1083-1091.

Gerold, V. and Nabarro, F. R. N. (1979). "Dislocations in solids." North Holland, The Netherlands.

George, E. Dieter (1988). "Mechanical Metallurgy." *McGraw-Hill*, London.

Gopi, K.R., Nayaka, H.S. and Sahu, S. (2016). "Investigation of Microstructure and Mechanical Properties of ECAP-Processed AM Series Magnesium Alloy." *J. Mater. Eng. Perform.*, 25(9), 3737-3745.

Gong, X., Kang, S.B., Li, S. and Cho, J.H. (2009). "Enhanced plasticity of twin-roll cast ZK60 magnesium alloy through differential speed rolling." *Mater. Des.*, 30(9), 3345-3350.

Guo, W., Wang, Q. D., Ye, B., Liu, M. P., Peng, T., Liu, X. T. and Zhou, H. (2012). "Enhanced microstructure homogeneity and mechanical properties of AZ31 magnesium alloy by repetitive upsetting." *Mater. Sci. Eng. A*, 540, 115-122.

Guo, W., Wang, Q.D., Li, W.Z., Zhosu, H., Zhang, L. and Liao, W.J. (2017). "Enhanced microstructure homogeneity and mechanical properties of AZ91-SiC nanocomposites by cyclic closed-die forging." *J. Compos. Mater.*, 51(5), 681-686.

Hall, E.O. (1951). "The deformation and ageing of mild steel." *Proc. Phys. Soc., Sect B*, 64(9), 747-753.

Hakamada, M., Nakamoto, Y., Matsumoto, H., Iwasaki, H., Chen, Y., Kusuda, H. and Mabuchi, M. (2007). "Relationship between hardness and grain size in electrodeposited copper films." *Mater. Sci. Eng. A*, 457(1), 120-126.

- Hadzima, B., Janecek, M., Bukovina, M. and Kral, R. (2009). "Electrochemical properties of fine-grained AZ31 magnesium alloy." *Int. J. Mater. Res.*, 100(9), 1213-1216.
- Hofmann, D. C. and Vecchio, K. S. (2005). "Submerged friction stir processing (SFSP): An improved method for creating ultra-fine-grained bulk materials." *Mater. Sci. Eng. A*, 402(1), 234-241.
- Hoche, H., Blawert, C., Broszeit, E. and Berger, C. (2005). "Galvanic corrosion properties of differently PVD-treated magnesium die cast alloy AZ91." *Surf. Coat. Technol.*, 193(1), 223-229.
- Hu, H. J., Fan, J. Z., Wang, H., Zhai, Z. Y., Li, Y. Y. and Ou, Z. (2015). "Dry sliding wear behavior of ES-processed AZ31B magnesium alloy." *Russ. J. Non-Ferrous Met.*, 56(4), 392-398.
- Huot, J. (2016). "High-Pressure Torsion, in: Enhancing Hydrogen Storage Properties of Metal Hydrides: Enhancement by Mechanical Deformations." Springer International Publishing AG Switzerland, 11.
- Huang, H., Tang, Z., Tian, Y., Jia, G., Niu, J., Zhang, H., Pei, J., Yuan, G. and Ding, W. (2015). "Effects of cyclic extrusion and compression parameters on microstructure and mechanical properties of Mg-1.50Zn-0.25Gd alloy." *Mater. Des.* 86, 788-796.
- Ion, S.E., Humphreys, F.J. and White, S.H. (1982). "Dynamic recrystallisation and the development of microstructure during the high temperature deformation of magnesium." *Acta Metall.*, 30(10), 1909-1919.
- Ivanisenko, Y., Kulagin, R., Fedorov, V., Mazilkin, A., Scherer, T., Baretzky, B. and Hahn, H. (2016). "High Pressure Torsion Extrusion as a new severe plastic deformation process." *Mater. Sci. Eng. A*, 664, 247-256.
- Iwahashi, Y., Wang, J., Horita, Z., Nemoto, M. and Langdon, T. G. (1996). "Principle of equal-channel angular pressing for the processing of ultra-fine grained materials." *Scripta Mater.*, 35(2), 143-146.
- Iwahashi, Y., Horita, Z., Nemoto, M. and Langdon, T. G. (1997). "An investigation of microstructural evolution during equal-channel angular pressing." *Acta Mater.*, 45(11), 4733-4741.
- Jahedi, M. and Paydar, M.H. (2010). "Study on the feasibility of the torsion extrusion (TE) process as a severe plastic deformation method for consolidation of Al powder." *Mater. Sci. Eng. A*, 527(20), 5273-5279.

- Jahadi, R., Sedighi, M. and Jahed, H. (2014). "ECAP effect on the micro-structure and mechanical properties of AM30 magnesium alloy." *Mater. Sci. Eng. A*, 593, 178-184.
- Janecek, M., Cizek, J., Gubicza, J. and Vratna, J. (2012). "Microstructure and dislocation density evolutions in MgAlZn alloy processed by severe plastic deformation." *J. Mater. Sci.*, 47(22), 7860-7869.
- Jiang, D. M., Ning, J. L., Sun, J. F., Hu, Z. M. and Yi, H. O. U. (2008). "Annealing behavior of Al-Mg-Mn alloy processed by ECAP at elevated temperature." *Trans. Non-Ferrous Met. Soc. China*, 18(2), 248-254.
- Jiang, J., Aibin, M.A., Saito, N., Zhixin, S.H.E.N., Dan, S.O.N.G., Fumin, L.U., Nishida, Y., Donghui, Y.A.N.G. and Pinghua, L.I.N. (2009). "Improving corrosion resistance of RE-containing magnesium alloy ZE41A through ECAP." *J. Rare Earths*, 27(5), 848-852.
- Jin, L., Lin, D., Mao, D., Zeng, X., Chen, B. and Ding, W. (2006). "Microstructure evolution of AZ31 Mg alloy during equal channel angular extrusion." *Mater. Sci. Eng. A*, 423(1), 247-252.
- Johansen, N.A., Adams, G.B. and Van Rysselberghe, P. (1957). "Anodic oxidation of aluminum, chromium, hafnium, tantalum, titanium, vanadium, and zirconium at very low current densities." *J. Electrochem. Soc.*, 104(6), 339-346.
- Jung, K.H., Kim, Y.B., Lee, G.A., Lee, S., Kim, E.Z. and Choi, D.S. (2014). "Formability of ZK60A Magnesium Alloy Determined by Compression and Backward Extrusion." *Mater. Manuf. Processes*, 29(2), 115-120.
- Kapoor, R., Sarkar, A., Yogi, R., Shekhawat, S.K., Samajdar, I. and Chakravartty, J.K. (2013). "Softening of Al during multi-axial forging in a channel die." *Mater. Sci. Eng. A*, 560, 404-412.
- Khosravifard, A., Jahedi, M. and Yaghtin, A.H. (2012). "Three dimensional finite element study on torsion extrusion processing of 1050 aluminum alloy." *Trans. Non-ferrous. Met. Soc. China*, 22(11), 2771-2776.
- Kim, H. K. and Kim, W. J. (2004). "Microstructural instability and strength of an AZ31 Mg alloy after severe plastic deformation." *Mater. Sci. Eng. A*, 385(1), 300-308.
- Kim, W.J., Hong, S.I., Kim, Y.S., Min, S.H., Jeong, H.T. and Lee, J.D. (2003). "Texture development and its effect on mechanical properties of an AZ61 Mg alloy fabricated by equal channel angular pressing." *Acta Mater.*, 51(11), 3293-3307.

- Kim, H.K., Lee, Y.I. and Chung, C.S. (2005). "Fatigue properties of a fine-grained magnesium alloy produced by equal channel angular pressing." *Scripta Mater.*, 52(6), 473-477.
- Kojima, Y. (2000). "Handbook Advanced Mg Technology." *Kallos Publishing Co., Ltd.*, Tokyo.
- Komura, S., Furukawa, M., Horita, Z., Nemoto, M. and Langdon, T. G. (2001). "Optimizing the procedure of equal-channel angular pressing for maximum superplasticity." *Mater. Sci. Eng. A*, 297(1), 111-118.
- Kral, R., Minarik, P., Lesna, I. K., Skublova, L., Harcuba, P., Hadzima, B. and Janecek, M. (2011). "Effect of Grain Refinement on Electrochemical Characteristics in AE42 Magnesium Alloy." *WDS'11 Proceedings of Contributed Papers, Part III*, 136-140.
- Kulyasova, O., Islamgaliev, R., Mingler, B. and Zehetbauer, M. (2009). "Microstructure and fatigue properties of the ultrafine-grained AM60 magnesium alloy processed by equal-channel angular pressing." *Mater. Sci. Eng. A*, 503(1), 176-180.
- Lavrentev, F. F. (1980). "The type of dislocation interaction as the factor determining work hardening." *Mater. Sci. Eng.*, 46(2), 191-208.
- Lee, S. W., Chen, Y. L., Wang, H. Y., Yang, C. F. and Yeh, J. W. (2007). "On mechanical properties and superplasticity of Mg–15Al–1Zn alloys processed by reciprocating extrusion." *Mater. Sci. Eng. A*, 464(1), 76-84.
- Lee, S. and Langdon, T. G. (1999). "Influence of equal-channel angular pressing on the superplastic properties of commercial aluminium alloys." In *MRS Proceedings*, Cambridge University Press, 601, 359.
- Li, P., Lei, M.K. and Zhu, X.P. (2010). "Dry sliding tribological behavior of AZ31 magnesium alloy irradiated by high-intensity pulsed ion beam." *Appl. Surf. Sci.*, 257(1), 72-81.
- Liao, J., Hotta, M. and Yamamoto, N. (2012-a). "Corrosion behavior of fine-grained AZ31B magnesium alloy." *Corros. Sci.*, 61, 208-214.
- Li, B., Joshi, S., Azevedo, K., Ma, E., Ramesh, K.T., Figueiredo, R.B. and Langdon, T.G. (2009). "Dynamic testing at high strain rates of an ultrafine-grained magnesium alloy processed by ECAP." *Mater. Sci. Eng. A*, 517(1), 24-29.
- Liao, J., Hotta, M. and Mori, Y. (2012-b). "Improved corrosion resistance of a high-strength Mg-Al-Mn-Ca magnesium alloy made by rapid solidification powder metallurgy." *Mater. Sci. Eng., A*, 544, 10-20.

- Liao, W., Ye, B., Zhang, L., Zhou, H., Guo, W., Wang, Q. and Li, W. (2015). "Microstructure evolution and mechanical properties of SiC nanoparticles reinforced magnesium matrix composite processed by cyclic closed-die forging." *Mater. Sci. Eng. A*, 642, 49-56.
- Lin, J., Wang, Q., Peng, L. and Roven, H. J. (2009). "Microstructure and high tensile ductility of ZK60 magnesium alloy processed by cyclic extrusion and compression." *J. Alloys Compd.*, 476(1), 441-445.
- Lin, H.K., Huang, J.C. and Langdon, T.G. (2005). "Relationship between texture and low temperature superplasticity in an extruded AZ31 Mg alloy processed by ECAP." *Mater. Sci. Eng. A*, 402(1), 250-257.
- Lowe, T.C. and Valiev, R.Z. (2004). "The use of severe plastic deformation techniques in grain refinement." *JOM*, 56 (10), 64-68.
- Luo, A. A. and Sachdev, A. K. (2007). "Development of a new wrought magnesium-aluminium-manganese alloy AM30." *Metall. Mater. Trans. A*, 38(6), 1184-1192.
- Luo, A., Renaud, J., Nakatsugawa, I. and Plourde, J. (1995). "Magnesium castings for automotive applications." *JOM*, 47(7), 28-31.
- Majumdar, J.D., alun, R.G., Mordike, B.L. and Manna, I. (2003). "Effect of laser surface melting on corrosion and wear resistance of a commercial magnesium alloy." *Mater. Sci. Eng., A*, 361(1), 119-129.
- Matsubara, K., Miyahara, Y., Horita, Z. and Langdon, T. G. (2003). "Developing superplasticity in a magnesium alloy through a combination of extrusion and ECAP." *Acta Mater.*, 51(11), 3073-3084.
- Makar, G. L. and Kruger, J. (1993). "Corrosion of magnesium." *International mater. reviews*, 38(3), 138-153.
- Masoudpanah, S. M. and Mahmudi, R. (2010). "Effects of rare earth elements and Ca additions on high temperature mechanical properties of AZ31 magnesium alloy processed by ECAP." *Mater. Sci. Eng., A*, 527(16), 3685-3689.
- Masoudpanah, S. M. and Mahmudi, R. (2009). "Effects of rare-earth elements and Ca additions on the microstructure and mechanical properties of AZ31 magnesium alloy processed by ECAP." *Mater. Sci. Eng., A*, 526(1), 22-30.
- Ma, A., Jiang, J., Saito, N., Shigematsu, I., Yuan, Y., Yang, D. and Nishida, Y. (2009). "Improving both strength and ductility of a Mg alloy through a large number of ECAP passes." *Mater. Sci. Eng., A*, 513, 122-127.

- Minarik, P., Kral, R. and Janecek, M. (2013). "Effect of ECAP processing on corrosion resistance of AE21 and AE42 magnesium alloys." *Appl. Surf. Sci.*, 281, 44-48.
- Miyahara, Y., Horita, Z. and Langdon, T. G. (2006). "Exceptional superplasticity in an AZ61 magnesium alloy processed by extrusion and ECAP." *Mater. Sci. Eng., A*, 420(1), 240-244.
- Mordike, B. L. and Ebert, T. (2001). "Magnesium: properties-applications-potential." *Mater. Sci. Eng., A*, 302(1), 37-45.
- Mohamed Ibrahim. (2011). "Influence of the pre-homogenization treatment on the microstructure evolution and the mechanical properties of Al-Cu alloys processed by ECAP." *Mater. Sci. Eng., A*, 528(22), 6946-6957.
- Mostaed, E., Hashempour, M., Fabrizi, A., Dellasega, D., Bestetti, M., Bonollo, F. and Vedani, M. (2014). "Microstructure, texture evolution, mechanical properties and corrosion behavior of ECAP processed ZK60 magnesium alloy for biodegradable applications." *J. Mechanical Behavior of Biomed. Mater.*, 37, 307-322.
- Mostaed, E., Fabrizi, A., Dellasega, D., Bonollo, F. and Vedani, M. (2015). "Microstructure, mechanical behavior and low temperature superplasticity of ECAP processed ZM21 Mg alloy." *J. Alloys Compd.*, 638, 267-276.
- Nakashima, K., Horita, Z., Nemoto, M. and Langdon, T.G. (2000). "Development of a multi-pass facility for equal-channel angular pressing to high total strains." *Mater. Sci. Eng., A*, 281(1), 82-87.
- Nakamura, K., Neishi, K., Kaneko, K., Nakagaki, M. and Horita, Z. (2004). "Development of severe torsion straining process for rapid continuous grain refinement." *Mater. Trans.*, 45(12), 3338-3342.
- Orlov, D., Ralston, K. D., Birbilis, N. and Estrin, Y. (2011). "Enhanced corrosion resistance of Mg alloy ZK60 after processing by integrated extrusion and equal channel angular pressing." *Acta Mater.*, 59(15), 6176-6186.
- Pardo, A., Merino, M.C., Coy, A.E., Viejo, F., Arrabal, R. and Feliu Jr., S. (2008). "Influence of microstructure and composition on the corrosion behaviour of Mg/Al alloys in chloride media." *Electrochim. Acta*, 53(27), 7890-7902.
- Pardo, A., Merino, M. C., Coy, A. E., Arrabal, R., Viejo, F. and Matykina, E. (2008). "Corrosion behaviour of magnesium/aluminium alloys in 3.5 wt.% NaCl." *Corros. Sci.*, 50(3), 823-834.
- Panigrahi, S.K. and Jayaganthan, R. (2008). "A study on the mechanical properties of cryorolled Al-Mg-Si alloy." *Mater. Sci. Eng., A*, 480(1), 299-305.

Petch, N.J. (1953). "The cleavage strength of polycrystals." *J. Iron Steel Inst.*, 174, 25-28.

Ralston, K. D. and Birbilis, N. (2010). "Effect of grain size on corrosion: a review." *Corrosion*, 66(7), 075005-075005.

Rajinikanth, V., Arora, G., Narasaiah, N. and Venkateswarlu, K. (2008). "Effect of repetitive corrugation and straightening on Al and Al-0.25 Sc alloy." *Mater. Lett.*, 62(2), 301-304.

Raab, G. J., Valiev, R. Z., Lowe, T. C. and Zhu, Y. T. (2004). "Continuous processing of ultrafine grained Al by ECAP-Conform." *Mater. Sci. Eng., A*, 382(1), 30-34.

Raei, M., Toroghinejad, M.R. and Jamaati, R. (2011). "Nano/Ultrafine Structured AA1100 by ARB Process." *Mater. Manuf. Processes*, 26(11), 1352-1356.

Sakai, G., Nakamura, K., Horita, Z. and Langdon, T. G. (2005). "Developing high-pressure torsion for use with bulk samples." *Mater. Sci. Eng., A*, 406(1), 268-273.

Saito, Y., Utsunomiya, H., Tsuji, N. and Sakai, T. (1999). "Novel ultra-high straining process for bulk materials-development of the accumulative roll-bonding (ARB) process." *Acta Mater.*, 47(2), 579-583.

Semiatin, S.L. and Jonas, J.J. (1984). "Formability and workability of metals: plastic instability and flow localization." *Amer. Soc. Met.*, 299.

Shin, D.H., Park, J.J., Kim, Y.S. and Park, K.T. (2002). "Constrained groove pressing and its application to grain refinement of aluminum." *Mater. Sci. Eng. A*, 328(1), 98-103.

Shaarbaf, M. and Toroghinejad, M. R. (2008). "Nano-grained copper strip produced by accumulative roll bonding process." *Mater. Sci. Eng. A*, 473(1), 28-33.

Sharifzadeh, M., Ali ansari, M., Narvan, M., Behnagh, R. A., Araee, A. and Givi, M. K. B. (2015). "Evaluation of wear and corrosion resistance of pure Mg wire produced by friction stir extrusion." *Trans. Non-Ferrous Met. Soc. China*, 25(6), 1847-1855.

Shi, Z., Liu, M. and Atrens, A. (2010). "Measurement of the corrosion rate of magnesium alloys using Tafel extrapolation." *Corros. Sci.*, 52(2), 579-588.

Song, G. (2005). "Recent progress in corrosion and protection of magnesium alloys." *Adv. Eng. Mater.*, 7(7), 563-586.

Song, D., Ma, A., Jiang, J., Lin, P., Yang, D. and Fan, J. (2010). "Corrosion behavior of equal-channel-angular-pressed pure magnesium in NaCl aqueous solution." *Corros. Sci.*, 52(2), 481-490.

- Song, D., Ma, A. B., Jiang, J. H., Lin, P. H., Yang, D. H. and Fan, J. F. (2011). "Corrosion behaviour of bulk ultra-fine grained AZ91D magnesium alloy fabricated by equal-channel angular pressing." *Corros. Sci.*, 53(1), 362-373.
- Song, G., Atrens, A. and StJohn, D. (2001). "An hydrogen evolution method for the estimation of the corrosion rate of magnesium alloys." *Magnesium Technol.*, 254-262.
- Song, G. and Atrens, A. (2003). "Understanding magnesium corrosion-a framework for improved alloy performance." *Adv. Eng. Mater.*, 5(12), 837-858.
- Stolyarov, V. V., Zhu, Y. T., Alexandrov, I. V., Lowe, T. C. and Valiev, R. Z. (2001). "Influence of ECAP routes on the microstructure and properties of pure Ti." *Mater. Sci. Eng. A*, 299(1), 59-67.
- Stolyarov, V. V., Lapovok, R., Brodova, I. G. and Thomson, P. F. (2003). "Ultrafine-grained Al-5 wt.% Fe alloy processed by ECAP with backpressure." *Mater. Sci. Eng. A*, 357(1), 159-167.
- Su, C.W., Lu, L. and Lai, M.O. (2008). "Recrystallization and grain growth of deformed magnesium alloy." *Philos. Mag.*, 88(2), 181-200.
- Sunil, B.R. (2015). "Repetitive Corrugation and Straightening of Sheet Metals." *Mater. Manuf. Processes*, 30(10), 1262-1271.
- Surendarnath, S., Sankaranarayanan, K. and Ravisankar, B. (2014). "A Comparative Study of Commercially Pure Aluminum Processed by ECAP Using Conventional and New Die." *Mater. Manuf. Processes*, 29(10), 1172-1178.
- Suh, J., Victoria-Hernandez, J., Letzig, D., Golle, R., Yi, S., Bohlen, J. and Volk, W. (2015). "Improvement in cold formability of AZ31 magnesium alloy sheets processed by equal channel angular pressing." *J. Mater. Process. Technol.*, 217, 286-293.
- Sunil, B. R., Kumar, K. K., Jojibabu, P., Kumar, T. S. and Chakkingal, U. (2014). "Effect of processing route and working temperature on microstructure evolution of AZ31 magnesium alloy during equal channel angular pressing." *Procedia Mater. Sci.*, 5, 841-846.
- Suwas, S., Gottstein, G. and Kumar, R. (2007). "Evolution of crystallographic texture during equal channel angular extrusion (ECAE) and its effects on secondary processing of magnesium." *Mater. Sci. Eng. A*, 471(1), 1-14.
- Taltavull, C., Rodrigo, P., Torres, B., Lopez, A.J. and Rams, J. (2014). "Dry sliding wear behavior of AM50B magnesium alloy." *Mater. Des.*, 56, 549-556.
- Tian, Y., Huang, H., Yuan, G. and Ding, W. (2015). "Microstructure evolution and mechanical properties of quasicrystal-reinforced Mg-Zn-Gd alloy processed by cyclic extrusion and compression." *J. Alloys Compd.* 626, 42-48

- Valiev, R.Z., Estrin, Y., Horita, Z., Langdon, T.G., Zechetbauer, M.J. and Zhu, Y.T. (2006). "Producing Bulk Ultrafine-Grained Materials by Severe Plastic Deformation." *JOM*, 58(4), 33-39.
- Valiev, R.Z., Islamgaliev, R. K. and Alexandrov, I.V. (2000). "Bulk nanostructured materials from severe plastic deformation." *Prog. Mater sci.*, 45(2), 103-189.
- Valiev, R. Z. and Langdon, T. G. (2006). "Principles of equal-channel angular pressing as a processing tool for grain refinement." *Prog. Mater sci*, 51(7), 881-981.
- Verlinden, B. (2005). "Severe plastic deformation of metals." *Metalurgija*, 11(3), 165-182.
- Watanabe, K., Matsuda, K., Gonoji, T., Kawabata, T., Sakakibara, K., Sanpei, Y., Saikawa, S. and Ikeno, S. (2010). "Effect of Casting Method and Al Contents on Microstructure in AM-Type Magnesium Alloys." *Mater. Sci. Forum*, 654, 663-666.
- Wang, L., Shinohara, T. and Zhang, B. P. (2009). "Corrosion behavior of AZ31 magnesium alloy in dilute sodium chloride solutions." *Zairyo-to-Kankyo*, 58(3), 105-110.
- Wang, R.M., Eliezer, A. and Gutman, E.M. (2003). "An investigation on the microstructure of an AM50 magnesium alloy." *Mater. Sci. Eng., A*, 355(1), 201-207.
- Wang, C.T., Gao, N., Wood, R.J. and Langdon, T.G. (2011). "Wear behavior of an aluminum alloy processed by equal-channel angular pressing." *J. Mater. Sci.*, 46(1), 123-130.
- Xing, Z.P., Kang, S.B. and Kim, H.W. (2002). "Structure and properties of AA3003 alloy produced by accumulative roll bonding process." *J. Mater. Sci.*, 37(4), 717-722.
- Xin, Z. H. A. O., Wang, J. F. and Jing, T. F. (2007). "Gray cast iron with directional graphite flakes produced by cylinder covered compression process". *J. Iron and Steel Res.*, 14(5), 52-55.
- Xu, J., Wang, X., Zhu, X., Shirooyeh, M., Wongsangam, J., Shan, D., Guo, B. and Langdon, T. G. (2013). "Dry sliding wear of an AZ31 magnesium alloy processed by equal-channel angular pressing." *J. Mater. Sci.*, 48(11), 4117-4127.
- Yan, K., Sun, Y. S., Bai, J. and Xue, F. (2011). "Microstructure and mechanical properties of ZA62 Mg alloy by equal-channel angular pressing." *Mater. Sci. Eng., A*, 528(3), 1149-1153.
- Yadav, P.C., Sinhal, A., Sahu, S., Roy, A. and Shekhar, S. (2016). "Microstructural Inhomogeneity in Constrained Groove Pressed Cu-Zn Alloy Sheet." *J. Mater. Eng. Perform.* 25(7), 2604-2614.

Yamashita, A., Yamaguchi, D., Horita, Z. and Langdon, T. G. (2000). "Influence of pressing temperature on microstructural development in equal-channel angular pressing." *Mater. Sci. Eng., A*, 287(1), 100-106.

Yu, H.L., Lu, C., Tieu, A.K. and Kong, C. (2014). "Fabrication of Nanostructured Aluminum Sheets Using Four-Layer Accumulative Roll Bonding." *Mater. Manuf. Processes*, 29(4), 448-453.

Zhan, M.Y., Li, Y.Y. and Chen, W.P. (2008). "Improving mechanical properties of Mg-Al-Zn alloy sheets through accumulative roll-bonding." *Trans. Non-Ferrous Met. Soc. China*, 18(2), 309-314.

Zhang, Y., Chen, J., Lei, W. and Xv, R. (2008). "Effect of laser surface melting on friction and wear behavior of AM50 magnesium alloy." *Surf. Coat. Technol.*, 202(14), 3175-3179.

Zhilyaev, A.P. and Langdon, T.G. (2008). "Using high-pressure torsion for metal processing: Fundamentals and applications." *Prog. Mater. Sci.*, 53(6), 893-979.

Zhu, Y.T., Lowe, T.C., Jiang, H. and Huang, J. (2001). "Method for producing ultrafine-grained materials using repetitive corrugation and straightening." U.S. Patent No. 6197129 B1.

Zrnik, J., Dobatkin, S. V. and Mamuzic, I. (2008). "Processing of metals by severe plastic deformation (SPD)-structure and mechanical properties respond." *Metalurgija*, 47(3), 211.

BIO-DATA

1. **Name** : Gopi K R
2. **Father's Name** : K M Rangaraju
3. **Date of Birth** : 21-09-1983
4. **Nationality** : Indian
5. **Marital Status** : Married
6. **Address:**

Permanent Address

Lekhana Nilaya, 1st stage Jayanagar,
Behind Adavigowda petrol bunk,
M G Road-573202, Hassan (Dist),
Karnataka, India.

Present Address

Department of Mechanical Engineering
National Institute of Technology Karnataka
Surathkal-575025, Srinivasanagar,
Dhakshina Kannada (Dist), Karnataka, India.

7. **Mobile Number** : +91-9916666873
8. **E-mail id.** : nitkgopi@gmail.com

9. Educational Qualification:

Qualification	College/school	University/Board	Year of Passing	Performance
Ph.D. in Mechanical Engineering	National Institute of Technology Karnataka	National Institute of Technology Karnataka	2017	7.64 (CGPA)
M. Tech in Mechanical Engineering	M S Ramaiah Institute of Technology	Autonomous institute (Affiliated to VTU)	2013	9.47 (CGPA)
B. E in Automobile Engineering	Malnad college of Engineering	Visvesvaraya Technological University (VTU)	2005	70.00%

10. Research Publications:

Number of papers published in International Journals	Number of papers published in International Conference/Symposium
4	2

11. Work Experience:

Name of the Organization	Duration	Position
Cyient, Bangalore	2007-2014	Team Lead
Hindustan Aeronautics Limited, Bangalore	2005-2006	Contract Engineer

I declare that above information is true and correct to best of my knowledge.

(Gopi K R)